Lava tubes on Earth, Moon and Mars: A review on their size and morphology revealed by comparative planetology

Lava tubes on Earth, Moon and Mars: a review on their size and morphology revealed by comparative planetology

Francesco Sauro[1,2], Riccardo Pozzobon[3]*, Matteo Massironi[3], Pierluigi De Berardinis[1], Tommaso Santagata[4], Jo De Waele[1]

1) Department of Biological, Geological and Environmental Sciences, Italian Institute of Speleology, University of Bologna, Via Zamboni 67, 40126, Bologna, Italy
2) European Space Agency, ESA PANGAEA program, European Astronaut Centre, Cologne, Germany
2) Department of Geosciences, University of Padova
3) Virtual Geographic Agency, Reggio Emilia, Italy
*Correspondence to: Riccardo Pozzobon, email riccardo.pozzobon@unipd.it

Abstract

Sinuous collapse chains and skylights in lunar and Martian volcanic regions have often been interpreted as collapsed lava tubes (also known as pyroducts). This hypothesis has fostered a forty years debate among planetary geologists trying to define if analogue volcano-speleogenetic processes acting on Earth could have created similar subsurface linear voids in extra-terrestrial volcanoes. On Earth lava tubes are well known thanks to speleological exploration and mapping in several shield volcanoes, with examples showing different genetic processes (inflation and overcrusting) and morphometric characters. On the Moon subsurface cavities have been inferred from several skylights in Maria smooth plains and corroborated using gravimetry and radar sounder, while on Mars several deep skylights have been identified on lava flows with striking similarities with terrestrial cases. Nonetheless, the literature on this topic is scattered and often presents inaccuracies in terminology and interpretation. A clear understanding of the potential morphologies and dimensions of Martian and lunar lava tubes remains elusive.

Although it is still impossible to gather direct information on the interior of Martian and lunar lava tube candidates, scientists have the possibility to investigate their surface expression through the analysis of collapses and skylight morphology, morphometry and

their arrangement, and compare these findings with terrestrial analogues. In this review the state of the art on terrestrial lava tubes is outlined in order to perform a morphological and morphometric comparison with lava tube candidate collapse chains on Mars and the Moon. By comparing literature and speleological data from terrestrial analogues and measuring lunar and Martian collapse chains on satellite images and digital terrain models (DTMs), this review sheds light on tube size, depth from surface, eccentricity and several other morphometric parameters among the three different planetary bodies. The dataset here presented indicates that Martian and lunar tubes are 1 to 3 orders of magnitude more voluminous than on Earth, and suggests that the same processes of inflation and overcrusting were active on Mars, while deep inflation and thermal entrenchment was the predominant mechanism of emplacement on the Moon. Even with these outstanding dimensions (with total volumes exceeding 1 billion of m^3), lunar tubes remain well within the roof stability threshold. The analysis shows that aside of collapses triggered by impacts/tectonics, most of the lunar tubes could be intact, making the Moon an extraordinary target for subsurface exploration and potential settlement in the wide protected and stable environments of lava tubes.

Keywords: lava tube; inflation; subsurface; comparative planetology; volcanospeleology

1. Introduction

The recent years have seen a rapid expansion of international participation in lunar and Martian exploration, with thousands of publications on planetary geology based on images and data obtained through satellites and rover missions (Burns, 2010). Comparative planetology allows the analysis and interpretation of geological features on different planets. The comparison can be applied both to morphologies and processes considering the differences in planetary parameters such as gravity, temperature, pressure, density and composition of the atmosphere, geological history and others (Chahine et al., 2010). However, while the surfaces of terrestrial planets of our solar system have been documented with high resolution, multispectral cameras, and even by rover missions, very little is known about the subsurface and the potential presence of underground voids.

Early in the seventies, planetary geologists had already identified peculiar collapse sinkhole-like morphologies in several volcanic areas of Mars and in the lunar Maria (Carr et al., 1977; Carr, 1973). These “sinkholes” are often referred to as “collapse” or “pit” chains when they are aligned (Fig. 1). Since these features lack the elevated crater rim and ejecta deposits that are typically associated with impact craters, they have been thought to represent collapses of underground cavities. Because most of these features are found on lava flows or along the sides of volcanic edifices, they were very early associated to the putative presence of “lava tubes”, also known as “pyroducts” (Kempe, 2012, 2019). Lava tubes are well known on terrestrial shield volcanoes thanks to volcanological and speleological research (Bunnell, 2008), even though also other processes could be accounted for the formation of pits and volcanic non-eruptive depressions (Halliday, 2004; Okubo and Martel, 1998). The lava tube collapse hypothesis was also proposed by several authors to explain the formation of sinuous lunar rills, that would represent collapsed tubes (Cruikshank and Wood, 1972; Greeley, 1971a; Oberbeck, 1969). Nonetheless, several authors have shown that also on Mars and the Moon not all sinkholes can be directly related to lava tubes and other volcanic and tectonic processes are most likely driving the formation of these features (Cushing, 2017; Wyrick et al., 2004). Hence, the potential presence of still intact lava tubes below the surface of the Moon and Mars is a matter of debate since more than fifty years.

In recent times, the availability of high resolution images of the surface of Mars from High Resolution Imaging Science Experiment camera (HiRISE, 0.25 m/pixel resolution) on board Mars Reconnaissance Orbiter (MRO) and the Moon from the Lunar Reconnaissance Orbiter Narrow Angle Camera Camera (LROC NAC, 0.5 m/pixel resolution) on board Lunar Reconnaissance Orbiter (LRO) has allowed identifying peculiar holes characterized by vertical or overhanging walls, named “skylights”, often proposed as “cave-entrance” candidates (Cushing, 2012; Haruyama et al., 2012). Until now, more than 300 of these potential cave entrances have been identified on the Moon (Wagner and Robinson, 2019) and more than 1000 on Mars (Cushing, 2017). Most of them are isolated features but several are associated with collapse chains on Mars or sinuous rilles on the Moon. While in sinkholes, detritus from the collapse could obstruct the access to the intact tube, skylight features represent direct ceiling accesses to underlying still intact lava tubes. The most

spectacular examples of these entrances are situated in the volcanic plateau of Marius Hills on the Moon (Haruyama et al., 2012), and on the lava plains of Arsia and Olympus volcanoes on Mars (Cushing et al., 2007). Robotic technologies, could allow to examine stratigraphic sections of lava flows from skylights allowing to collect new data on the formation of plateau basalts on the Moon and shield volcanoes on Mars (Kerber et al., 2018). Intact, open segments of lava tubes could provide stable shelters for human habitats shielded by cosmic radiation and micrometeorite impacts on the Moon (Haruyama et al., 2012). These voids could have dimensions suitable for housing a permanent base providing potential access to several resources, including volatiles and possibly water ice trapped in cave sediments (Blamont, 2014; Williams et al., 2010). In addition, skylights could provide direct access to the subsurface of Mars, which is considered one of the main targets for the search of past and present life traces on the red planet (Boston et al., 2001; Léveillé and Datta, 2010; Michalvsky et al., 2018).

Nonetheless, aside of identifying the presence of lava tube collapses and skylights, scientists have very few hints on the potential dimension and morphology of subterranean voids on these planetary bodies. On the Moon recent studies have attempted to evaluate the dimensions of intact lava tube fragments below the surface using the radar sounder system (Kaguya) (Kaku et al., 2017) and gravity mass deficit by Gravity Recovery and Interior Laboratory mission (GRAIL) (Chappaz et al., 2017), targeting pits and sinuous rilles regions. These studies seem to confirm that subsurface voids certainly exist, but the available limited resolution of the instruments have only allowed to retrieve partial information on their size, depth and shape. Finite element modelling of ceiling stability (Blair et al., 2017; Theinat et al., 2020) was used to estimate the sustainable potential dimensions of lunar and Martian lava tubes by iteratively varying roof thickness and strength of the material. However, this approach is limited to the stability range of these voids in the different planetary bodies without providing direct evidences of their real existence and any information on their genetic processes. Recently, tubular sinuous ridges hundred of meters wide and hundred of kilometers long on the lava plains of Southwest Tharsis on Mars have been proposed as undrained tubes based upon several morphological analogies with terrestrial examples (Zhao et al., 2017). Other studies in Noctis Labyrinthus on Mars have interpreted pit chains and linear depressions as collapses above hundred-

kilometers long lava tubes but have failed to provide any evidence of their subsurface development and dimensions (Leone, 2014).

On the other hand - on Earth - several morphological and genetical studies have been performed on lava tubes in terrestrial shield volcanoes (Kempe, 2012, 2019) with hundreds of kilometers of lava tubes and associated collapses and skylights mapped by speleological organizations. Detailed morphological descriptions and topographic surveys of kilometer-long tubes are available thanks to speleological explorations on Hawai'i (USA) (Bunnell, 2008; Greeley, 1971b; Kauahikaua et al., 1998; Peterson et al., 1994), the Canary Islands (Spain) (Sauro et al., 2019; Wilkens et al., 2009), Iceland (Hróarsson and Jónsson 1991), Northern Queensland (Australia) (Atkinson et al., 1975), Sicily (Italy) (Calvari and Pinkerton, 1999), Jeju Island (South Korea) (Woo et al., 2008), the Galapagos (Ecuador) (Jorda-Bordehore et al., 2016), and many other lava fields in the world (Kempe, 2012, 2019). This huge amount of data can be used for comparative planetology studies in order to infer lava tube dimensions and morphologies in the different planetary bodies of the inner solar system.

Although the morphological similarities of several collapse chains and skylights on Mars and the Moon with terrestrial lava tube features have been underlined by several authors (Cushing et al., 2007; Cushing, 2012; Léveillé and Datta, 2010), to date, a detailed morphological and morphometric comparison among the three planetary bodies has not yet been provided. Given the direct genetic relationship between the collapses, the skylights and the lava tubes, morphometric analysis can be used to estimate the dimension and general morphology of intact sections of the tube along the same collapse chain line.

In this review, we discuss the genetic mechanisms and related morphologies of lava tubes on Earth and we provide morphological evidences to recognize lava tube collapse chains and associated skylights on Mars and the Moon. We also define morphometric and morphological relationships between collapses and underlying intact segments of the tubes on Earth, allowing for morphological and volumetric estimation of the Martian and lunar cases.

To this aim, we have examined the most important morphometric parameters of collapse chains and skylights associated to lava tubes observed in satellite images and DTMs from Earth, the Moon and Mars. For the terrestrial lava tubes we can relate these measurements

with the dimensions of the still intact tube, which has been mapped through standard speleological surveys or laser scanner technologies and the relationship between surface and subsurface lava tube features can be extended to the other bodies.

This review and the associated comparative analysis provide, for the first time, direct evidence of the size, depth and morphology of lunar and Martian lava tube candidates in comparison with terrestrial ones, providing new clues on their genetic processes and implications on volcanology, habitability and astrobiology (Boston et al., 2004; Léveillé and Datta, 2010). These data constitute the basis for planning of future robotic and human exploration missions of these subsurface planetary features.

2. Lava tube genetic mechanisms and morphologies on Earth

A lava tube, also known as pyroduct (Kempe, 2012, 2019), is defined by Halliday (2004) as a "roofed conduit of flowing lava, either active, drained, or plugged". The lengths of lava tubes on Earth vary from a few meters up to tens of kilometers (Bunnell, 2008). Their width and height vary from 0.5 m up to 30 m, developing from few centimeters below the surface up to a depth of few tens of meters. Lava tubes are in most of the cases sub-parallel to the surface itself. Cross-sections of lava tubes are usually arched, round, oval, or alternatively keyhole shaped, due to accretion of lava to the sidewalls and downcutting by thermal and physical erosion (Allred and Allred, 1997; Fagents and Greeley, 2001; Greeley et al., 1998).

Lava tubes can present different patterns: a) single tubes, sinuous or rectilinear, b) braided tubes, with bifurcations and conjunctions c) multilevel tubes with different levels connected by lava falls and shafts, d) a combination of braided tubes on different levels. This range of morphologic variability is due to different genetic processes (Fig. 2) controlled mainly by the effusion rate, the slope of the land surface on which the lava flows, the underlying paleo-topography, and the composition and related rheology of the lava.

The first genetic observations of actively forming lava tubes are those of Peterson and Swanson (1974) and Peterson (1994) during long-lasting effusive eruptions at Kīlauea volcano in the Hawai'i. They observed most of the tubes forming by "overcrusting" of an open lava channel. This process is based on the principle that the outer surface of an active

lava flow chills quickly because of the temperature difference between the molten lava and the atmospheric air. The cooling surface becomes progressively more viscous and finally solidifies (Dragoni et al., 1995), insulating the molten lava below. The insulation slows the rate of cooling inside the closed tube helping to maintain heat and low viscosity over long distances and time. The overcrusting of the channel can happen through slightly different mechanisms, depending on the flow rate, turbulence and channel geometry (Fig. 2 A-B): 1) the growth of solidified rooted crusts from lava stream banks; 2) overflows and spatters accreted to form shelves and levees that progressively grow forming a roof across the stream; 3) plates and lithoclasts of solidified lava floating downstream welding together and forming a blocky roof. The three mechanisms are not mutually exclusively and frequently the channel is overcrusted through a combination of these three processes.

When the feeding source of the lava runs out, the flow slowly evacuates the conduit leaving an empty tube. Usually overcrusted tubes are limited to the width and depth of the channels where they originally formed, with roofed sections not exceeding few tens or maximum hundreds of meters in length and a few meters in diameter. The discharge rates of these tubes are often moderate, between 1 to 5 m^3 s^{-1}. If the lava flow reaches the sea, the chilled crust solidifies much more quickly forming "littoral" tubes that show characteristic features in association with pillows (Peterson et al., 1994). These tubes however are rarely drained and mostly plugged, and generally have limited extensions. Examples of overcrusted tubes, aerial and littoral, have been described in most of the terrestrial shield volcanoes (Rossi, 1997).

Another overwhelmingly more frequent genetic process forming lava tubes is shallow inflation and draining of inflated pahoehoe lobes (Fig. 2 C). This process has been widely described by Hon et al. (1994) and Peterson (1994): initially inflation acts within thin sheets of pahoehoe lava, but when the chilling crust is strong enough, the increasing internal pressure results in uniform uplift of the entire sheet flow lobe. As the flow advances, preferred pathways develop in the older portions of the liquid-cored flow; these pathways can evolve into elliptical lava tube systems that sometimes can be drained and leave an open tunnel (Cooper an Kauahikaua, 1992). In case of long-lasting eruptions several small tubes can merge focusing the flow along one main path. The focused flow has

stronger thermic erosion potential and can enlarge and entrench the conduit (Kempe, 2019).

Lava tubes formed by shallow inflation are usually characterized by a superficial bulge (due to the inflation) along its development, and by an original horizontal elliptical cross section that can be entrenched by thermal erosion. The most remarkable examples on Earth are on Hawai'i (Kempe, 2019), on the Canary Islands (Sauro et al., 2019) and on Iceland (Hróarsson and Jónsson, 1991) but they are in any case present in all major shield volcanoes on Earth.

Inflation can act also in long-lasting aa lava flows as described by Calvari and Pinkerton (1998) (Fig. 2 D). In this case the inflation acts mainly at the front where the flow stops, thickens and widens. Since lava continues to be supplied at a uniform rate but cannot reach further than the front, the internal pressure increases and inflation propagates from the front region backwards forming a tube network. When the pressure overcomes the tensile strength of the crust in the front area, tumuli or new ephemeral vents open and a new flow is fed by the upper tube system (Duncan et al., 2004). These peculiar lava tubes in aa flows are usually characterized by higher discharge rates compared to pahoehoe, in the order of 10-20 m^3 s^{-1}. Because of these peculiar genetic mechanisms, lava tubes in aa flows are usually bigger than in pahoehoe, but are more segmented into primary and secondary flows.

Tumuli hosting small chambers and short low-ceiling caves can also be associated to both aa and pahoehoe inflationary tubes s a result of lava being injected from below (Pedersen et al., 2017; Table 1).

In addition to overcrusted and shallow inflated lava tube morphotypes, few cases on Earth have been proposed as a very peculiar example of "deep inflated-entrenched" lava tubes (Fig. 2 E). These formed through inflation along deep inception horizons following previous lava flow boundaries where, after inflation, the conduit has been enlarged by downward thermic erosion and breakdown phenomena (Tonello, 2017; Kempe, 2019). These lava tubes are among the biggest in size on Earth, with the most famous examples being Corona Lava Tube in Lanzarote (Sauro et al., 2019) and the Undara Lava Tube in Queensland (Atkinson et al., 1975). In these cases, the flow discharge can reach values of over 50 m^3 s^{-1}.

Sometime the conduit can form also along fractures and eruptive fissures (Fig. 2 F), through processes described as ”evacuated dike tunnels” sensu Cushing et al. (2015). An example of a very deep plug pressure tube along a fracture is the Wood Valley Pit Crater in Hawai‘i (Favre, 1993). Here the thermal erosion created a lava tube conduit through plug flow along a fracture, at almost 90 meters of depth below the surface (Okubo and Martel, 1998). The fracture doesn’t reach the surface being probably sealed by younger flows on top. In this case, this peculiar lava tubes controlled by a fracture present vertical elliptical cross sections.

In all genetic cases, chains of collapses aligned along the tube development represent the surface expression of these conduits (Fig. 1 A-C). Collapses of the ceiling form during the genesis of the lava tube through flow overpressure (pseudo-vents), or, more commonly, by gravitational effects when the tube is finally drained, including block stoping transferring the void from deep conduits to the surface (Cushing et al., 2015). These collapses, called “*pukas*” in Hawai‘i or “*jameos*” in the Canary archipelagos (Fig. 1 A-C), typically form sinuous chains and are mostly elongated along the direction of the tube (Fig. 1 A-E). It is worth mentioning that in literature collapses associated to lava tubes are often confused with other volcanic vertical pit types - frequently named “pit craters” - that can be associated to other processes like tectonic or fissural magma flow (Halliday, 2004a; Cushing et al., 2015). In this review we will use the Canarian term “*jameos*” for the lava tube-associated terrestrial cases, as reported in the most updated edition of *Glossary of Geology* from the American Geological Institute (Jackson, 2005). *Jameos* is a genetic-specific term referred to a collapse that is certainly related to lava tube formation, while pit crater is a more general term, not necessarily due to lava tube collapse but potentially related also to other types of cavities (Okubo and Martel, 1998).

On Earth a collapse can represent different stages: 1) proper *jameos*, which are collapses that involve the whole tube width with vertical or steeply descending detrital slopes (Fig. 1 B-C), 2) skylights with vertical or overhanging walls where the opening is much smaller than the tube width below (Fig. 1D). *Jameos* are frequently filled by detritus, while skylights are just openings on the roof of the conduit. Between one *jameo*/skylight and the subsequent one the underground tunnel can be intact and accessible for exploration and mapping (Fig. 1A).

3. Collapses and skylights related to lava tube candidates on the Moon and Mars

The putative presence of lava tubes on planetary bodies such as Mars and the Moon has been proposed as early as in the sixties (Oberbeck, 1969) with their evidence expressed as sinuous rilles and sinkholes in volcanic terrains. The terms "collapse" or "pit" are commonly used in the planetary geology literature to define lunar or Martian morphologies characterized by sinking circular or elliptical topographic depressions that lack the elevated crater rim and ejecta deposits typical of impact craters. Several authors have associated collapse chains in planetary volcanic terrains to the breaking of lava tube ceilings, exactly like *jameos* on Earth (Cushing, 2012; Leone, 2014; Wagner and Robinson, 2014). Nonetheless, the direct relationship of these features and lava tubes cannot be inferred easily without direct exploration. Several other genetic processes have been proposed for collapse/pit chains such as dike intrusions, collapses of shallow magma chambers, dilational faults and voids created by tensional fractures (Cushing, 2012; Ferrill et al., 2004; Ferrill et al., 2011; Leone, 2014; Rubin, 1992; Scott and Wilson, 2002; Smart et al., 2011; Wilson and Head III, 2002; Wyrick et al., 2004).

Also skylights have been associated to lava tubes. Even so, other speleogenetic processes have been proposed as well, like hypogenic and sulfate karstification, tectonic caves and shallow magma chamber evacuation on Mars. The Mars Global Cave Candidate (MGC3) catalogue (Cushing, 2017) differentiates between: 1) lava tube candidate *jameos* along rilles, channels and collapse chains, 2) Atypical Pit Craters (APCs) usually isolated with peculiar morphological characteristics, 3) Small Rimless Pits (SRPs) along flow channels 4) Pinholes which are likely very small entrances and 5) lateral entrances on cliffs. Applying this classification only 1, and 3 can be directly associated with lava flows and can therefore be considered potential lava tubes entrances. Atypical pit craters instead remain controversial features with an unclear origin.

Likewise, on the Moon not all skylights formed in volcanic terrains, but also in impact melts, therefore in these cases other processes are probably responsible for their formation (Wagner and Robinson, 2014).

For these reasons, any study aiming to identify lava tube collapses and skylight candidates on the surface of these planetary bodies has to follow a rigorous approach based on a geomorphological comparison with terrestrial analogues.

As discussed by Wyrick et al. (2004), several pit chains on Mars are related to dilational faults that are distributed along the flanks of volcanic edifices of the Tharsis region and on flat-lying floors of broad basins, with striking similarities with terrestrial analogues on Iceland (Ferrill et al., 2011) and Hawai'i (Okubo and Martel, 1998). On the Moon, dilational pit chains are common within and around Mare basins, mainly related to tensional tectonic regions (Watters et al., 2012). Tectonic pit chains are often rectilinear or curvilinear and are mostly associated with tectonic lineaments or bounded within grabens (Pozzobon et al., 2015). Frequently, there are transitions along strike from visible faulting to faults and pits to pit chain alone (Mège et al., 2003). Tectonic pits are often coalescent depressions forming scalloped troughs and do not necessary follow the maximum slope.

Conversely, lava tube *jameos* on Earth (and by analogy lava tube associated collapses on Mars and Moon) present important morphological differences that make them easily discernible from tectonic counterparts (Tab. 1). The main characteristic, which makes them distinguishable from the tectonic chains, is their sinuosity (Cushing et al., 2007).

Additionally, also some remarkable morphological differences are expected between collapse chains related to overcrusted or inflated lava tubes (Dragoni et al., 1995; Kauahikaua et al., 1998; Kempe et al., 2010; Orr et al., 2015) (Tab. 1). Overcrusted tubes are formed mainly within lava channels and therefore their topographic expression can be followed from one collapse to the other along the channel benches (Dragoni et al., 1995; Kempe et al., 2010). Being the flow gravity-driven (Sakimoto et al., 1997), overcrusted tubes always follow the line of maximum steepness. An example of a putative overcrusted lava tube collapse chain on Mars is shown by Cushing (2012) on the lava plains to the north of Arsia Mons. This sinuous chain of *jameos*, with a total length of 40 km, shows clear bulges/benches that can be followed on the surface from one collapse to another (Fig. 1G). Conversely, inflated tubes usually do not present any linear evidence on the surface aside of collapses or wide bulged areas and tumuli (Orr et al., 2015). Because this genetic type of lava tube is pressure-plug driven (Sakimoto et al., 1997) with subsurface inflation able to follow prominent inception horizons (discontinuities like fractures or lava flow

boundaries), their directions can also slightly deviate from the steepest slope line. Typical examples of this type of collapse chains are those on the southern flanks of Arsia or Hadriaca on Mars and the Gruithuisen chain on the Moon (Fig. 1 I-O). Inflated can also be braided and develop on different levels as shown in several terrestrial examples, like Cueva del Viento on the island of Tenerife (Montoriol-Pous and de Mier, 1974). Examples of braided collapse chains have been identified on flanks of Olympus Mons (Fig. 1N), whereas no evidences of their presence have been detected on the Moon so far.

Lava tubes collapse chains can be discriminated from other genetic types also by the presence of a vent at the top of the chain. While on Earth, this is usually a volcanic cone and crater, there are evidences that in the shield volcanoes of Mars or in the fissural volcanic field of the Moon this is often represented by a deeper and wider depression which can represent their feeding vent. Smaller circular skylights with vertical or overhanging walls can be indeed found along lava tube collapse chains, usually with a smaller width compared to the collapses (Fig. 1D, 1H, 1L). All these characteristics are useful to properly distinguish lava tube collapse (*jameos*) chains on the Moon and Mars, however these criteria are solely based on the analogies with terrestrial lava tubes, while other unknown or slightly diverse emplacement mechanisms could be acting on different planetary bodies.

4. Morphology of collapses related to tube stability and emplacement mechanisms

Terrestrial examples can also help to define the morphometric relationship between collapse chains and intact lava tube segments on the Moon and Mars. In most terrestrial lava tubes, *jameos* appear in plan view as ellipses elongated along the conduit development direction and their width (*W*) approximates the underlying lava tube average width (*Wt*) of the intact sectors (Fig. 1A). However, in case of braided superposed branches, collapse chains follow the development of the shallowest part of the tube while other segments can remain stable and thus without any expression at the surface. *Jameos* can have vertical or high angle slope sidewalls when the ceiling is completely collapsed forming depressions elongated along the tube lateral limits (Fig. 1B). Skylights instead have vertical or overhanging walls forming smaller circular depressions (Fig. 1C-D). Indeed, skylights on the ceiling have a smaller width *W* compared to the tube *Wt* (Fig. 1D). In all surveyed

terrestrial lava tube chains, skylights are by definition much smaller than *jameos* (Bunnell, 2008). Their circular shape is guaranteed by the uniform horizontal stress field on the ceiling (i.e., being σ1 vertical, and σ2 = σ3) when tube sidewalls confinement is not yet reached transforming the skylight into an elongated *jameos.* Thus even the collapse planar ellipticity can be used as a distinctive character among lava tube openings.

The scaling factor *f=W/Wt* between *jameos* and intact tube segments is shown in Fig. 3 for three different terrestrial examples. In the case of a braided multilevel tube like Kazumura in Hawai'i (Allred and Allred, 1997) *f* is slightly smaller than 1, with most of the collapses still with vertical walls. The width of the tube is not changing in proximity of the *jameos*. Conversely, *jameos* in the deep-inflated Corona lava tube in Lanzarote are situated in areas where the conduit was wider in average. These larger areas are mainly located where the lava tube changes its direction, and the lateral enlargement was probably due to flow overpressure and lateral thermal erosion. The transition from an $f<1$ to an $f>1$ is related to the predominance of a gravity-driven flow or of a pressure-driven flow in the tube, respectively (Sakimoto et al., 1997).

The pressure-driven flow is even more evident in the inflated tube of Undara in Queensland (Atkinson and Atkinson, 1995) where *jameos* are much wider than the intact tube *Wt* (f=5.3). In some cases, collapses seems even unrelated to the tube development, being interpreted as lateral pressure overflows forming local lava ponds that afterwards drained back into the lava tube (Atkinson, 1991).

These different scaling factors are clearly controlled by different emplacement mechanisms. Therefore in order to provide estimates of lava tube dimensions based on associated collapse morphometry on the Moon and Mars, it is necessary to consider the different genetic hypotheses by carefully investigating the morphological characteristics able to discern overcrusted from shallow/deep inflated cases (Table 1).

5. Morphometry: materials and methods

5.1 Lava tube and related jameo*/sinkhole morphometric parameters*

In the last years morphometry has been used as a tool for comparing genetically related features on different planetary bodies (Ansan and Mangold, 2013; De Toffoli et al., 2019;

Plescia, 2004; Pozzobon et al., 2019). Using DTMs we extracted profiles along the chains and a wide range of comprehensive morphometric parameters of lava tube collapses on Earth, Mars and the Moon, including volumes (Table 2). For each *jameo*/skylight along a chain the following parameters have been extracted: length (*L*), width (*W*, considered as the minor axis of elliptical collapses), depth (*D*), collapse total volume (*V*), linear volume (V_1, the average volume of 1-m-long cross-sections), asymmetry ratio (*AR*, the ratio between width and depth). For the whole collapse chain it is possible to measure the following parameters: total length (*Ctl*), collapse chain sinuosity (*Si*), and slope (*S*). In the case of Earth, thanks to speleological exploration, terrestrial laser scanning, and topographic surveys, it is possible to directly acquire the width (*Wt)*, height (*Ht*) and linear volume (V_1t) of the intact tube between collapses, as well as the total length of the underground void (*Ttl*).

Finally, the expected intact tube length (*Tutl*) is given by the difference between the chain total length (*Ctl*) and the sum of all collapse lengths (*L*).

5.2 Case studies and dataset generation

5.2.1 Earth

The terrestrial examples analyzed are Corona (Lanzarote, Spain), among the most voluminous tubes known on Earth (Carracedo et al., 2003), Kazumura (Hawai'i, USA), the longest terrestrial lava tube (Allred et al., 1997), and the Undara lava tube in North Queensland (Australia) (Whitehead, 2010). In total, we gathered a dataset of 120 *jameos* and skylights measured in the three sites. These three examples have been chosen as terrestrial maximum size end-members in terms of dimension, being considered among the most voluminous lava tubes on Earth (Allred and Allred, 1997; Atkinson and Atkinson, 1995; Sauro et al., 2019). A detailed description of each lava tube and associated *jameos*/skylights is provided in the Suppl. Mat.

The 6.5 km long Corona lava tube system (Supplementary Fig. 1) above the sea-level was entirely mapped together with its *jameos* during three different survey campaigns in 2017 using a combination of Terrestrial Laser Scanning (TLS) and Mobile Mapping (MM). The final result is one of the longest 3D surveys of terrestrial lava tubes to date (Santagata et al., 2018; Sauro et al., 2019). The main path of the entire cave system was mapped with an

unprecedented resolution of 6 mm point spacing on average. The laser scanner surveys within the caves were georeferenced on the surface through differential GPS and using DTMs derived from regional airborne Light Detection and Ranging data (LIDAR, 2.5 m point spacing from Spanish Geological Survey) and Unmanned Aerial Vehicles (UAVs) photogrammetric surveys of the *jameos* and surrounding terrains. All the morphometric parameters of Corona lava tube were thus retrieved using this high-resolution dataset.

The morphometric data for *jameos*/skylights in Kazumura and Undara were obtained through existing speleological maps and databases. The measurements of Kazumura have been performed with the aid of the Kazumura Atlas (Allred et al., 2002) providing plan views and profiles of the entire tube length, including *jameos* and skylights (Supplementary Fig. 2). The measurements of morphometric parameters on the digitalized maps where performed in a Geographic Information System (GIS) environment. For Undara we relied on existing data from previous publications (Atkinson, 1991; Atkinson and Atkinson, 1995) and speleological maps, including average measurement of conduit *Wt* and *Ht* (Supplementary Fig. 3).

5.2.2 Mars

On Mars, a total of 122 collapses related to five lava tube candidate chains were examined on Arsia, Olympus and Hadriaca volcanoes (Table 3, Fig. 2, Supplementary Figures 4-8). The analysis was extended for comparison also to a typical graben-bounded tectonic pit chain in Ascraeus Mons (Wyrick et al., 2004) (Supplementary Figure 9). This was achieved through high-resolution stereo DTMs (18 m of grid size) generated from Context camera images (CTX, 6 m/pixel on board MRO)(Malin et al., 2007). CTX images present indeed a good compromise between resolution (~5.5 m/pixel) and areal extent (swath width of 30 km and length variable between 50 and 300 km) providing broad coverage and sufficient resolution for mapping and morphometric analyses. By contrast, the high resolution stereo pairs provided by the HiRISE camera (0.25 m/pixel, with associated DTMs with 1 m of grid spacing) have a small field of view (6x12 km in the RED channel) and an extremely limited coverage on the areas of our interest and thus could not provide the needed areal extent to carry out our analysis

The best overlapping CTX images were selected using the Planetary Image Locator Tool (PILOT) stereo analyzer for targeted regions (Bailen et al., 2015) which is able to compute the stereo angles of the image pairs and the expected vertical precision of the final output (Supplementary Table 1).

All the stereo pairs were pre-processed with Integrated Software for Imagers and Spectrometers (ISIS3) suite from USGS (United States Geological Survey) (Gaddis et al., 1997; Torson and Becker, 1997). The bundle adjustment of the stereo pairs and stereo matching was performed with Ames Stereo Pipeline (ASP, Beyer et al., 2014; Moratto et al., 2010; Shean et al., 2016). The point clouds were aligned with the Mars Orbiter Laser Altimeter Precision Experiment Data Records (MOLA PEDR) for absolute height reference and the DTM was gridded with a resolution of 18 m. The associated ortho-images at 6m/pixel resolution were also produced for each site.

5.2.3 Moon

On the Moon a total of 27 collapses putatively related to lava tubes were analyzed in three different collapse chains in Marius Hills and Gruithuisen (Table 3, Fig. 2, Supplementary Figures 10-12) using the Kaguya/LOLA merged DTMs (59 m of grid spacing, Barker et al., 2016). In both cases, we have carefully selected the collapse chains that for their morphological characteristics (Table 1) can be differentiated from tectonic pit chains (Wyrick et al., 2004) on LROC NAC image mosaics. In addition, the same DTM approach has been performed for comparison on the graben bounded tectonic pit chain of Hyginus Rill (Wilson et al., 2011) (Supplementary Fig. 13).

Lunar lava tube traces and collapses were mapped on LROC NAC images (Supplementary Table 2) that, with ISIS 3, were calibrated, destriped, attached to the spacecraft navigation and pointing kernels (SPICE) and exported as 32bit geotiffs allowing to perform contrast stretch during the mapping and analysis of the collapses.

5.3 Topographic profiles and extraction of collapse maximum depth (D)

We traced the profiles of the collapses on Mars and the Moon by calculating the second derivative of the DTM (Wood, 1996). This variable produces a line along the collapse chain perpendicular to the direction of the maximum slope, visually providing the trace of the

deepest path from which the topographic profiles were extracted (Supplementary Fig. 14). This was achieved using the *r.param.scale* GRASS GIS module with a kernel size of analysis of 11x11 pixels (Wood, 1996).

The problem of no-data areas in correspondence of shadowed regions is particularly relevant for some collapses (~30%) on Mars where LiDAR data by MOLA did not reach a sufficient resolution to merge them with stereo DTMs. On the Moon the DTM dataset used is a combination of LOLA laser altimeter able to map shaded areas merged with stereo photogrammetry from Selene-Kaguya images. On Mars the areas presenting hard shadows in the images typically do not converge in the stereo matching and most softwares apply a hole-filling technique during the post-processing to mitigate this effect. In some cases, like in Arsia's largest collapse chains, almost one third of the depression is shadowed. In order to keep the information as much similar to the ground truth we did not use any hole filling technique. Indeed, the region interested by such hard shadows is typically one side wall of the deepest collapses, whereas the profile line matches the bottom floor which is covered by DTM.

The absolute maximum depth of each collapse was obtained by subtracting from the height values of the topographic profile, the profile traced on a DTM where holes were "filled" with synthetic surfaces (Supplementary Fig. 15). For this purpose we used a technique based on the creation of a synthetic surface constrained to the collapse edges in order to approximate the original topography before collapses and creating a DTM where holes are filled as shown in Pozzobon et al. (2018) and Pozzobon et al. (*in press*). This is obtained by digitizing the edges of the collapses on a combination of optical images and maximum profile curvature extracted from the DTM using the *r.param.scale* GRASS module (Wood, 1996) and with the aid of an overlaid ortho-image in transparency. The nodes of the polygon retracing the collapse edges were used to triangulate the synthetic surface, that was subsequently merged with the DTM obtaining a "filled" surface best approximating the pristine pre-collapse condition. The two stacked profiles and the absolute depth are presented in supplementary figures for each collapse chain (Supplementary Materials).

To be sure to extract the actual local maximum depth in each of the collapses we treated the obtained absolute depth data as a waveform and performed a peak analysis in MATLAB

environment extracting local peaks within the collapses and hence identifying univocally the greatest depth value.

For the smaller *jameos* of Arsia North and the skylights along all collapse chains, the very high contrast between the shaded areas and the surroundings bear no information usable for stereo correlation. However, knowing the azimuth and incidence angle of the light source on the ground from image metadata and by measuring the shadow it is possible to derive the depth of each *jameo*/skylight. The depths where extracted by using the *shadow height* tool in the *qview* program of the ISIS3 software suite. For each *jameo*/skylight we measured 10 profiles parallel to the illumination direction extracting maximum and average depth.

5.4 Collapse and conduit volume extraction

To correctly perform a volume calculation of collapses based on DTMs on all three planetary bodies it is necessary to take into account the high variability of the surrounding terrain as well as its general steepness, slope and roughness. In this case, opposite to the profile extraction phase, we applied a hole-filling technique of the shadows/no data areas in the DTMs in order to obtain a closed surface. A simple volume estimation based on average height of the collapse is thus not possible. The volumes enclosed between the reference synthetic surface and the real one were calculated with the *surface difference* in the 3D analyst toolbox of ArcGIS obtaining an estimate in cubic meters. It is worth to emphasize that the calculated volumes correspond to the minimum volume of the collapse, since some mass wasting from the walls and aeolian infilling is to be expected.

The terrestrial laser scan model of the Corona lava tube served as a starting point to build on comparative planetology and as a reference to check the performance and reliability of morphometric calculations based on DTMs. In particular, to validate the methodology of volumes extraction from DTMs described above, we compared the volumes obtained from TLS of the Corona collapses (Supplementary Fig. 16), with the same ones extracted using the airborne LiDAR data at 5 m resolution. The results gave an almost perfect match (R^2=0.9989) with volumes obtained through terrestrial laser scanning slightly higher than those extracted from the LIDAR DTM; this is most probably due to sporadic lateral overhanging walls that cannot be resolved by airborne LiDAR surveys.

By using the point cloud of the terrestrial laser scan model of the Corona lava tube we also derived the volumes of the intact sections of the tube together with the collapsed ones (Supplementary Movie 1). This operation was carried out by importing the aligned point clouds in Auto-Cad 2017 and extracting vertical cross-sections orthogonal to the tube path using 5 m interval for the intact tube and 1 m for the collapses (*jameos*) (Supplementary Figure 16, Supplementary Movie 1).

All of the lava tube cross-sections were digitized in 2D cad polylines subsequently cut into 1 m thick discrete slices (also referred to as linear volumes V_1 for *jameos* sections and V_1t for intact tube sections). The total volumes of the *jameos* were instead closed at the surface by interpolating their edges and laterally by interpolating the margin of their openings towards the intact conduit.

In the cases of Kazumura and Undara where 3D models and high resolution DTMs were not available, because of the two-dimensional nature of the cave maps such as (plan and profile views), we approximated the collapse volumes through the simple equation $[(D*W)/2]*\pi$, where D is the average depth and W the width of the tube. Tube linear volumes V_1t were instead approximated assuming an elliptical cross-section of the conduits following the equation $(Ht/2)*(Wt/2)*\pi$ where Ht is the height of the conduit and Wt is the width of the conduit. The same equations have been used for the dataset of the collapse chain of Arsia North on Mars, where the average depths (D) of collapses have been calculated through the shadow method and used to calculate V_1 of the collapses.

6. Results

6.1 Morphometry of terrestrial cases

Lava tube *jameos* measured on terrestrial shield volcanoes have an elliptical plan shape with the long axis parallel to the direction of subsurface tube development (Fig. 1A). Along the same chain, the minor axes of the *jameos* (perpendicular to the subsurface tube development) show comparable W, which is representative of the width of the underlying lava tube (Fig. 1A, Fig. 3, Fig. 4). Morphometric data are reported in Table 4. In the case of Kazumura, the mean collapse W is 7.3 m (σ=2.9), with the main portions of the intact tube characterized by a comparable Wt of 10.5 m (σ=4.7). Bigger dimensions can be found in the

Corona lava tube where the mean collapse *W* is 37.6 m (σ=12.1) while the intact tube departing from the collapses shows slightly smaller dimensions with *Wt* between 7 to 27 m with an average *Wt*=13.7 m (σ=5). According to Atkinson (1991) similar dimensions can be found also in the Undara lava tube with a *Wt* of 15-20 m, but here the related collapses can reach up to 50-60 meters in *W*. The depth *D* of the collapses is more homogeneous in the four cases (respectively in average 5.2, 9.8, and 10.0 for Kazumura, Corona and Undara) and is well comparable to the heights *Ht* of the intact tube sections (respectively in average 8.1, 9.7, and 6.5). Following the increase of *W* in the three cases while maintaining similar *D*, the asymmetry ratio (*AR*) of the collapses is growing from Kazumura (1.4) to Corona (3.8) and Undara (5 to 12). Linear volumes (volume along a 1 m thick cross-section) have also been measured in the three cases, both along the collapses (V_1) and along the intact tube sections (V_1t). The average linear volume represents an estimation of the collapse/conduit size independently from their asymmetry ratio and allows to calculate a volumetric conversion factor (*f*) between the intact tube and the collapse, as $f=V_1/V_1t$ resulting in 0.4, 2.9 and 5.2 respectively for Kazumura, Corona and Undara. In Kazumura the tube is intact along 97 % of the collapse chain, while in Corona and Undara the intact portions cover 73-74 % of the chain but they are not always accessible due to rockfall and infillings.

Few skylights of the cave ceiling show a much smaller *W* along the chains (Fig. 2). These skylight outliers in each chain dataset are usually rounded (*L*=*W*) and present peculiar morphologies with overhanging walls opening on the conduit roof. Skylights are common in Kazumura, but they characterize also some parts of Corona.

6.2 Morphometry of lava tube collapse chains on Mars

Similar morphological characteristics can be found in the four lava tube candidates measured on Mars (Fig. 1 G-O). The chains here show a higher density of collapses compared to Earth, with only from 20 to 40 % of intact portions along the whole chain (Table 5). An exception to this range is the chain of Arsia North, where the pristine lava tube parts reach 95%. In all cases collapses are elongated along the sinuous chain development. In the chains of Arsia South-A, Arsia South-B and Arsia North smaller outliers

where *L*=*W* have been identified as overhanging skylights, similar to those observed in terrestrial examples (Fig. 1H and 1L, Supplementary Figures 4-5-6).

Arsia North collapses have the smallest average *W* of 44 m (σ=11) and depth *D* of 16 m (σ=4), while the other cases show much bigger dimensions. The collapse chain of Arsia South-A shows an average *W* of 283 m (σ=84) and depth *D* of 25 m (σ=17). Slightly bigger dimensions are found in Arsia South-B (*W*=415 m, σ=108; *D*=60 m, σ=34), and in the chains analyzed in Hadriaca (*W*=374 m, σ=144; *D*=35 m, σ=18) and Olympus (*W*=366 m, σ=149 m; *D*=45 m, σ=36). The ratio between width and depth *AR* of the collapses is comparable to Earth only for Arsia North (2.8), while it is much higher for the other cases (11.2 and 6.9 for Arsia South-A and Arsia South-B, 10.8 in Hadriaca, 8.1 for Olympus). Most of the collapses show an important infilling of windborne deposits, that could be responsible for the high asymmetry ratio.

The two smaller and rounded skylights along Arsia South A and B appear to be filled with more aeolian sediment than the bigger depressions. Arsia South-A skylight is 58.8 meters deep on average and presents a maximum depth of 64.7 meters, whereas Arsia South-B is 49.6 meters deep on average with a maximum depth of 61.4 meters. Both present a slight infilling of unconsolidated aeolian material bulging towards the center, and some boulders resulted from the roof collapse with an average width of 10 m and protruding from the aeolian deposits for about 2 m of height.

Both the Arsia South and the Olympus cases show at the upstream termination of the chain one or two much deeper and wider depressions possibly representing the original tube-feeding vent (Fig. 2 I-N, Fig. 4). These show a depth of over 250 m in Arsia South-A (versus a *jameos* mean depth of 25 m) and, 210-230 m in Arsia South-B and Olympus (versus a *jameos* mean depth of 60 and 45 m, respectively). In Hadriaca the vent has not been identified, most probably because the initial part of the chain has been eroded by the nearby Dao Vallis. However, the area of Hadriaca is characterized by other three putative lava tube chains departing from a rounded caldera (Fig. 1 O).

6.3 Morphometry of lava tube collapse chains on the Moon

Collapse chains are less common on the Moon than on Mars, while continuous rills are dominant morphologies in several areas of the Maria (Hurwitz et al., 2013; McCall, 1970). Steep pits are usually isolated and in few cases associated to rill features (Robinson et al., 2012; Wagner and Robinson, 2014). Nonetheless, it was possible to identify and analyze three collapse chains that share very similar characteristics with the Martian and terrestrial ones (Fig. 1 P-R; Supplementary Figures 10-12). We informally called them Marius Hills A, Marius Hills B and Gruithuisen chains. As on Mars the percent of intact portions along the tube is around 40% of the chain (Table 5). All chains start with a deeper depression possibly representing the tube-feeding vent (respectively 320, 345, and 1240 m deep; Fig. 4). Aside of this initial depression they continue with a series of smaller collapses sharing comparable *W* and *D*, two or three times bigger than the Martian ones. More in detail, in Marius Hills A the collapses show an average *W*=574 m (σ=141), and *D*=87 (σ=33), very similar to Marius Hills B (*W*=527 m, σ=197; *D*=96, σ=30). These values are only slightly lower than those of Gruithuisen, which show an average *W*=858 m (σ=322) and an average *D*=190 m (σ=84). In general, the ratio between width and depth *AR* is similar or slightly smaller than on Mars, with a mean value of 6.6 for Marius Hills A, 5.5 for Marius Hills B and 4.5 for Gruithuisen. In the short chain of Marius Hills B it was also possible to identify a roundish skylight with much smaller dimension compared to the other collapses, and with debris material at the bottom (Fig. 1S).

6.4 Morphometric differences between tectonic pits and lava tube collapses

The data obtained from lava tube candidate collapse chains on Earth, Mars and the Moon can be compared to tectonic examples, as shown in Fig. 5. For Earth we compared the *jameos* of Corona and Kazumura with the tectonic pits measured in Iceland by Ferrill et al. (2011), while for Mars and the Moon we chose very typical graben-bounded chains. The profile distribution of collapses is much more regular and homogenous in the putative lava tube candidates compared to the tectonic ones (Fig. 4 and Supplementary Figures 13 and 9). Also, the tectonic chains present clearly more coalescent pits while the lava tube ones show a more regular depth and are often separated from each other (Fig. 4, Supplementary Figures 9 and 13). The initial larger and deeper depression (interpreted as potential lava

tube vent) is also typical of lava tube chains and not present on tectonic pit chains. In terms of morphometric statistics, tectonic pit chains present a stronger positive correlation between the width (*W*) and depth (*D*) of the collapse (Fig. 5 E-H). This is not the case of lava tube candidates, where this correlation is weaker or absent. These results show that morphometry can differentiate between different collapse genetic mechanisms. All the examples shown in this review from Mars and the Moon are within the morphometric constrains that exclude a potential tectonic origin, favoring the lava tube emplacement as the main process forming the subsurface voids creating the chain.

7. Discussion

The morphometric characteristics of a collapse chain are the expression of the main processes and parameters controlling the tube emplacement. These are the effusion rate, slope, rheology and driving forces like gravity or plug pressure (Sakimoto et al., 1997). Nonetheless, it is known from terrestrial examples that important morphological differences arise between channel overcrusting or shallow/deep inflation lava tubes (Dragoni et al., 1995; Kauahikaua et al., 1998; Kempe et al., 2010). Hence size estimations of Martian and lunar tubes remain mainly speculative if these different genetic processes are not taken into account.

Indeed, looking exclusively at morphologies, the lava tube collapse chains on Earth share several common characteristics with those proposed here as potential candidates on Mars and the Moon (Fig. 1), among them: a) most of the collapse chains here analyzed are sinuous and not related to tectonic lineaments; b) the minor axes *W* and depths *D* of the collapses are comparable along each chain, with *W* perpendicular to the tube development line; c) in most cases the deeper depression at the beginning of the chain could represent the feeding source of the tube; d) the presence of steeper overhanging and roundish skylights in the Martian chain in the Arsia examples and in Marius Hills B on the Moon indicates that between one collapse and the other there should be an intact portion of the lava tube. All these morphological and morphometric characteristics suggest that these collapse chains are genetically related and clearly different from pit chains formed along

tectonic dilational faults, grabens and dike swarms (e.g. Ferrill et al., 2004; Wyrick et al., 2004) (Fig. 4).

However, while morphologies and elevation profiles (Fig. 4) are strikingly similar, the morphometric range is mainly homogeneous in each planetary body, but significantly differs among Earth, Mars, and the Moon (Fig. 6). The minor axis *W* of the collapses shows a relevant increasing trend from Earth (maximum few tens of m), to Mars (from 40 to 400 m), and to the Moon (500-900 m) (Fig. 6A). The average linear volume of the collapses follows the same trend in all three planetary bodies, being up to 80 times bigger on Mars than on Earth, and with the greatest magnitude on the Moon, which presents collapses from 300 to 700 times bigger than on Earth (Fig. 6B; Table 4).

Aside from the dimensions, drastically increasing from Earth to Mars and to the Moon, also width/depth ratio *AR* varies considerably (Fig. 7B). This parameter provides information on the expected eccentricity of the conduit, which in turn is related to its genetic mechanisms. On Earth the variation in *AR* from Kazumura, Corona and Undara (respectively 1.4, 3.9 and 5 to 6; Table 4), are certainly related to different processes of tube emplacement (overcrusting versus inflation) and effusion rates (Kauahikaua et al., 1998; Kempe et al., 2010; Orr et al., 2015). The different volumetric factor *f* between collapses and intact tube linear volumes (V_1t) in the three examples is also an expression of the emplacement process. Surely there is a difference not only in effusion rates but also in the speleogenesis of the three terrestrial examples: Kazumura was formed through a combination of overcrusting of small channels and shallow inflation evolving in a master tube (Allred and Allred, 1997) entrenched by thermal erosion (emplacement driven by gravity flow), the formation of the other considered terrestrial tubes, Corona and Undara, is related to deeper and more persistent inflation processes (Tonello, 2017; Whitehead, 2010) (emplacement driven by pressure flow). In these two latter cases, the difference in dimensions between the still intact tube and the wider collapses is related to flow overpressure and lateral thermic erosion in specific sections of the tube forming wider areas that have collapsed as soon as the internal pressure decreased (Fig. 3). Undara represents an extreme example where tube pressure overflow filled lava lakes within the collapses, draining back inside the tube at the end of the eruption (Atkinson, 1991; Whitehead, 2010). Therefore, for analogy with the terrestrial cases, also on Mars and the

Moon *f* is expected to be close or minor to 1 in the case of channelized overcrusted tubes, and greater than 1 with the predominance of inflation processes.

Also on Mars the variability of width/depth ratio *AR* (Table 4) found in the different examples could be related to different lava tube genetic processes. Arsia North presents clear channel benches along its development and shows smaller dimensions and *AR* (2.8) compared to the other cases (Fig. 1G, 7B, Table 4), being comparable to the biggest terrestrial cases. The morphological characters point to an overcrusted origin of this tube, with smaller collapse chains with the same characteristics also in other areas of the northern flank of Arsia (Cushing 2012; for example the channels and associated collapses and skylights at -2.098/-122.150, -2.577°/-127.110, -0.467°/-123.606, Fig. 8). Small skylights along Arsia North could provide an easy access to the still intact segments of the tube (Fig. 1H).

On the other hand, the collapse chains along the lava flows of Arsia South, Olympus and Hadriaca do not show any surface expression aside of collapses and skylights (Fig. 1 I-M, Fig. 9), and have a range of *AR* (from 6 to 11) suggesting that the underlying lava tube might present a high degree of eccentricity in cross-section. Because of these characteristics this type of collapse chains are most probably related to a predominance of deep inflation controlled by the boundaries between pre-existing lava flows (Tonello, 2017). This hypothesis can be tested looking specifically at the collapse chain profile examined in Arsia South-A (Fig. 1I; Fig. 4). Here the depth of the original conduit is expected to follow the maximum depth of the collapses, which regularly decreases from the vent (70-50 m) to the distal part of the chain (30-20 m). This depth of emplacement is in agreement with lava flow thickness measured on the flanks of Arsia Mons (Mouginis-Mark and Rowland, 2008), suggesting that the lava tube is confined within lava flow boundaries. In addition, inflation is pressure-driven and therefore has the ability to inject the tube mainly along the existing most favorable inception horizons and not necessarily along the steepest slope, as can be observed in the lower part of Arsia South-B (Supplementary Figure 6). In Arsia these morphological characteristics seem to be repeated not only in Arsia South-A and Arsia South-B, but also in at least other two cases with starting vents and skylights to the southwest of the Arsia edifice (Fig. 9; at coordinates -14.876/-120.212, -14.949/-120.609). In addition the lava flows in this area present other 75 skylights,

Atypical Pit Craters, or cave entrance candidates registered in the MGC3 (Cushing, 2017). The average depth of the 37 skylights reported in MG3 that can be measured with the shadow method is 65 meters, supporting the hypothesis that a network of inflated tubes probably exists at these depths since this value represents the typical lava flow thickness on Arsia Mons (Mouginis-Mark and Rowland 2008). The morphologies of these collapse chains imply that on the southern apron of Arsia the emplacement of lava tubes was frequent and acting mainly in the subsurface through deep inflation.

Nonetheless, the high width/depth ratio *AR* of these Martian chains might be overestimated because of the partial infilling of the depressions with aeolian sediments (decreasing collapse depths), which appear to be ubiquitous from HiRISE images both in Arsia (Fig. 1L), Olympus and Hadriaca.

Looking to the skylights at Arsia North, most of these are occupied by aeolian sediment cones with heights of 10-20 meters in some places (Fig. 1H). Considering a similar thickness of the sediment infilling, the original *AR* is probably in the order of 1 or 2 instead of the observed 3, as happens in overcrusted terrestrial cases. Similarly, looking at the outcropping part of boulders from the collapsed roofs partially buried by aeolian sediments at the bottom of the two skylights in Arsia South-A and Arsia South-B (in average 10 m in diameter and protruding 2 m out of the sediments) it is possible to estimate the thickness of these deposits in the order of 5-10 meters. This value could be even higher for the more open collapses, suggesting that the original pre-infilling *AR* could be around 5-8 instead of 7-10, and thus more comparable to terrestrial deep inflated cases.

The collapse chain analyzed in Olympus presents similar characteristics to those in Arsia, but here the chain is splitting into two branches showing a braided pattern (Fig. 1N), which is typical of several terrestrial examples including some portions of Kazumura and Corona. On Hadriaca the chain also shares very similar characteristics (Fig. 1O) but the frequency of the collapses is much higher with a limited spacing between them. This means that most of the tube has collapsed and that erosion and weathering agents have partially obliterated its course, as described in general for the Hadriaca edifice (Williams et al., 2007).

As observed on inflated examples on Earth, intact tube dimension on Mars could be characterized by a scaling factor compared to the related collapses (Fig. 3). The volumetric scaling factor f is unknown for the Martian case but, considering by analogy f=1 for

overcrusted examples, we can estimate a linear tube volume of V_l $6*10^2$ for Arsia North (Fig. 7A), with conduit width *Wt* from 20 up to 70 m and heights *Ht* of the lava tube from 10 to 25 meters. If we apply a *f*=1 also for the other cases (Arsia South, Hadriaca and Olympus) we can estimate a linear tube volume range of V_l $6\text{-}21*10^3$ (Fig. 7A), with conduit width *Wt* from 100 up to 450 m (Fig. 6). Quite low heights of the lava tubes passages (*Ht*) are expected due to the high width/depth ratio *AR*, in the range of a few tens of meters. However, because inflation is prevailing, as in the inflation cases analyzed on Earth, an *f*>1 is a more realistic value, therefore these tubes could have linear volumes from three to six times smaller than the previous values.

These morphometric outcomes are in agreement with those found in sinuous ridges interpreted as shallow, only partially drained inflated tubes on Syria Planum (Zhao et al., 2017), showing typical width *W* of 300-500 m and low height of the inflated bulge of 10-20 m. This also confirms the typically high asymmetry ratio of the Martian lava tubes due to the predominant inflation process.

On the Moon the examined lava tube collapse chains are among the very few detected on lunar volcanic regions (Hurwitz et al., 2013). The collapse chains present the same morphological characteristics observed on Mars, but with volumes one order of magnitude greater (Table 3, Fig. 6 A-B-C). In addition, the width/depth ratios *AR* are lower than on Mars but still comparable to inflated examples on Earth (Fig. 7B). Lower *AR* are not surprising on the Moon because the higher effusion rates and the stronger thermal erosion (Williams et al., 2000; Wilson and Head III, 1983) facilitate the evolution of inflated tubes to entrenched conduits with lower eccentricity. Considering an *f*=1 it is possible to estimate a maximum linear lava tube volume V_lt of $4\text{-}14*10^4$ m^3, with tube width *Wt* ranging between 500 and 800 m and its height *Ht* of 80-190 m (Fig. 6-7). The *Ht* value is indeed confirmed by the Lunar Radar Sounder analysis of Kaguya in the Marius Hills region (Kaku et al., 2017), showing a comparable putative depth of the tube between 75 and 150 m. However, as explained in the case of Mars, also on the Moon *f* could have a slightly higher value if inflation processes are predominant, and the conduits could be from a half to one-third smaller than the above reported estimation.

All these lunar values for the collapses fit into the stability range as calculated by Blair et al. (2017) and Theinat et al. (2020) even considering roof thickness of few tens of meters and

conduits with an asymmetry ratio between 4 and 7. This could explain why collapse chains are not common on the Moon compared to Mars and we should expect the presence of several still intact conduits lying below the smooth Maria plains. Indeed collapse chains on the Moon are unlikely generated by gravitational instabilities and should require collapse triggers such as meteorite impacts (Martellato et al., 2013) or tectonic events. Indeed, all the lunar chains analyzed in this study are characterized by a non-gravity related collapse trigger candidate (Fig. 10): in Marius Hills A an important impact crater superposes and partially obliterates the chain (Figures 1Q, 10A), while in Marius Hills B and Gruithuisen a wrinkle ridge partially follows or crosses the collapse chains (Fig. 1P-R; see also Supplementary figures 10-11-12). It is hence possible that those chains formed during the tectonic activity of those structures. In addition an impact has also been proven as collapse trigger for the Marius Hills skylight studied by Robinson et al. (Fig. 10D)(Martellato et al., 2013; Robinson et al., 2012). Hence, our results suggest that below the main rilles of the Marius Hills plateau there could be intact tubes with dimensions comparable to those estimated for the collapse chains of Marius Hills A and B. Recent studies on the morphology and genesis of Rima Rilles have shown the high probability that this feature could also be related to the continuous collapse of a lava tube (Roberts and Tracy, 2019). Dimensions (*W* and *H*) are comparable to our results, in the hypothesis that the ceiling was not thick enough to remain stable after the draining. In this specific case, Sakimoto and Gregg (2019) modelled the thermal erosion and flow showing that in order to create such feature a closed ceiling tunnel is much more effective thermally than an open channel. All these data suggest that some deeper lunar rills could represent original tubes that collapsed right after the draining and other shallower ones, like in Marius Hills, could represent the still intact ceiling of intact tubes.

Considering together the percentage of intact tube segments along the chains and the linear volume estimations (Table 5), we can calculate that below the overcrusted example examined on Mars there could be almost $3*10^7$ cubic meters of intact voids. In inflated Martian cases this value rises to a maximum of $10*10^7$. The volume value increases even by one order of magnitude for the lunar cases, reaching up to $12*10^8$ cubic meters for the Gruithuisen case. If we consider the possible existence of lava tubes still intact all along their full development below the surface of the Moon and thus with length and V_1

comparable to the Gruithuisen case, accessible tunnel-like voids on Moon Maria might easily reach up to 8-10 billions of cubic meters opening new intriguing scenarios for future exploration and utilization.

8. Future space missions for lava tube detection and exploration

The comparative analysis and the morphological similarities presented in this review show a great potential for exploration of enormous intact lava tubes on the Moon and, on a less extent, Mars. However these outcomes are mainly based on comparison with terrestrial cases, while direct evidences are still limited. Aside of the radar signals reported by Kaku et al. (2017), and the gravity anomalies detected by GRAIL (Chappaz et al., 2017), we do not have yet a clear understanding on the lava tube extent and genetic processes underneath Moon Maria. The same applies for Mars, where the Shallow Radar (SHARAD on board MRO) sections have not yet proven the presence of subsurface lava tubes because of an inappropriate resolution and coverage (Perry et al., 2019; Bardabelias et al., 2020).

In the last two decades, several scientists have proposed mission scenarios to access candidate lava tube entrances to verify the presence of subsurface caves (Blamont, 2014). On the Moon most of the attention has been focused on the pits of Marius Hills and Mare Tranquillitatis (Wagner and Robinson, 2014), following scientific objectives driven mainly by the uniqueness of the outcrop exposure along the pit walls, rather than for their potential of accessing much bigger underground voids (Kerber et al., 2018). On Mars, a robotic mission to these features is still problematic, because of the time delay in operations, the required autonomy in navigation and problems related to landing in the high volcanic plateaus of the Tharsis volcanic region.

This review emphasizes the need of specific remote sensing and ground truth data to finally assess the existence of lava tubes and their genetic processes on the different planetary bodies. The morphometric data provided here could be the starting point for dedicated missions aiming to detect and measure dimensions - depth and width at the least - of intact sections of lava tubes on the Moon and Mars.

In this regard, several new specific satellite mission approaches have been recently proposed: ground penetrating radar from orbiters (Sood et al., 2016; Carrer et al., 2018)

small satellites arrays for multi-frequency radar sounding (Carrer et al 2019), and the very promising use of passive sounding through radio emissions from Sun and Jupiter (Romero-Wolf et al., 2020). Also the deployment of surface rover missions dedicated to subsurface analysis, with specific geophysical instruments, could provide definitive proofs of the existence of these voids and information on their subsurface development (Caroll et al., 2015). On the other hand, robotic missions devoted to the direct exploration of skylights could only confirm the existence of the tubular cavities, but probably their capability of accessing relevant parts of the cave would still be very limited. A roadmap for subsurface exploration of the Moon and Mars is strongly needed, and should involve ground penetrating remote sensing before carrying out robotic approaches below ground.

9. Conclusions

In conclusion, this review and the morphometric study show that terrestrial lava tube collapse chains present striking morphological similarities with those proposed here as candidates on Mars and the Moon. However, dimensions and morphometric parameters like width/depth ratio *AR* have peculiar ranges each pertaining a different planetary body. Volumes of collapses and related conduits show increasing orders of magnitude from Earth, to Mars and to the Moon (Fig. 7). The minor axis *W* of the collapses shows a relevant increasing trend from Earth (maximum 20-30 m), to Mars (from 40 to 400 m), and to the Moon (500-900 m) (Fig. 6). The average linear volume of the collapses follows the same trend in all three planetary bodies, being almost 80 times bigger on Mars than on Earth, and with the greatest magnitude on the Moon, which presents collapses from 300 to 700 times bigger than on Earth (Tab. 4). This increasing trend of lava tube size from Earth to Mars and the Moon can be correlated to the different gravity parameters of each planetary body. Lower gravity bodies present higher effusion rates and longer and thicker lava flows, favoring the emplacement of flood basalts where pressure flow prevails over gravity flow (Wilson and Head III). Also lower gravity allows the emplacement of wider conduits within the stability threshold also favoring the emplacement of lava tubes instead of open lava channels.

AR values suggest that both overcrusted and inflation cases are present on Mars, while on the Moon deep inflation is probably predominant but thermal erosion could have favored a lower eccentricity because of the higher effusion rates and longer duration of the eruptions (Wilson and Head III, 1983). The size estimation indicates that on the Moon, the typical volume $V_l t$ and *AR* of lava tubes with ceiling thickness of some tens of meters are not high enough to reach the roof instability threshold and cause collapse, as often happens on Earth and Mars. Indeed, on Mars intact portions of lava tubes surely exist, especially in overcrusted examples, but in most cases the biggest deep inflated tubes present more frequent collapses due to the higher width/depth ratio *AR* although aeolian dusts could have partially filled them.

Therefore, among the three planetary bodies, the Moon presents the highest potential for lava tube development and conservation. Most of its tubes are probably intact and stable along their full length exceeding a total volume of some billions of cubic meters each, but with few accessible entrances from the surface. These impressive volumetric values clearly show how future space missions devoted to the investigation of these voids could open a promising era of subsurface lunar and Martian exploration and a completely new perspective in planetary exploration.

Acknowledgments

We would like to thank Kevin Allred, Doug Medville, Peter Bannink and the Hawai'i Speleological Survey for providing the Kazumura Atlas for this study. Our gratitude goes to the Leica and VIGEA for the support provided in the realization of the TLS survey of the Corona lava tube, together with the survey operators Marta Lazzaroni, Umberto Del Vecchio, Norma Damiano, Ivana Guidone, , Farouk Kadded, Raphael Goudard and Marco Camorani. Our gratitude goes also to all ESA staff organizing and supporting the ESA PANGAEA-X program in whose framework part of the TLS survey has been performed. We would also like to thank Austin Jackson, Robbie Shone and Armstrong Osborne for providing photographs of different lava tubes on Earth. Thanks also to Samuel Payler for reviewing the text and to Prof. Jay Melosh and one other anonymous reviewer for the positive comments that allowed for further improvements of the final manuscript. Author contributions: FS contributed in concept, data elaboration, writing of the original draft, and

figure elaboration; RP contributed in concept, methodology, formal analysis, writing and figure elaboration; MM contributed with data interpretation and writing; PdB contributed with data acquisition and elaboration; TS contributed in the TLS surveys, methods, data and figures elaboration; JdW contributed with concept development and writing; Competing interests: Authors declare no competing interests; Data and materials availability: All data are available in the main text or in the Supplementary material.

References

Allred, K. and Allred, C., 1997. Development and morphology of Kazumura cave, Hawaii. Journal of Caves and Karst Studies, 59: 67-80.

Allred, K., Allred, C. and Richards, R., 1997. Kazumura Cave Atlas, Island of Hawai ʻi. Special Publication Hawai ʻi Speleological Survey, National Speleological Society, Huntsville, AL, 81.

Allred, K., Allred, C. and Richards, R., 2002. Kazumura Cave Atlas, Island of Hawai ʻi. Special Publication of the Hawaii Speleological Survey.

Ansan, V. and Mangold, N., 2013. 3D morphometry of valley networks on Mars from HRSC/MEX DEMs: Implications for climatic evolution through time. Journal of Geophysical Research: Planets, 118(9): 1873-1894.

Atkinson, A., 1991. The Undara lava tube system, North Queensland, Australia: Updated data and notes on mode of formation and possible lunar analogue, Proc. 6th Intern. Symp Volcanospeleol., Hilo, pp. 95-120.

Atkinson, A. and Atkinson, V., 1995. Undara Volcano and its lava tubes: a geological wonder of Australia in Undara Volcanic National Park, North Queensland. Vernon and Anne Atkinson.

Atkinson, A., Griffin, T. and Stephenson, P., 1975. A major lava tube system from Undara Volcano, North Queensland. Bulletin Volcanologique, 39(2): 266-293.

Bailen, M., Herkenhoff, K., Howington-Kraus, A. and Becker, K., 2015. Finding stereo pairs with the Pds planetary image locator tool (Pilot), Second Planetary Data Workshop.

Bardabelias, N.M., Holt, J.W. and Christoffersen, M.S., 2020. Potential Detection of martian Lava Tubes from Mars Global Cave Candidate Catalog Skylight Locations Using SHARAD. LPICo, 2197, p.1068.

Barker, M., Mazarico, E., Neumann, G., Zuber, M., Haruyama, J. and Smith, D., 2016. A new lunar digital elevation model from the Lunar Orbiter Laser Altimeter and SELENE Terrain Camera. Icarus, 273: 346-355.

Beyer, R., Alexandrov, O. and Moratto, Z., 2014. Aligning terrain model and laser altimeter point clouds with the Ames Stereo Pipeline, Lunar and Planetary Science Conference, pp. 2902.

Blair, D.M., Chappaz, L., Sood, R., Milbury, C., Bobet, A., Melosh, H.J., Howell, K.C. and Freed, A.M., 2017. The structural stability of lunar lava tubes. Icarus, 282: 47-55.

Blamont, J., 2014. A roadmap to cave dwelling on the Moon and Mars. Advances in Space Research, 54(10): 2140-2149.

Boston, P., Frederick, R., Welch, S., Werker, J., Meyer, T., Sprungman, B., Hildreth-Werker, V. and Thompson, S., 2004. Extraterrestrial subsurface technology test bed: Human use and scientific value of martian caves, AIP Conference Proceedings. American Institute of Physics, pp. 1007-1018.

Boston, P., Spilde, M., Northup, D., Melim, L., Soroka, D., Kleina, L., Lavoie, K., Hose, L., Mallory, L. and Dahm, C., 2001. Cave biosignature suites: microbes, minerals, and Mars. Astrobiology, 1(1): 25-55.

Bunnell, D., 2008. Caves of Fire: Inside America's Lava Tubes. National Speleological Society.

Burns, J.A., 2010. The four hundred years of planetary science since Galileo and Kepler. Nature, 466(7306): 575.

Calvari, S., Pinkerton, H., 1998. Formation of lava tubes and extensive flow field during the 1991-1993 eruption of Mount Etna. Journal of Geophysical Researches. 103: 27291-27301.

Calvari, S. and Pinkerton, H., 1999. Lava tube morphology on Etna and evidence for lava flow emplacement mechanisms. Journal of Volcanology and Geothermal Research, 90(3-4): 263-280.

Carr, M., Greeley, R., Blasius, K., Guest, J. and Murray, J., 1977. Some martian volcanic features as viewed from the Viking orbiters. Journal of Geophysical Research, 82(28): 3985-4015.

Carr, M.H., 1973. Volcanism on mars. Journal of Geophysical Research, 78(20): 4049-4062.

Carracedo, J., Singer, B., Jicha, B., Guillou, H., Badiola, E.R., Meco, J., Torrado, F.P., Gimeno, D., Socorro, S. and Láinez, A., 2003. La erupción y el tubo volcánico del Volcán Corona (Lanzarote, Islas Canarias). Estudios Geológicos, 59(5-6): 277-302.

Carrer, L., Gerekos, C. and Bruzzone, L., 2018. A multi-frequency radar sounder for lava tubes detection on the Moon: Design, performance assessment and simulations. Planetary and Space Science, 152, pp.1-17.

Carrer, L., Gerekos, C., Bovolo, F. and Bruzzone, L., 2019. Distributed Radar Sounder: A Novel Concept for Subsurface Investigations Using Sensors in Formation Flight. IEEE Transactions on Geoscience and Remote Sensing, *57*(12), pp.9791-9809.

Carroll, K.A., Hatch, D., Ghent, R., Stanley, S., Urbancic, N., Williamson, M.C., Garry, W.B. Talwani, M., 2015, March. Exploring Subsurface Lunar Voids Using Surface Gravimetry. In Lunar and Planetary Science Conference, Vol. 46, p. 1746.

Chahine, M.T., A'Hearn, M.F., Rahe, J., Solomon, P. and Nickle, N.L., 2010. Comparative Planetology with an Earth Perspective. Springer.

Chappaz, L., Sood, R., Melosh, H.J., Howell, K.C., Blair, D.M., Milbury, C. and Zuber, M.T., 2017. Evidence of large empty lava tubes on the Moon using GRAIL gravity. Geophysical Research Letters, 44(1): 105-112.

Cooper. K.M., Kauahikaua, J.P., 1992. Morphology of extinct lava tubes and the implications for tube evolution, Chain of Craters Road, Hawaii Volcanoes National Park, Hawaii. US Geol Surv Open-File Report 92-352, pp 1-44.

Cruikshank, D. and Wood, C., 1972. Lunar rilles and Hawaiian volcanic features: Possible analogues. The Moon, 3(4): 412-447.

Cushing, G.E., 2012. Candidate cave entrances on Mars. Journal of Cave and Karst Studies, 74(1): 33-47.

Cushing, G.E., 2017. Mars Global Cave Candidate Catalog (MGC3), Astrobiology Science Conference (LPI Contrib. No. 1965).

Cushing, G.E., Titus, T., Wynne, J. and Christensen, P., 2007. THEMIS observes possible cave skylights on Mars. Geophysical Research Letters, 34(17).

Cushing, G.E., Okubo, C.H. and Titus, T.N., 2015. Atypical pit craters on Mars: New insights from THEMIS, CTX, and HiRISE observations. Journal of Geophysical Research: Planets, 120(6):1023-1043.

De Toffoli, B., Pozzobon, R., Massironi, M., Mazzarini, F., Conway, S. and Cremonese, G., 2019. surface expressions of subsurface sediment Mobilization Rooted into a Gas Hydrate-Rich Cryosphere on Mars. Scientific reports, 9(1), pp.1-9.

Dragoni, M., Piombo, A. and Tallarico, A., 1995. A model for the formation of lava tubes by roofing over a channel. Journal of Geophysical Research: Solid Earth, 100(B5): 8435-8447.

Duncan, A.M., Guest, J.E., Stofan, E.R., Anderson, S.W., Pinkerton, H. and Calvari, S., 2004. Development of tumuli in the medial portion of the 1983 aa flow-field, Mount Etna, Sicily. Journal of Volcanology and Geothermal Research, 132: 173-187.

Fagents, S.A. and Greeley, R., 2001. Factors influencing lava-substrate heat transfer and implications for thermomechanical erosion. Bulletin of Volcanology, 62(8): 519-532.

Favre, G., 1993. Some observations of Hawaiian pit craters and relations with lava tubes, Proceedings of the 3rd International Symposium on Vulcanospeleology. International Speleological Foundation Seattle, Wash, pp. 37-41.

Ferrill, D.A., Wyrick, D.Y., Morris, A.P., Sims, D.W. and Franklin, N.M., 2004. Dilational fault slip and pit chain formation on Mars. GsA Today, 14(10): 4-12.

Ferrill, D.A., Wyrick, D.Y. and Smart, K.J., 2011. Coseismic, dilational-fault and extension-fracture related pit chain formation in Iceland: Analog for pit chains on Mars. Lithosphere, 3(2): 133-142.

Gaddis, L., Anderson, J., Becker, K., Becker, T., Cook, D., Edwards, K., Eliason, E., Hare, T., Kieffer, H. and Lee, E., 1997. An overview of the integrated software for imaging spectrometers (ISIS), Lunar and Planetary Science Conference, pp. 387.

Greeley, R., 1971a. Lava tubes and channels in the lunar Marius Hills. The Moon, 3(3): 289-314.

Greeley, R., 1971b. Observations of actively forming lava tubes and associated structures, Hawaii.

Greeley, R., Fagents, S.A., Harris, R.S., Kadel, S.D., Williams, D.A. and Guest, J.E., 1998. Erosion by flowing lava: Field evidence. Journal of Geophysical Research: Solid Earth, 103(B11): 27325-27345.

Halliday, W., 2004. Volcanic caves. Encyclopedia of Caves and Karst Science. Fitzroy Dearborn, New York, 760: 764.

Haruyama, J., Morota, T., Kobayashi, S., Sawai, S., Lucey, P.G., Shirao, M. and Nishino, M.N., 2012. Lunar holes and lava tubes as resources for lunar science and exploration, Moon. Springer, pp. 139-163.

Hon, K.E.N., Kauahikaua, J.I.M., Denlinger, R. and Mackay, K., 1994. Emplacement and inflation of pahoehoe sheet flows: Observations and measurements of active lava flows on Kilauea Volcano, Hawaii. Geological Society of America Bulletin, *106*(3): 351-370.

Hróarsson, B., & Jónsson, S. S., 1991. Lava Caves in the Hallmundarhraun Lava Flow, Western Iceland. In *Proceedings of the 6 th International Symposium on Vulcanospeleology*, pp. 85-88.

Hurwitz, D.M., Head, J.W. and Hiesinger, H., 2013. Lunar sinuous rilles: distribution, characteristics, and implications for their origin. Planetary and Space Science, 79: 1-38.

Jackson, J.A., 2005. Glossary of Geology, by JA Jackson. 2005 Approx. 900 p. 5th revised and enlarged ed. ISBN 3-540-27951-2. Berlin: Springer, 2005.: 5th.

Jorda-Bordehore, L., Toulkeridis, T., Romero-Crespo, P. L., Jordá-Bordehore, R., & García-Garizabal, I. (2016). Stability assessment of volcanic lava tubes in the Galápagos using engineering rock mass classifications and an empirical approach. *International Journal of Rock Mechanics and Mining Sciences*, *89*, 55-67.

Kaku, T., Haruyama, J., Miyake, W., Kumamoto, A., Ishiyama, K., Nishibori, T., Yamamoto, K., Crites, S.T., Michikami, T. and Yokota, Y., 2017. Detection of intact lava tubes at marius hills on the moon by selene (kaguya) lunar radar sounder. Geophysical Research Letters, 44(20).

Kauahikaua, J., Cashman, K.V., Mattox, T.N., Heliker, C.C., Hon, K.A., Mangan, M.T. and Thornber, C.R., 1998. Observations on basaltic lava streams in tubes from Kilauea Volcano, island of Hawai'i. Journal of Geophysical Research: Solid Earth, 103(B11): 27303-27323.

Kempe, S., 2012. Volcanic rock caves, Encyclopedia of Caves (Second Edition). Elsevier, pp. 865-873.

Kempe, S., 2019. Volcanic rock caves, Encyclopedia of Caves (Third edition). Academic Press, pp. 1118-1127.

Kempe, S., Bauer, I., Bosted, P., Coons, D. and Elhard, R., 2010. Inflationary versus crusted-over roofs of pyroducts (lava tunnels), Proceedings 14th International Symposium on Vulcanospeleology, pp. 93.

Kerber, L., Nesnas, I., Keszthelyi, L., Head, J., Denevi, B., Hayne, P., Mitchell, K., Ashley, J., Whitten, J. and Stickle, A., 2018. Moon diver: A discovery mission concept for understanding the history of the mare basalts through the exploration of a lunar mare pit, New Views of the Moon 2-Asia.

Leone, G., 2014. A network of lava tubes as the origin of Labyrinthus Noctis and Valles Marineris on Mars. Journal of Volcanology and Geothermal Research, 277: 1-8.

Léveillé, R.J. and Datta, S., 2010. Lava tubes and basaltic caves as astrobiological targets on Earth and Mars: a review. Planetary and Space Science, 58(4): 592-598.

Malin, M.C., Bell, J.F., Cantor, B.A., Caplinger, M.A., Calvin, W.M., Clancy, R.T., Edgett, K.S., Edwards, L., Haberle, R.M. and James, P.B., 2007. Context camera investigation on board the Mars Reconnaissance Orbiter. Journal of Geophysical Research: Planets, 112(E5).

Martellato, E., Foing, B. and Benkhoff, J., 2013. Numerical modelling of impact crater formation associated with isolated lunar skylight candidates on lava tubes. Planetary and Space Science, 86: 33-44.

McCall, G., 1970. Lunar rilles and a possible terrestrial analogue. Nature, 225(5234): 714-716.

Mège, D., Cook, A.C., Garel, E., Lagabrielle, Y. and Cormier, M.H., 2003. Volcanic rifting at martian grabens. Journal of Geophysical Research: Planets, 108(E5).

Michalski, J.R., Onstott, T.C., Mojzsis, S.J., Mustard, J., Chan, Q.H., Niles, P.B. and Johnson, S.S., 2018. The martian subsurface as a potential window into the origin of life. Nature Geoscience, *11*(1), pp.21-26.

Montoriol-Pous, J. and de Mier, J., 1974. Estudio vulcanoespeleológico de la Cueva del Viento (Icod de los Vinos, Isla de Tenerife, Canarias). Speleon, 21: 5-24.

Moratto, Z., Broxton, M., Beyer, R., Lundy, M. and Husmann, K., 2010. Ames Stereo Pipeline, NASA's open source automated stereogrammetry software, Lunar and Planetary Science Conference, pp. 2364.

Mouginis-Mark, P.J. and Rowland, S.K., 2008. Lava flows at Arsia Mons, Mars: Insights from a graben imaged by HiRISE. Icarus, 198(1): 27-36.

Oberbeck, V.R., 1969. On the origin of lunar sinuous rilles. Modern Geology, 1: 75.

Okubo, C.H. and Martel, S.J., 1998. Pit crater formation on Kilauea volcano, Hawaii. Journal of Volcanology and Geothermal Research, 86(1-4): 1-18.

Orr, T.R., Bleacher, J.E., Patrick, M.R. and Wooten, K.M., 2015. A sinuous tumulus over an active lava tube at Kīlauea Volcano: Evolution, analogs, and hazard forecasts. Journal of Volcanology and Geothermal Research, 291: 35-48.

Pedersen, G.B.M., Höskuldsson, A., Dürig, T., Thordarson, T., Jonsdottir, I., Riishuus, M.S., Óskarsson, B.V., Dumont, S., Magnússon, E., Gudmundsson, M.T. and Sigmundsson, F., 2017. Lava field evolution and emplacement dynamics of the 2014–2015 basaltic fissure eruption at Holuhraun, Iceland. Journal of Volcanology and Geothermal Research, *340*, pp.155-169.

Perry, M.R., Bain, Z.M., Crown, D.A., Scheidt, S.P. and Nunes, D.E., 2019. Detection and characterization of intact lava tubes on the western flank of Alba Mons in Mars Reconnaissance Orbiter Shallow Radar (SHARAD) Data. LPI Contributions, *2089*, p.6405.

Peterson, D.W., Swanson, D.A., 1974, Observed formation of lava tubes during 1970-71 at Kilauea Volcano, Hawaii. Studies in Speleology 2: 209-222

Peterson, D.W., Holcomb, R.T., Tilling, R.I. and Christiansen, R.L., 1994. Development of lava tubes in the light of observations at Mauna Ulu, Kilauea Volcano, Hawaii. Bulletin of Volcanology, 56(5): 343-360.

Plescia, J., 2004. Morphometric properties of martian volcanoes. Journal of Geophysical Research: Planets, 109(E3).

Pozzobon, R., Mazzarini, F., Massironi, M. and Marinangeli, L., 2015. Self-similar clustering distribution of structural features on Ascraeus Mons (Mars): implications for magma chamber depth. Geological Society, London, Special Publications, *401*(1), pp.203-218.

Pozzobon, R., Salvini, S., Mazzoli, C., Massironi, M. and Sauro, F., 2018. A DTM-based volume extraction approach: from micro-scale weathering forms to planetary lava tubes, EGU General Assembly 2018, Vienna, pp. EGU2018-8843.

Pozzobon, R., Mazzarini, F., Massironi, M., Rossi, A.P., Pondrelli, M., Cremonese, G. and Marinangeli, L., 2019. Fluids mobilization in Arabia Terra, Mars: Depth of pressurized reservoir from mounds self-similar clustering. *Icarus*, *321*, pp.938-959.

Pozzobon, R., Mazzoli, C., Salvini, S., Sauro, F., Massironi, M., Santagata, T., 2020. A DTM-based volume extraction approach: from micro-scale weathering forms to planetary lava tubes". 3D digital geological models: from terrestrial outcrops to planetary surfaces, AGU books, in press.

Roberts, C. E., Gregg T. K.P., 2019. Rima Marius, the Moon: Formation of lunar sinuous rilles by constructional and erosional processes. Icarus, 317: 682-688.

Robinson, M., Ashley, J., Boyd, A., Wagner, R., Speyerer, E., Hawke, B.R., Hiesinger, H. and Van Der Bogert, C., 2012. Confirmation of sublunarean voids and thin layering in mare deposits. Planetary and Space Science, 69(1): 18-27.

Robinson, M., Brylow, S., Tschimmel, M., Humm, D., Lawrence, S., Thomas, P., Denevi, B., Bowman-Cisneros, E., Zerr, J. and Ravine, M., 2010. Lunar reconnaissance orbiter camera (LROC) instrument overview. Space science reviews, 150(1-4): 81-124.

Rossi, M.J., 1997. Morphology of the 1984 open-channel lava flow at Krafla volcano, northern Iceland. Geomorphology, 20(1-2): 95-112.

Rubin, A.M., 1992. Dike - induced faulting and graben subsidence in volcanic rift zones. Journal of Geophysical Research: Solid Earth, 97(B2): 1839-1858.

Sakimoto, S.E., Crisp, J. and Baloga, S.M., 1997. Eruption constraints on tube - fed planetary lava flows. Journal of Geophysical Research: Planets, 102(E3): 6597-6613.

Sakimoto, S. E. H., Gregg, T. K. P., 2019, March. On the Formation of Lunar Sinuous Rilles: Insights from Multiphysics Modeling Techniques. Lunar and Planetary Science Conference (50).

Santagata, T., Sauro, F., Massironi, M., Pozzobon, R., Del Vecchio, U., Lazzaroni, M., Damiano, N., Tonello, M., Tomasi, I., Martínez-Frìas, J. and Mateo Medero, E., 2018. Subsurface laser scanning and photogrammetry in the Corona Lava Tube System, Lanzarote, Spain, EGU General Assembly 2018, pp. EGU2018-5290.

Sauro, F., Pozzobon, R., Santagata, T., Tomasi, I., Tonello, M., Martínez-Frías, J., Smets, L.M.J., Gómez, G.D.S. and Massironi, M., 2019. Volcanic Caves of Lanzarote: A Natural Laboratory for Understanding Volcano-Speleogenetic Processes and Planetary Caves, Lanzarote and Chinijo Islands Geopark: From Earth to Space. Springer, pp. 125-142.

Scott, E.D. and Wilson, L., 2002. Plinian eruptions and passive collapse events as mechanisms of formation for martian pit chain craters. Journal of Geophysical Research: Planets, 107(E4).

Shean, D.E., Alexandrov, O., Moratto, Z.M., Smith, B.E., Joughin, I.R., Porter, C. and Morin, P., 2016. An automated, open-source pipeline for mass production of digital elevation models (DEMs) from very-high-resolution commercial stereo satellite imagery. ISPRS Journal of Photogrammetry and Remote Sensing, 116: 101-117.

Smart, K.J., Wyrick, D.Y. and Ferrill, D.A., 2011. Discrete element modeling of martian pit crater formation in response to extensional fracturing and dilational normal faulting. Journal of Geophysical Research: Planets, 116(E4).

Sood, R., Melosh, H.J. and Howell, K., 2016. Lunar advanced radar orbiter for subsurface sounding (LAROSS): Lava tube exploration mission. In AAS/AIAA 26th Space Flight Mechanics Meeting.

Theinat, A.K., Modiriasari, A., Bobet, A., Melosh, H.J., Dyke, S.J., Ramirez, J., Maghareh, A. and Gomez, D., 2020. Lunar lava tubes: Morphology to structural stability. Icarus, 338: 113442.

Tonello, M., 2017. Origin and evolution of an inflated lava tube between the Mio-Pliocene volcanic complex of Famara and the Quaternary lava flows of La Corona in Lanzarote. , University of Padova, 111 pp.

Torson, J. and Becker, K., 1997. ISIS-A software architecture for processing planetary images, Lunar and Planetary Science Conference, pp. 1443.

Wagner, R. and Robinson, M., 2019. 3D Modeling of Lunar Pit Walls from Stereo Images, Lunar and Planetary Science Conference.

Wagner, R.V. and Robinson, M.S., 2014. Distribution, formation mechanisms, and significance of lunar pits. Icarus, 237: 52-60.

Watters, T.R., Robinson, M.S., Banks, M.E., Tran, T. and Denevi, B.W., 2012. Recent extensional tectonics on the Moon revealed by the Lunar Reconnaissance Orbiter Camera. Nature Geoscience, 5(3): 181.

Whitehead, P.W., 2010. The regional context of the McBride Basalt Province and the formation of the Undara Lava flows, tubes, rises and depressions. Organising Group, 14th International Symposium on Vulcanospeleology.

Wilkens, H., Iliffe, T.M., Oromí, P., Martínez, A., Tysall, T.N. and Koenemann, S., 2009. The Corona lava tube, Lanzarote: geology, habitat diversity and biogeography. Marine Biodiversity, 39(3): 155-167.

Williams, D.A., Fagents, S.A. and Greeley, R., 2000. A reassessment of the emplacement and erosional potential of turbulent, low - viscosity lavas on the Moon. Journal of Geophysical Research: Planets, 105(E8): 20189-20205.

Williams, D.A., Greeley, R., Zuschneid, W., Werner, S.C., Neukum, G., Crown, D.A., Gregg, T.K., Gwinner, K. and Raitala, J., 2007. Hadriaca Patera: insights into its volcanic history from Mars express high resolution stereo camera. Journal of Geophysical Research: Planets, 112(E10).

Williams, K., McKay, C.P., Toon, O. and Head, J.W., 2010. Do ice caves exist on Mars? Icarus, 209(2): 358-368.

Wilson, L., Hawke, B.R., Giguere, T.A. and Petrycki, E.R., 2011. An igneous origin for Rima Hyginus and Hyginus crater on the Moon. Icarus, 215(2): 584-595.

Wilson, L. and Head III, J.W., 1983. A comparison of volcanic eruption processes on Earth, Moon, Mars, Io and Venus. Nature, 302(5910): 663.

Wilson, L. and Head III, J.W., 2002. Tharsis - radial graben systems as the surface manifestation of plume - related dike intrusion complexes: Models and implications. Journal of Geophysical Research: Planets, 107(E8): 1-1-1-24.

Wood, J., 1996. The geomorphological characterisation of digital elevation models, University of Leicester, Leicester.

Wyrick, D., Ferrill, D.A., Morris, A.P., Colton, S.L. and Sims, D.W., 2004. Distribution, morphology, and origins of martian pit crater chains. Journal of Geophysical Research: Planets, 109(E6).

Zhao, J., Huang, J., Kraft, M.D., Xiao, L. and Jiang, Y., 2017. Ridge-like lava tube systems in southeast Tharsis, Mars. Geomorphology, 295: 831-839.

Figures

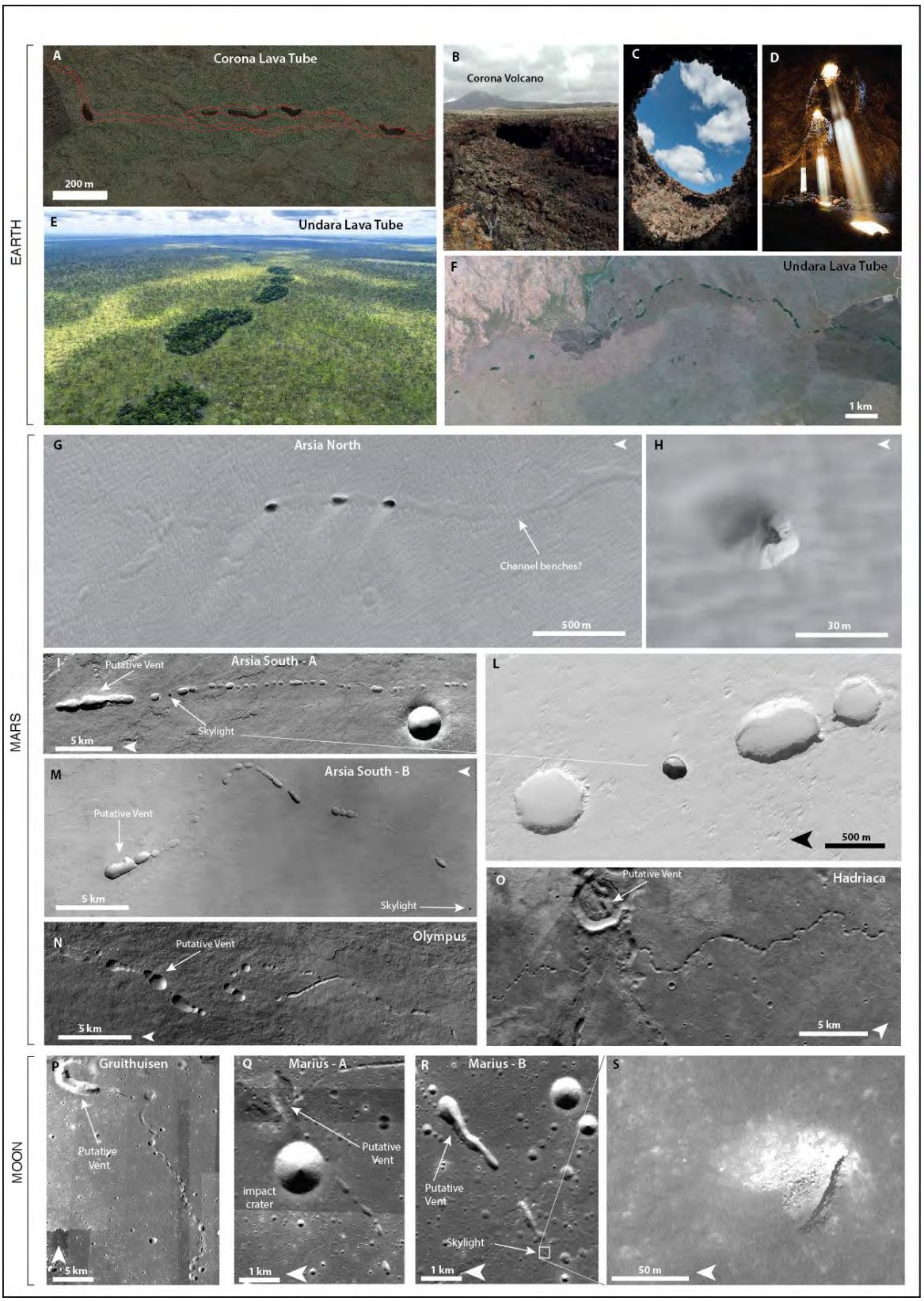
EARTH
MARS
MOON
A
Corona Lava Tube
200 m
B
Corona Volcano
C
D
E
Undara Lava Tube
F
Undara Lava Tube
1 km
G
Arsia North
Channel benches?
500 m
H
30 m
I
Putative Vent
Arsia South - A
Skylight
5 km
L
500 m
M
Arsia South - B
Putative Vent
5 km
Skylight
O
Putative Vent
Hadriaca
5 km
N
Putative Vent
Olympus
5 km
P
Gruithuisen
Putative Vent
5 km
Q
Marius - A
Putative Vent
impact crater
1 km
R
Marius - B
Putative Vent
Skylight
1 km
S
50 m

Fig. 1. Morphologies of lava tube collapse chains on Earth, Mars and the Moon. A) Satellite image of the collapse chains of the Corona lava tube showing the relationships between the subsurface tube development and collapses (red dotted lines represent the sidewalls of the tube surveyed with laser scanner). B) The *Jameo de la Puerta Falsa* (Corona lava tube) represents a typical elongated collapse with steep side slopes and overhanging walls at the two entrances to the intact lava tube. C) The *Jameo de La Gente* (Corona lava tube) shows vertical walls, steep slopes at the bottom and a less elongated shape in plan view. D) A series of three aligned skylights in the "Skylight Lava Tube" in Oregon (USA, photo A. Jackson): these holes in the ceiling of the conduit present a much smaller width compared to the intact tube. E-F) Collapse of the Undara Lava Tube are easily recognizable from air and satellite images because of the different vegetation. G-O) Examples of Martian lava tube candidate collapse chains in Arsia and Olympus Mons; H) A skylight showing a potential access to the tube along the Arsia North chain; L) A typical rounded skylight with overhanging walls along the collapse chain of Arsia-A; P-R) Examples of lunar lava tube candidate collapse chains in Gruithuisen and Marius Hills; S) A smaller collapse characterized by fallen boulders and vertical walls is a probable incipient skylight in the chain of Marius-B.

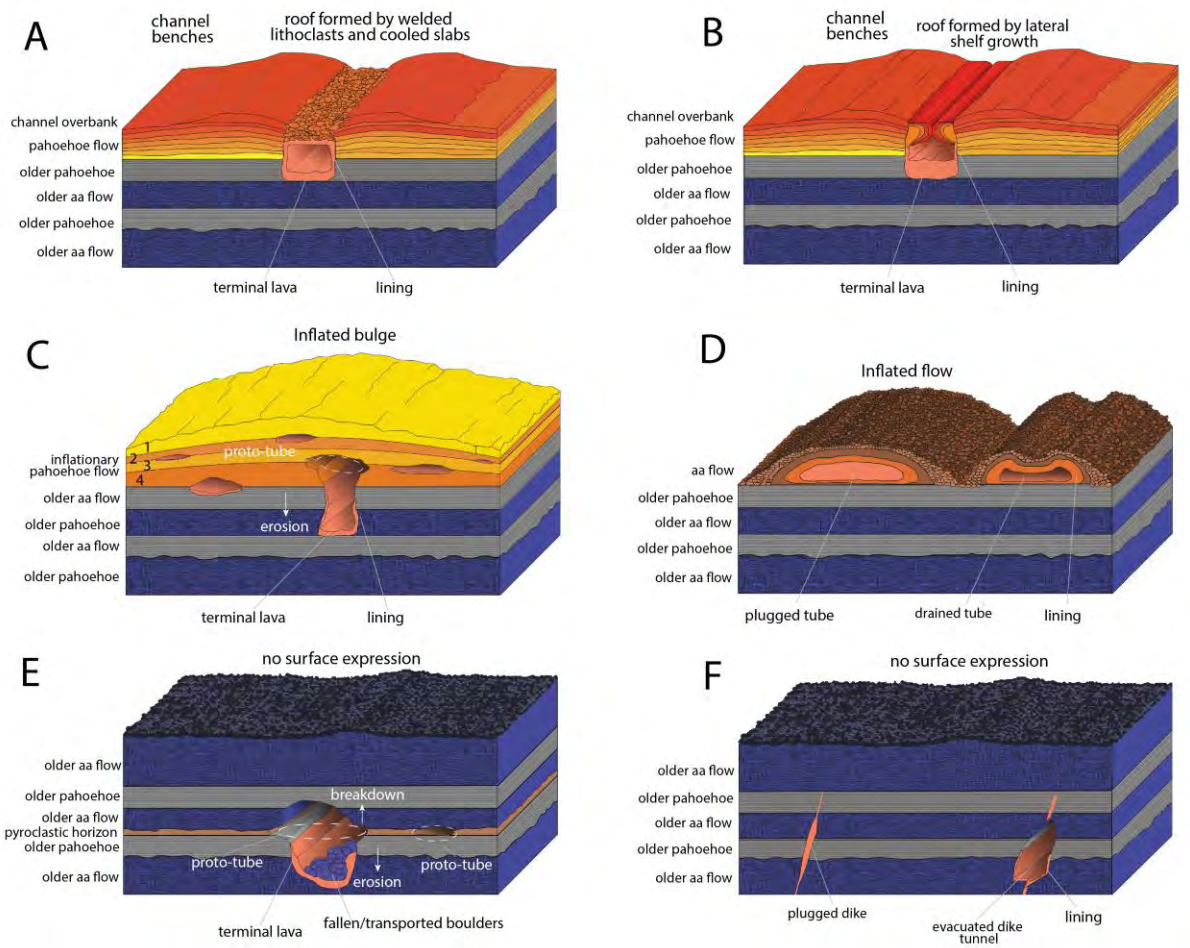

Fig. 2. Lava tube genetic processes (modified and integrated from Kempe et al., 2012): A) Lava tube formed by the crusting-over of channels by floating solidified slabs and lithoclasts welded together; B) Lava tube within a channel formed by lateral shelf accretion and consecutive closure; C) Lava tube formed by shallow inflation of pahoehoe sheets and later downward erosion; D) Lava tube formed by inflation and draining of aa flow nucleus; E) Lava tube formed by deep inflation along pre-existing lava flows boundaries or intra-flow pyroclastic deposits (inception horizons) enlarged by thermal erosion and breakdown; F) Tube formed through draining of a conduit formed by thermal erosion along a sealed fracture (eruptive fissure). .

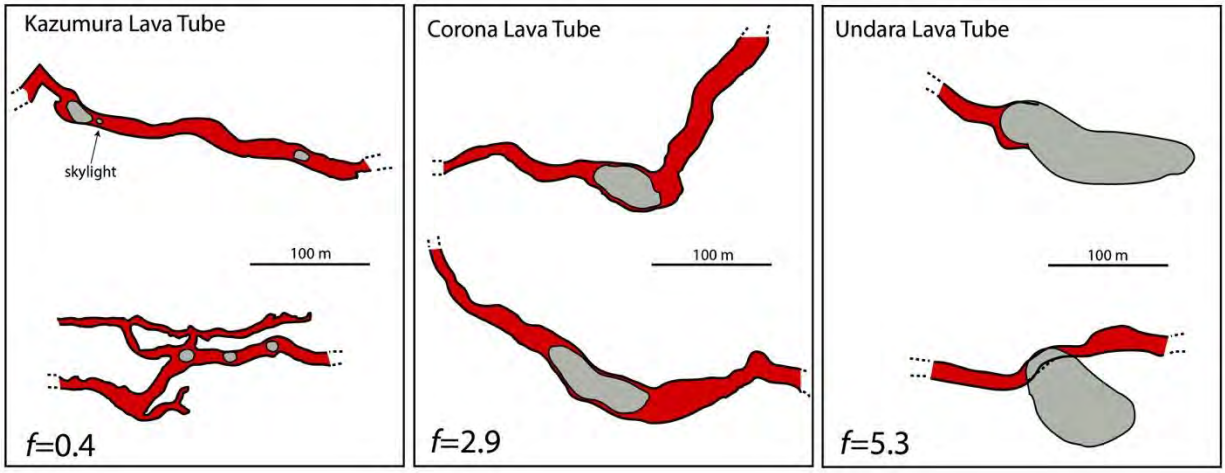

Fig. 3. Plan view maps of lava tubes showing different scaling factors *f* between collapses and intact tube segments. The two examples from Kazumura are from page 58a and 74 of the Kazumura Atlas. The Corona examples are derived from laser scanner mapping (above *Jameo de la Gente,* below *Jameo de la Puerta Falsa*). The Undara examples are from a modified figure in Atkinson et al. (1975).

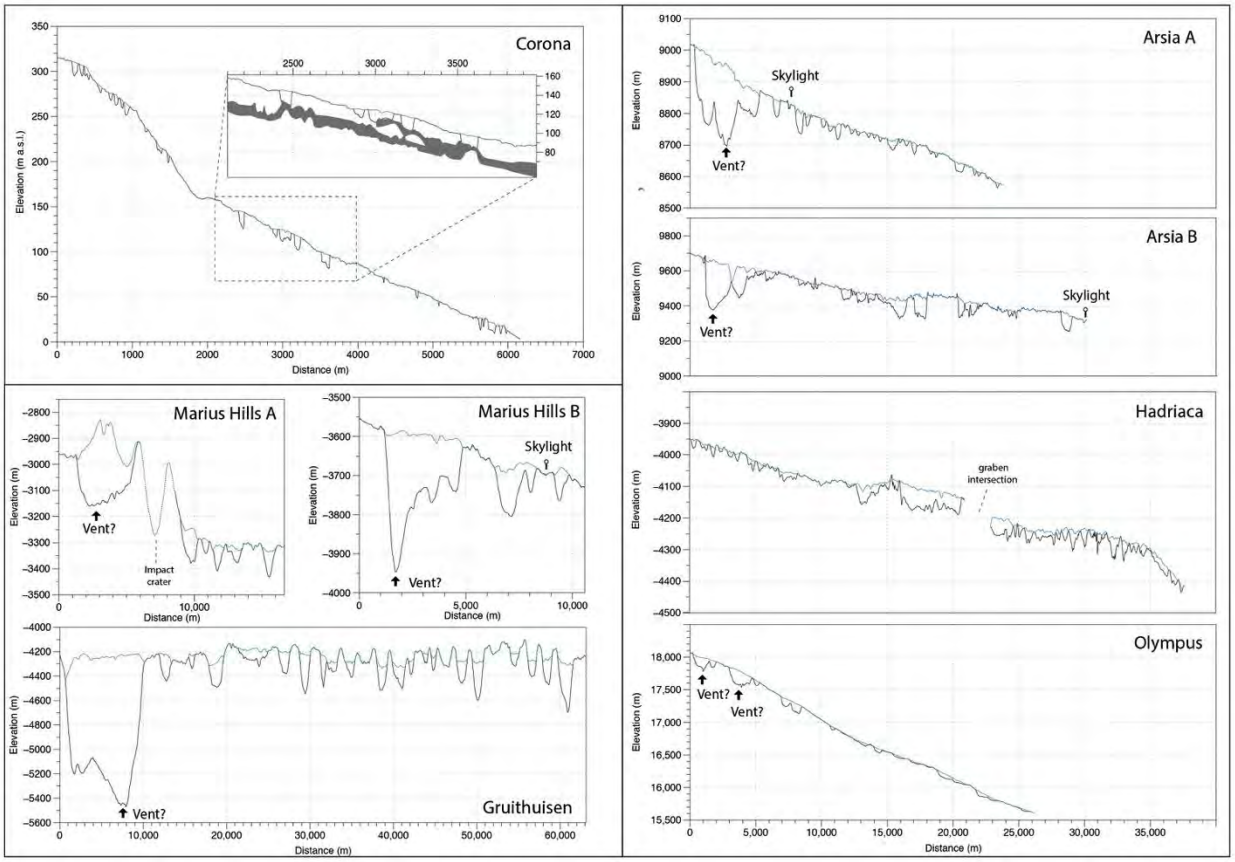

Fig. 4. Profiles of tube collapse pit chains (black lines) with superposed the extrapolated intact topography on Earth, Mars and the Moon. For the Corona terrestrial lava tube the inset shows the relationship between the collapses and the tube surveyed with laser scanner.

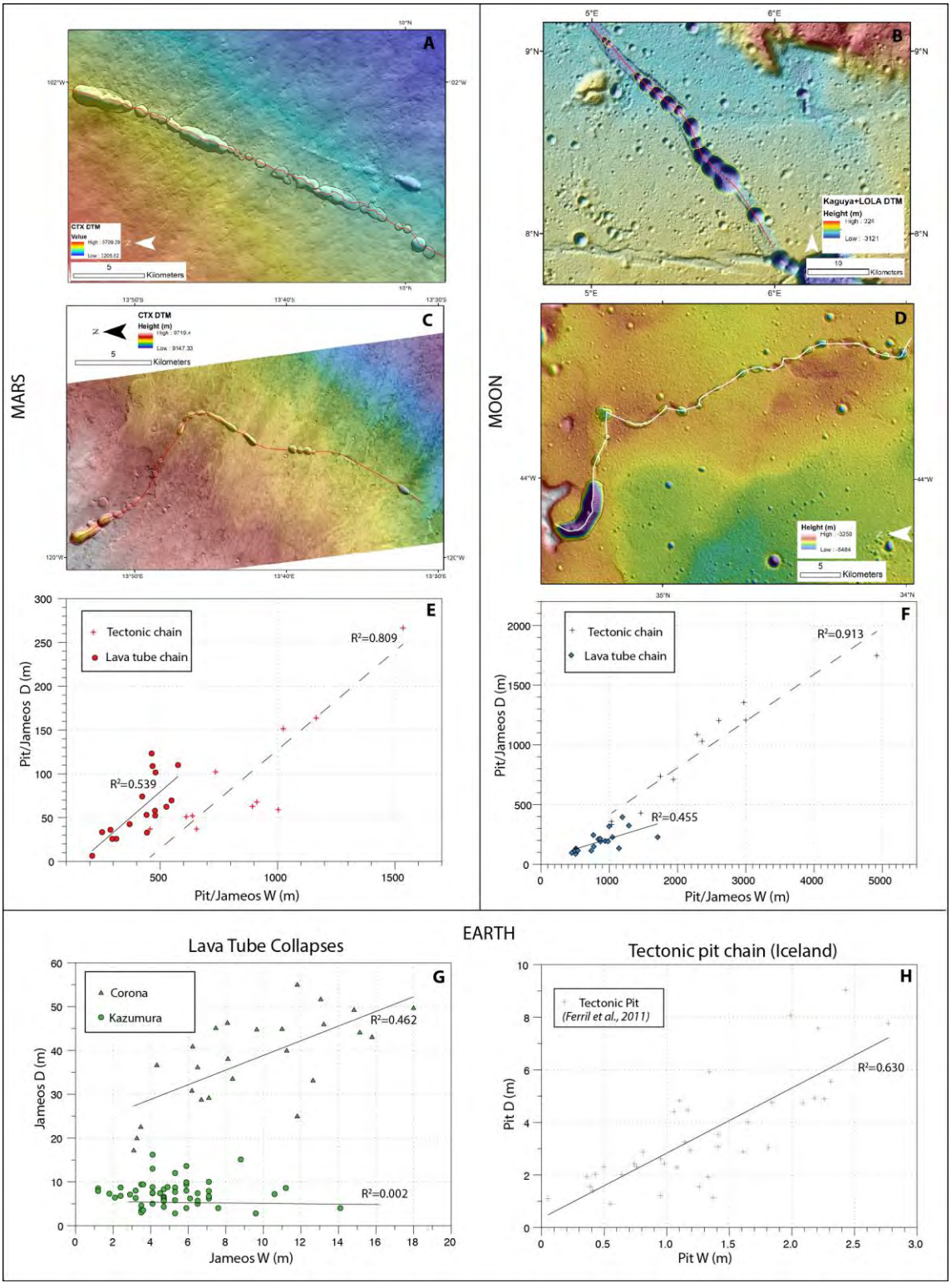

Fig. 5. Main morphological and morphometric characters of tectonic pit chains and lava tube collapse chains: Tectonic pit chains on Mars (A) and on the Moon (B) are characterized by coalescent pits and bounding grabens. Their development is rectilinear

and in the case of Mars (A) perpendicular to the steepest slope. Lava tube collapse chains on Mars (C) and on the Moon (D) are characterized by non-coalescent depressions and sinuous development. They often start with an initial deeper depression interpreted as the putative tube feeding vent. Width *W* and Depth *D* morphometric relationships of the three genetic cases, on Mars (E), the Moon (F), terrestrial lava tubes (G) and terrestrial tectonic pits in Iceland (H) from Ferril et al. (2011).

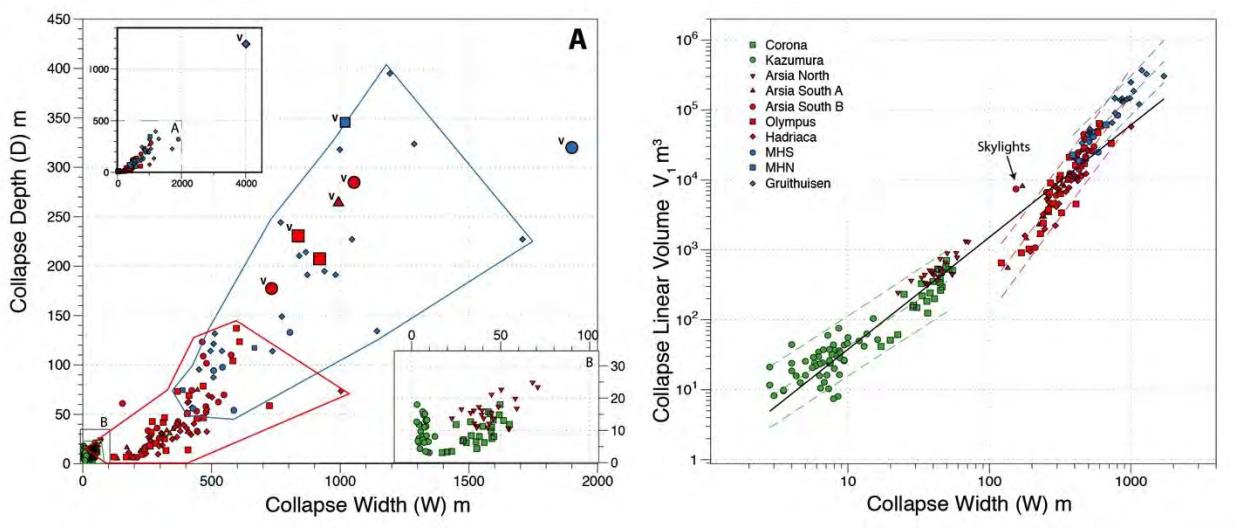

Fig. 6. Collapse chain morphometric parameter plots. A) The complete dataset showing the distribution of collapses width *W* and depth *D* (Earth in green, Mars in red, Moon in blue; legend for symbols is shown in D). Different line colors define the morphometric range for each planetary body. Bigger and deeper outliers are interpreted as putative vents (v in A) at the beginning of each chain (Gruithuisen vent shown in the upper left inset because of its exceptionally large size). The lower-right inset shows the partial overlap of terrestrial cases with putative overcrusted tubes in Arsia North on Mars. B) Collapse width *W* versus linear volume V_1 expressed in a logarithmic plot (putative vent outliers excluded); power laws trend lines for each planetary body and for the whole dataset (black line) are shown.

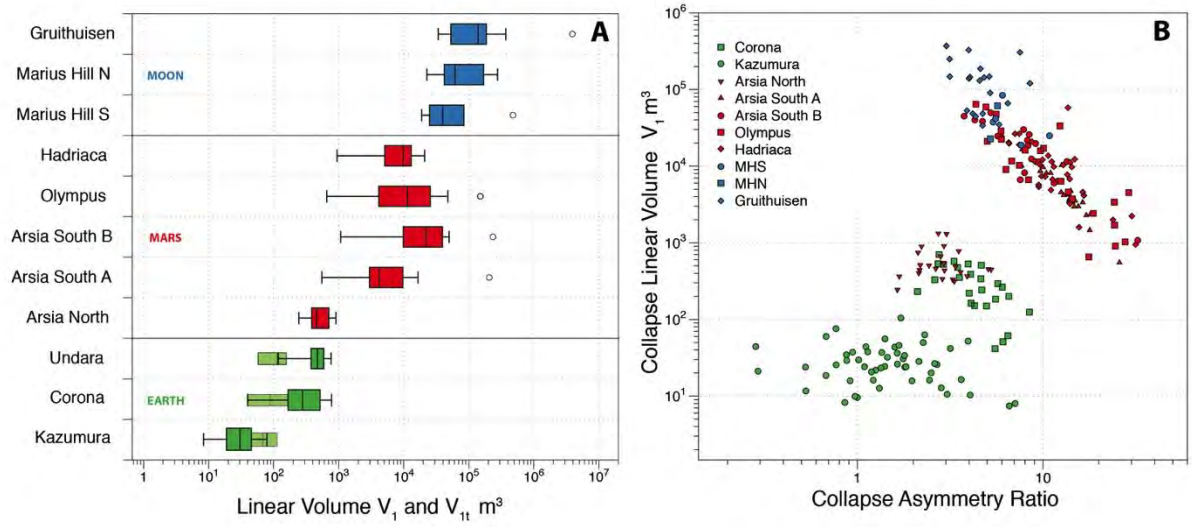

Fig. 7. A) Boxplot showing the quartiles, minimum and maximum distribution for V_1 of collapse chains analyzed in the three planetary bodies; outliers are the putative vents; for Earth the smaller and light green boxes show the quartile distribution of the intact tube V_1t in each chain (the data for Undara are derived from literature). B) Collapse asymmetry ratio versus V_1 in a logarithmic plot.

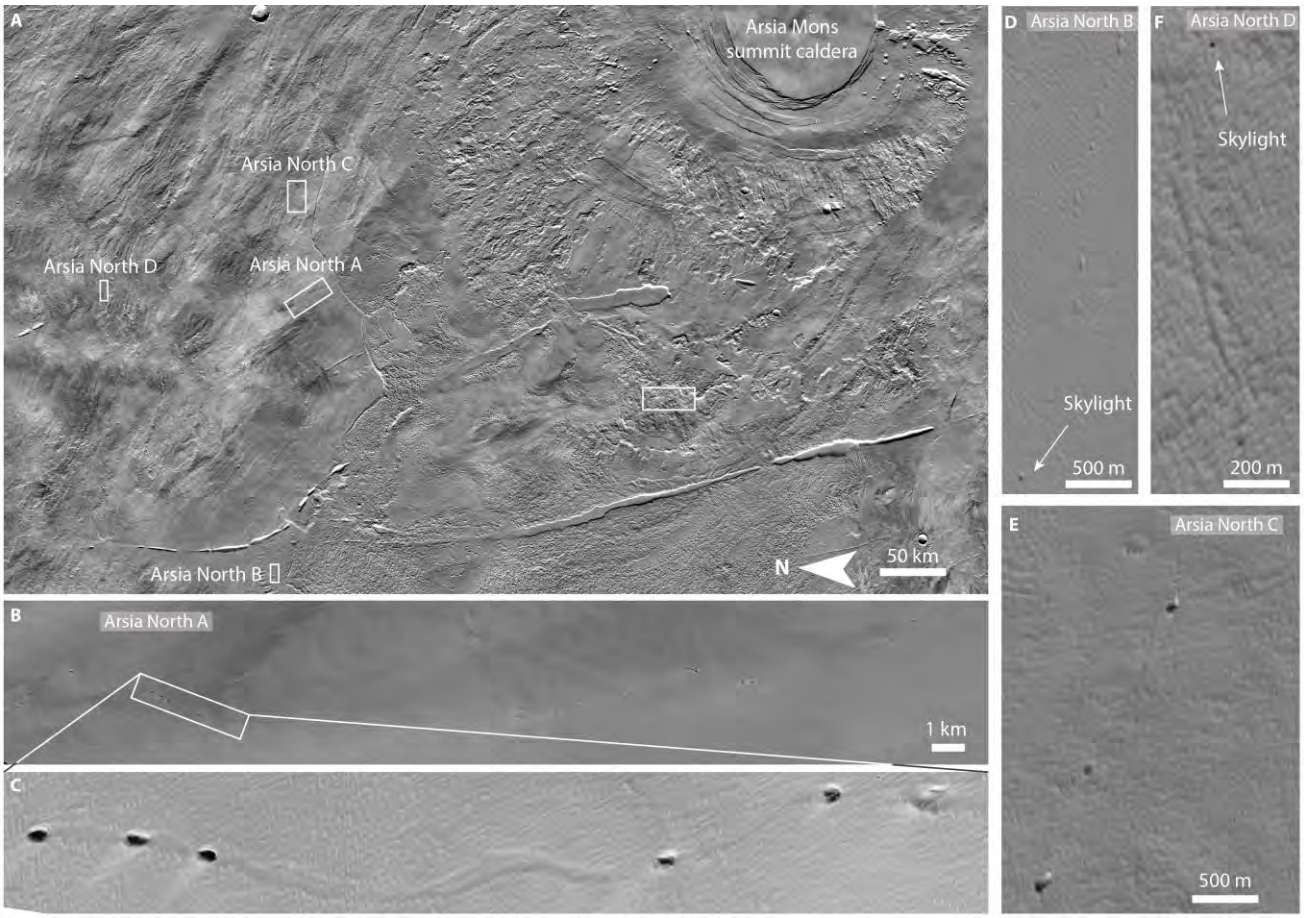

Fig. 8. Panel showing collapse chains with similar characteristics on the lava plains to the north of Arsia Mons (A). B-C) The collapse chain Arsia North measured in this study. D) A similar chain with skylights named Arsia North B. F) Two skylights with channel benches among them in the collapse chain named Arsia North D. E) A series of collapses connected by clear channel benches along Arsia North C.

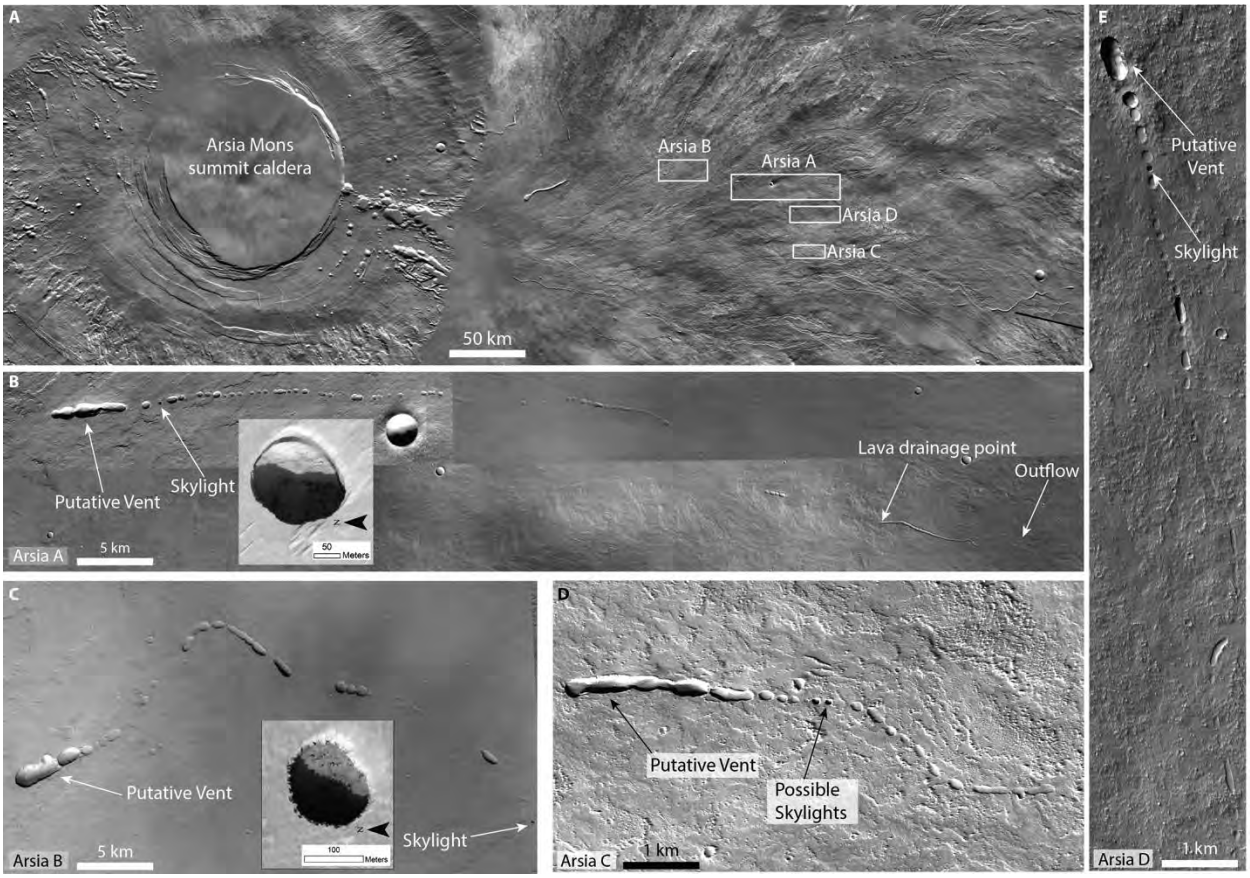

Fig. 9. Panel showing collapse chains with similar characteristics on the southern flank of Arsia Mons.

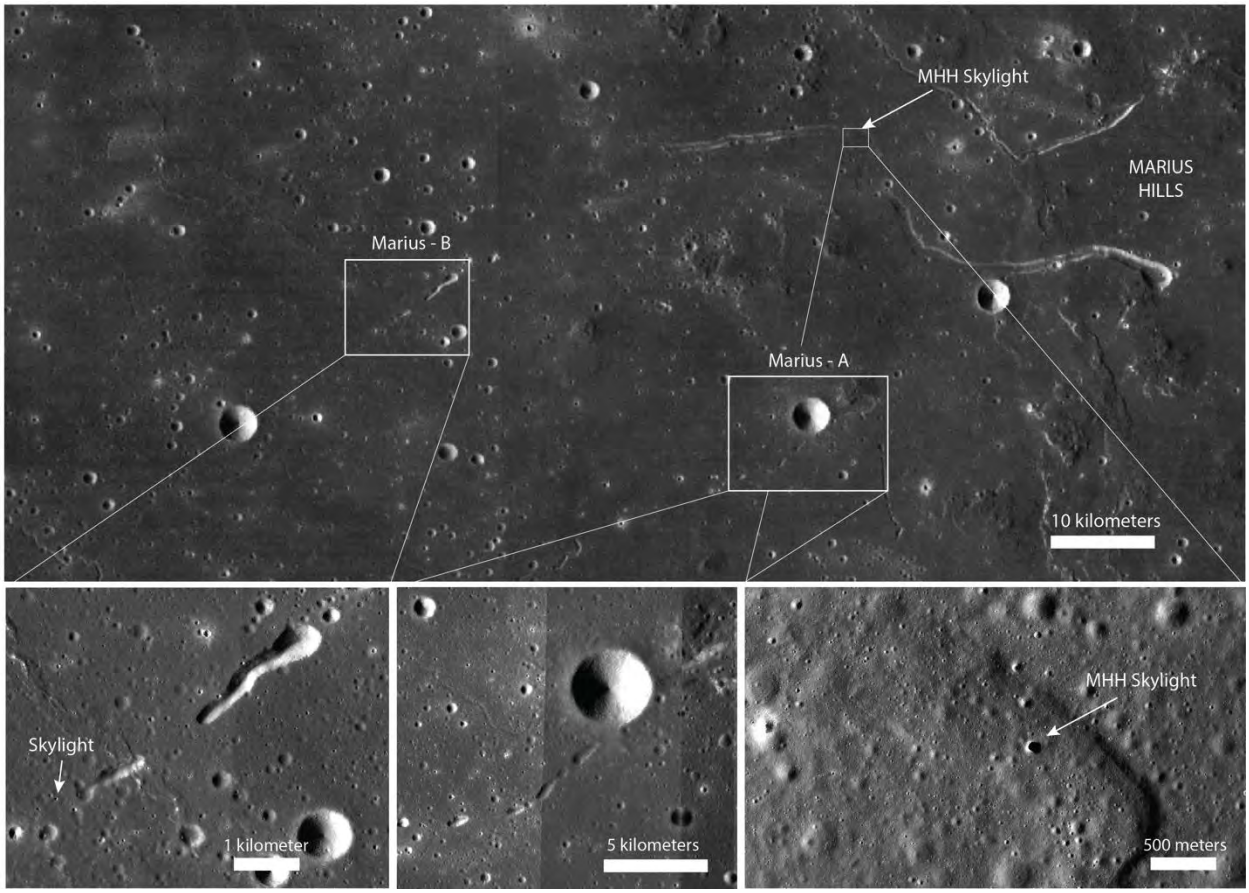

Fig. 10. Localization of collapse chains and skylights in the Marius Hills dome.

Chain morphological characters	Overcrusted	Shallow Inflated in pahoehoe	Shallow Inflated in aa	Deep inflated inception horizon	Deep inflated in Eruptive fissure	Tectonic
Rectilinear (R), curvilinear (C), Sinuous (S)	S	S	S, R along flow axes	S, rarely R	R, C	R, C
Braided	Rarely	Often	Rarely	Often	No	No
Collapse width (W) variability along the chain	Low	High	Low	Low	High	High
Coalescent pits	No	No	No	No	No	Yes
Following steepest slope line	Yes	Mostly but not always	Mostly but not always	Mostly but not always	Mostly but not always	No
Skylights	Common	Common	Common	Rare	Very rare	Rare
Initial vent on top of the chain	Yes	Yes, but not always	Also secondary vents	Yes	Yes, but not always	No
Within graben	No	No	No	No, or rarely	No	Yes
Within lava channels, sinuous rilles	Always	No, central part of the flow	No	Not always	No	No
Along one single lava flows	Always	Not always	Yes	Not always	No	No
Bulges or lateral benches between collapses	Often	Possible wide bulge/ridge, no benches,	Wide Bulge	No surface expression	No	No
Possible presence of other volcanic features	Lava falls, welded slabs and boulders in channel	Inflation clefts, tumuli and hornitos, degassing tracks	Inflation clefts, tumuli and hornitos, degassing tracks	Secondary vents	Deep pit craters like Wood Valley (Cushing et al. 2015)	No
Collapse asymmetry ratio	1 or <1	>1 (if not entrenched)	>1 (if not entrenched)	>1 (if not entrenched)	1 or <1	1

Table 1. Typical morphological characteristics of lava tube collapse chains (overcrusted/shallow inflated/deep inflated/eruptive fissures) compared to non-volcanic tectonic pit chains.

	Morphometric Parameters	Acronym	Source	Notes
Collapse (*jameos*/skylights) chain (Earth, Mars, Moon)	**Total Length**	*Ctl* (km)	Ortho-rectified and georeferenced satellite images	/
	Sinuosity Index	Si	*Sinuous AB path/Linear AB distance*	/
	V (Vertical Range)	*Vr* (m)	Total vertical topographic range from the highest to the lower collapse *height of A – height of B*	/
	Slope (steepness)	*CS* (°)	Average slope of the pit chain *Sin(CS)=Ctl/Vr*	/
Collapses (*jameos*/skylights) (Earth, Mars, Moon)	**Collapse Length**	*L* (m)	Major axis of the minimum bounding rectangle	/
	Collapse Width	*W* (m)	Minor axis of the minimum bounding rectangle	/
	Collapse Depth	*D* (m)	Maximum depth of the collapse	/
	Collapse Volume	*V* (m^3)	Surface difference *Synthetic Surface-DTM*	Calculated also from TLS for the Corona collapses
	Collapse Linear Volume	V_1 (m^3)	*The volume per 1 m thick cross section* $[(D*W)/2]*\pi$	
	Collapse Asymmetry Ratio	*AR*	*W/D*	Provide indications on the tube eccentricity
	Collapse Azimuth	*CA* (°)	Azimuth of the major axis of the minimum bounding rectangle	
Intact tube (Earth)	**Intact Tube Width**	*Wt* (m)	Width of the tube perpendicular to the tube development in a given cross section	In Corona and Kazumura *Wt* has been extracted from cross sections with 5 m spacing
	Intact Tube Height	*Ht* (m)	Maximum tube height in a given cross section	In Corona and Kazumura *Ht* has been extracted from cross sections with 5 m spacing
	Intact Tube linear volume	V_1t (m^3)	<u>For Corona</u> Direct measurement of the surface area of a given cross section of the 3D survey obtained with TLS <u>For Kazumura and Undara</u> $[(Ht*Wt)/2]*\pi$	
	Total tube length	*Ttl* (km)	Surveyed length of the whole intact tube sections	
	Tube collapse scaling factor	*f*	Average linear volume of the collapses divided per the average linear volume of the intact conduit V_1/V_1t	
Total conduit volumes (Earth, Mars, Moon)	**Total uncollapsed tube length**	*Tutl (m)*	The total length of the chain minus the total sum of collapses lengths *Ctl - Sum(L)*	Provide an estimation of the total length of intact sections
	Percent of uncollapsed sections along the chain	*Tutl (%)*	Same as above but in %	Provide an estimation of the percentage of intact sections
	Total volume of uncollapsed tube segments and total volume of the original tube	*TtV* (m^3) *TtoV* (m^3)	For Moon and Mars *Tutl* multiplied to the linear volume (of tube V_1t for the terrestrial cases, of collapse V_1 For the terrestrial cases, *Ttl* multiplied to the linear volume (of tube V_1t, of collapse V_1 for Moon and Mars)	Provide an estimate of the total volume of the intact tube sections without considering secondary infilling

Table 2. Morphometric parameters of collapse chains, individual collapses and intact tube sections provided in this study.

	Location	Coordinates	Data source and analysis method	Morphotype
Earth	Kazumura	19.412° -155.237°	Kazumura Atlas cave maps (Allred et al., 2002)	Overcrusted, entrenched, multilevel
	Corona	29.165° - 13.455°	Lidar DTMs (Spanish Geological Survey), Laser scans (Santagata et al., 2018)	Deep inflation along inception horizon, multilevel, partly braided
	Undara	-18.220° 144.628°	Cave maps (Atkinson, 1991; Atkinson and Atkinson, 1995)	Inflation and pressure overflow
Mars	Arsia North	-3.062° -123.930°	CTX, HiRiSe, shadow/height tool	Sinuous chain with continuous channel benches, collapses and skylights
	Arsia South-A	-14.377° -119.949°	CTX stereo-pairs DTM HiRiSe shadow/height tool (for skylights)	No surface expression aside of collapses, 1 skylight, deeper and wider depression at the beginning of the chain (vent?)
	Arsia South-B	-13.632° -119.869°	CTX stereo-pairs DTM HiRiSe shadow/height tool (for skylights)	Sinuous, no surface expression aside of collapses and 1 skylight, deeper and wider depression at the beginning of the chain (vent?)
	Olympus	19.456° -133.399°	CTX stereo-pairs DTM	Sinuous, braided, no surface expression aside of collapses and wider depression at the beginning of the chain (vent?)
	Hadriaca	-36.668° 89.394°	CTX stereo-pairs DTM	Sinuous, no surface expression aside of collapses, highly eroded
	Ascraeus Tectonic	10.123° -102.098°	CTX stereo-pairs DTM	Graben-bounded tectonic pit chain
Moon	Marius -A	13.096° -57.056°	LRO-NAC Kaguya/LRO LOLA DTMs	Sinuous, no surface expression aside of collapses, wider depression at the beginning of the chain (vent?)
	Marius-B	13.603° -58.047°	LRO-NAC Kaguya/LRO LOLA DTMs	No surface expression aside of collapses, 1 skylight, wider depression at the beginning of the chain (vent?)
	Gruithuisen	34.618° -43.467°	LRO-NAC Kaguya/LRO LOLA DTMs	Sinuous collapse chain, with some lava overflows and intersected by a wrinkle ridge, wider and much deeper depression at the beginning of the chain (vent?)
	Hyginus Rill Tectonic	8.384°, 5.630°	LRO-NAC Kaguya/LRO LOLA DTMs	Graben-bounded tectonic pit chain

Table 3. Lava tubes on Earth and candidate lava tube collapse chains on the Moon and Mars studied in this review for the morphometric analysis.

Collapse chain parameters

	Lava tube	N° Collapses	N° Skylight	Vent	Ctl (km)	Si	S	Vertical Range
Earth	Kazumura	53	29	Yes	32.1	1.3	1.9	1102
	Corona	25	2	Yes	6.5	1.1	2.91	240
	Undara*	>40	/	Yes	41	1.24	0,7-1,4	377
Mars	Arsia North	22	2	Yes	42	1.12	0.5	277
	Arsia South A	23	1	No	56	1.01	1.1	1094
	Arsia South B	17	1	Yes	30	1.23	0.9	315
	Olympus	25	0	Yes	29	1.1	5.2	2704
	Hadriaca	32	0	No	75.7	1.1	0.7	630
Moon	Marius Hill South	5	0	Yes	16.9	1	1.2	210
	Marius Hill North	2	1	Yes	8.5	1	0.01	60
	Gruithuisen	20	0	Yes	41	1.2	0.02	40

Collapses morphometry

	Lava tube	Av. L	σ L	Av. W	σ W	Av. D	σ D	Av. V	σ V	Av. V1	σ V1	Av. AR
Earth	Kazumura	13.9	7.3	7.4	2.9	5.2	2.5	/	/	29	18	1.4
	Corona	62.2	32.8	37.6	12.1	9.8	4.4	10263	9084	316	177	3.9
	Undara*	250	/	68	/	5-25	/	/	/	/	/	5-6
Mars	Arsia North	64	25	44.5	11.7	15.7	4,2	/	/	569	289	2.8
	Arsia South A	369.1	164.4	283.3	83.7	25.3	16.7	1410732	2181775	6740	6330	11.2
	Arsia South B	759.7	506.2	415.2	107.8	59.8	34	7324819	7079975	21514	14909	6.9
	Olympus	737.7	560.4	366.2	148.8	45	36.2	4549680	5714013	14970	17710	8.1
	Hadriaca	888.9	743.77	374.3	143.8	34.7	18.2	4648559	9511566	11700	10855	10.8
Moon	Marius Hill South	1070.3	374.5	573.9	141.5	87	32.9	16482675	13802402	41388	25543	6.6
	Marius Hill North	1358	802.6	527.4	197	95.8	30.2	21733653	22293270	42039	27341	5.5
	Gruithuisen	1333.7	629.4	858.5	322	189.9	83.54	81715413	78192450	141601	100929	4.5

Subsurface tube morphometry

	Lava tube	Ttl (km)	Av. Wt	σ Wt	Av. Ht	σ Ht	Av. V1t	σ V1t	*f*
Earth	Kazumura	41,8 (65,6)	10.5	4.7	8.11	3.44	69.21	37.4	0.4
	Corona	7.5	13.7	5.1	9.7	3.7	104	69	2.9
	Undara*	/	15-20	/	6.5	/	76-102	/	5.3

Tab. 4. Main morphometric parameters of collapse chains (for Earth, Mars and Moon) and of related intact tube sections (Earth). *Data for Undara are derived from existing literature and cave maps (Atkinson, 1991). Morphometric parameters acronyms are: *Ctl* – Chain total length; *Si* – Sinuosity index; *S* – Slope; *Vr* – Vertical range; *Av. L* – Average length of the collapses (major axis); σL - standard deviation of *L*; *Av. W* – Average width of the collapses (minor axis); σW - σ standard deviation of *W*; Av. D – Average depth of the collapses; σD -

standard deviation of D; Av. V – Average volume of the collapses; σV - standard deviation of *V*; *Av.Vl* – Average linear volume (along 1 meter thick cross section) of the collapses; σV_1 - standard deviation of V_1; *Av AR* – Average asymmetry Ratio; *Ttl* – Total tube length; *Av. Wt* – Average tube width; σWt - standard deviation of *Wt*; *Av. Ht* – Average height of the tube passages; σHt standard deviation of *Ht*; A*v. V_1t* – Average linear volume of the tube passages; $\sigma V_1 t$ - standard deviation of $V_1 t$; *f* - conversion factor collapse/tube.

Estimated total volumes

	Lava tube	Tutl (m)	Tutl (%)	TtV (m3) (*f*=1)	TtV (m3) (*f*=3)	TtoV (m3)
Earth	Kazumura	31281	97.44859813	2164645.2	/	2221320
	Corona	4538	73.71669916	471952	/	640224
	Undara*	29999	73.16829268	2699910	/	3690000
Mars	Arsia North	23359	94.04162808	13291271	4430423.667	14133391
	Arsia South A	9683	40.87551184	65263420	21754473.33	159663860
	Arsia South B	13615	45.12910604	292913110	97637703.33	649055866
	Olympus	20372	47.85304895	304968840	101656280	637302840
	Hadriaca	7193	20.18407835	84158100	28052700	416952900
Moon	Marius Hill A	6402	38.43659942	264965976	88321992	689358528
	Marius Hill B	4137	39.10947249	173915343	57971781	444688542
	Gruithuisen	27244	43.17591125	3857777644	1285925881	8935023100

Tab. 5. Estimation of total tube parameters: *Tutl* – total uncollapsed tube length; *TtV* – total uncollapsed tube volume (two scenarios: with *f*=1 and *f*=3); *TtoV* total original tube volume before collapses.

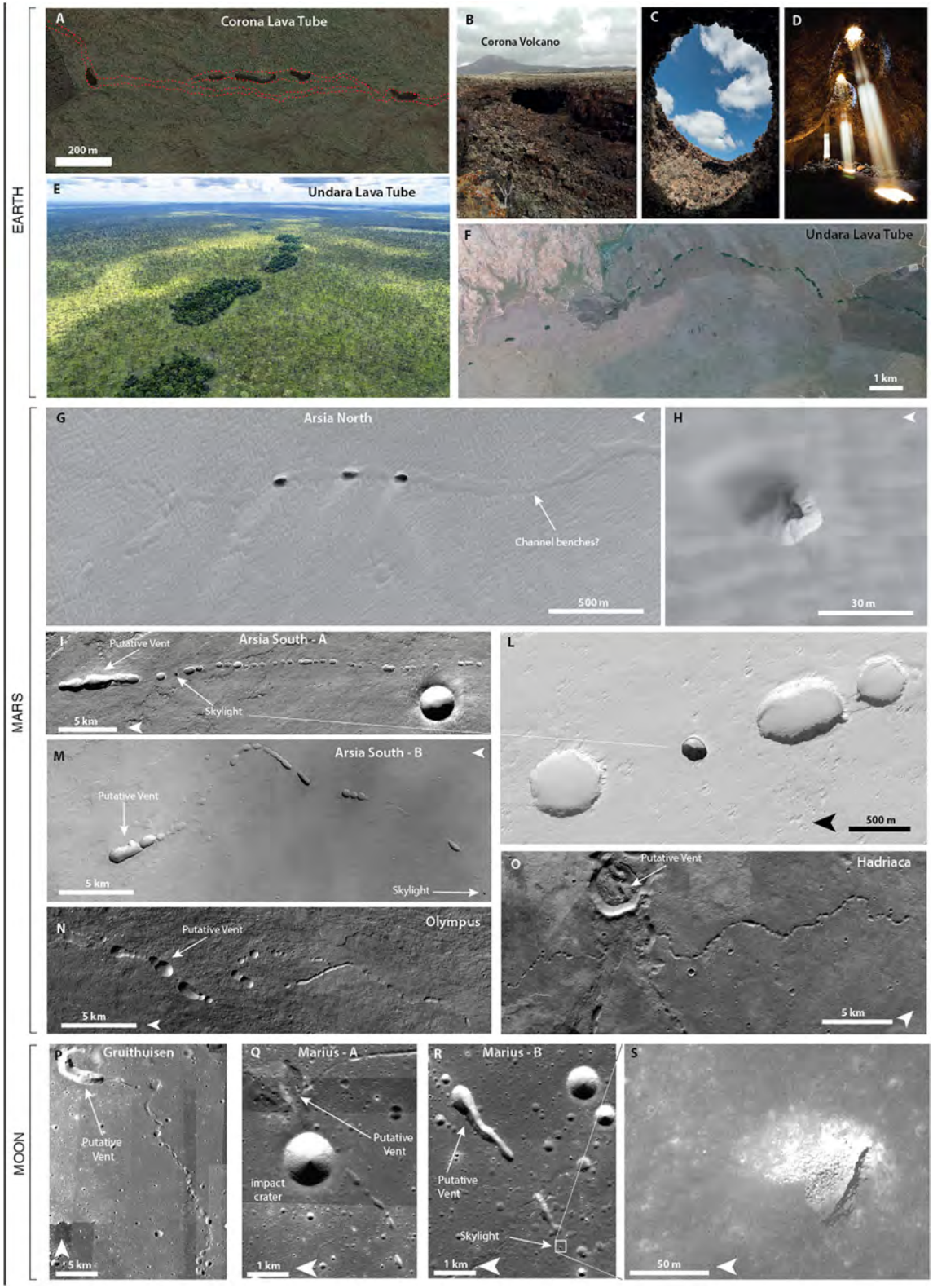
EARTH
A
Corona Lava Tube
200 m
B
Corona Volcano
C
D
E
Undara Lava Tube
F
Undara Lava Tube
1 km
MARS
G
Arsia North
Channel benches?
500 m
H
30 m
I
Putative Vent
Arsia South - A
Skylight
5 km
L
500 m
M
Arsia South - B
Putative Vent
5 km
Skylight
O
Putative Vent
Hadriaca
5 km
N
Putative Vent
Olympus
5 km
MOON
P
Gruithuisen
Putative Vent
5 km
Q
Marius - A
Putative Vent
impact crater
1 km
R
Marius - B
Putative Vent
Skylight
1 km
S
50 m

Figure 1

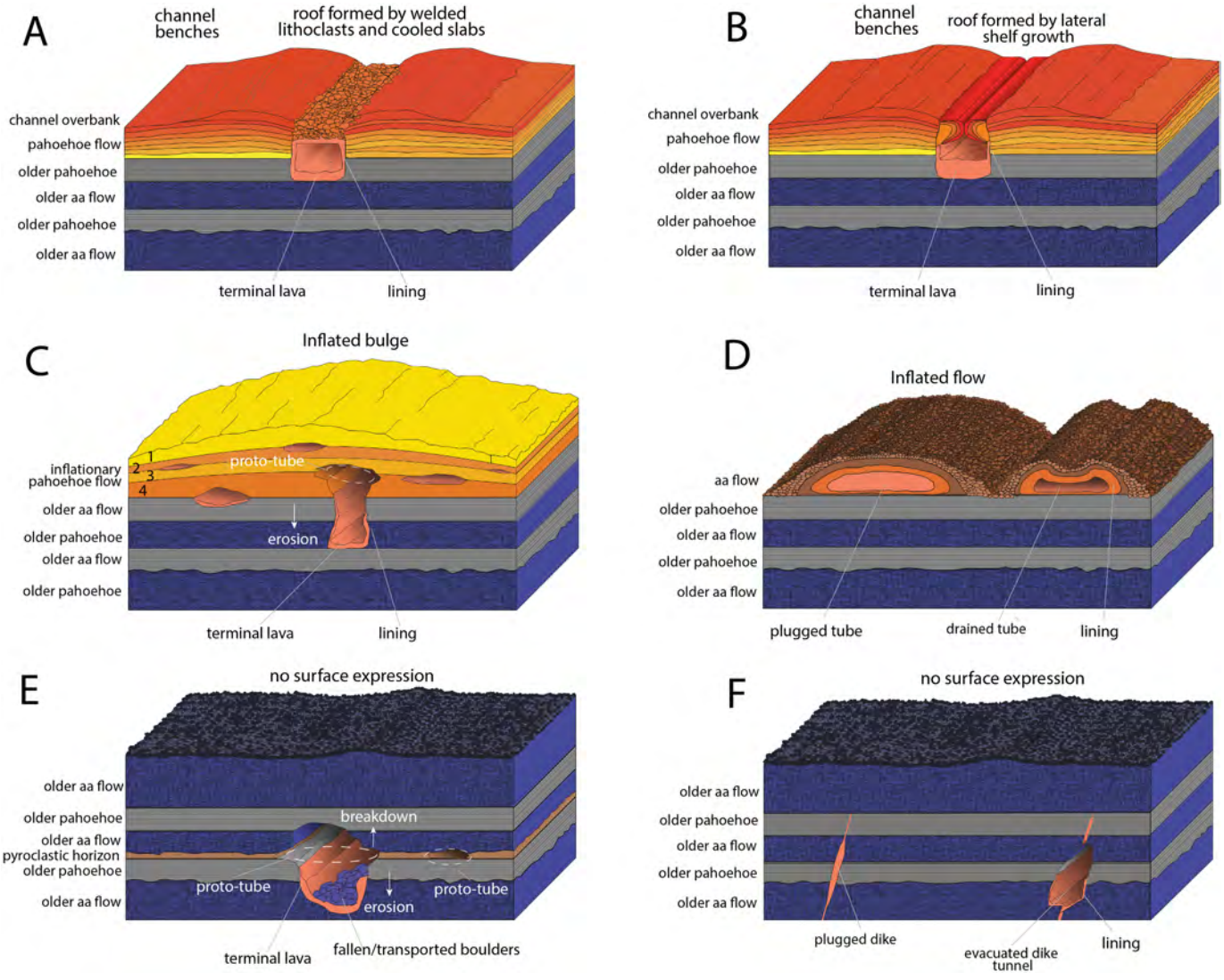
A
channel benches
roof formed by welded lithoclasts and cooled slabs
channel overbank
pahoehoe flow
older pahoehoe
older aa flow
older pahoehoe
older aa flow
terminal lava
lining
B
channel benches
roof formed by lateral shelf growth
channel overbank
pahoehoe flow
older pahoehoe
older aa flow
older pahoehoe
older aa flow
terminal lava
lining
C
Inflated bulge
inflationary pahoehoe flow
1
2
3
4
proto-tube
older aa flow
older pahoehoe
older aa flow
older pahoehoe
erosion
terminal lava
lining
D
Inflated flow
aa flow
older pahoehoe
older aa flow
older pahoehoe
older aa flow
plugged tube
drained tube
lining
E
no surface expression
older aa flow
older pahoehoe
older aa flow
pyroclastic horizon
older pahoehoe
older aa flow
breakdown
proto-tube
proto-tube
erosion
terminal lava
fallen/transported boulders
F
no surface expression
older aa flow
older pahoehoe
older aa flow
older pahoehoe
older aa flow
plugged dike
evacuated dike tunnel
lining

Figure 2

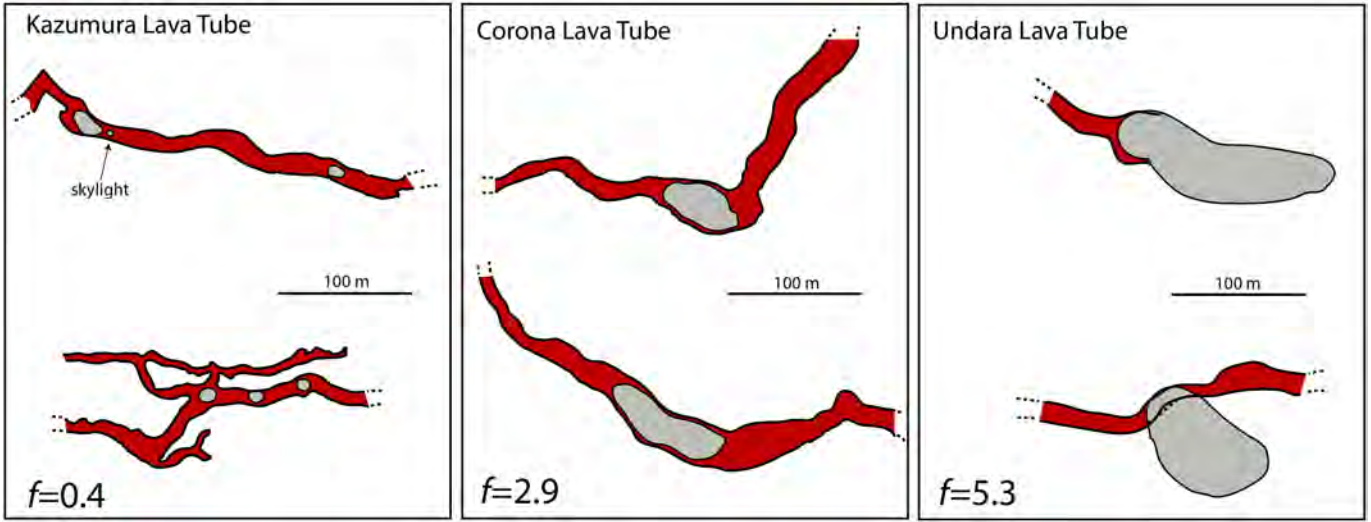
Kazumura Lava Tube
skylight
100 m
f=0.4
Corona Lava Tube
100 m
f=2.9
Undara Lava Tube
100 m
f=5.3

Figure 3

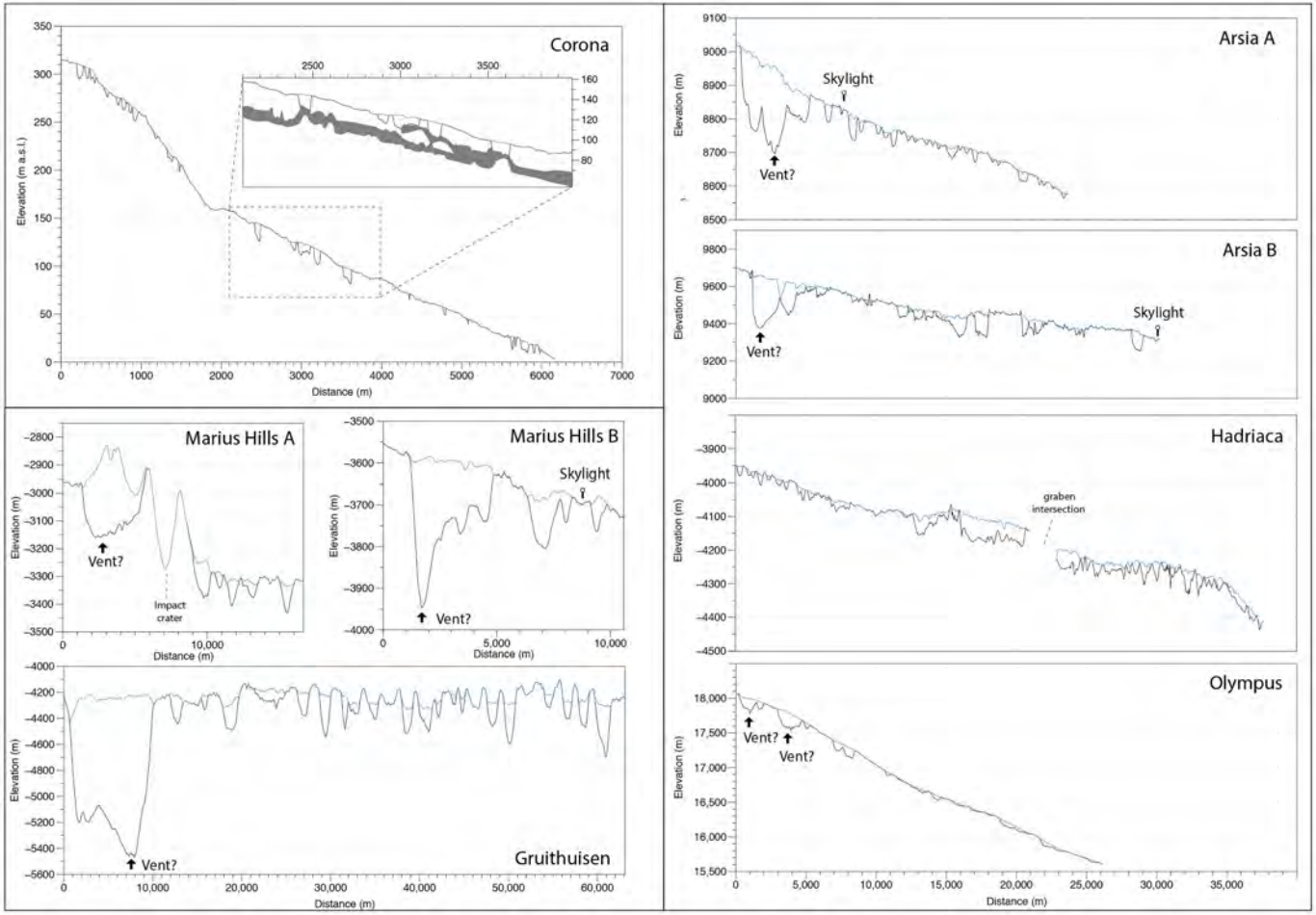
Corona
Elevation (m a.s.l.)
Distance (m)
Marius Hills A
Vent?
Impact crater
Marius Hills B
Skylight
Vent?
Gruithuisen
Vent?
Arsia A
Skylight
Vent?
Arsia B
Skylight
Vent?
Hadriaca
graben intersection
Olympus
Vent?
Vent?

Figure 4

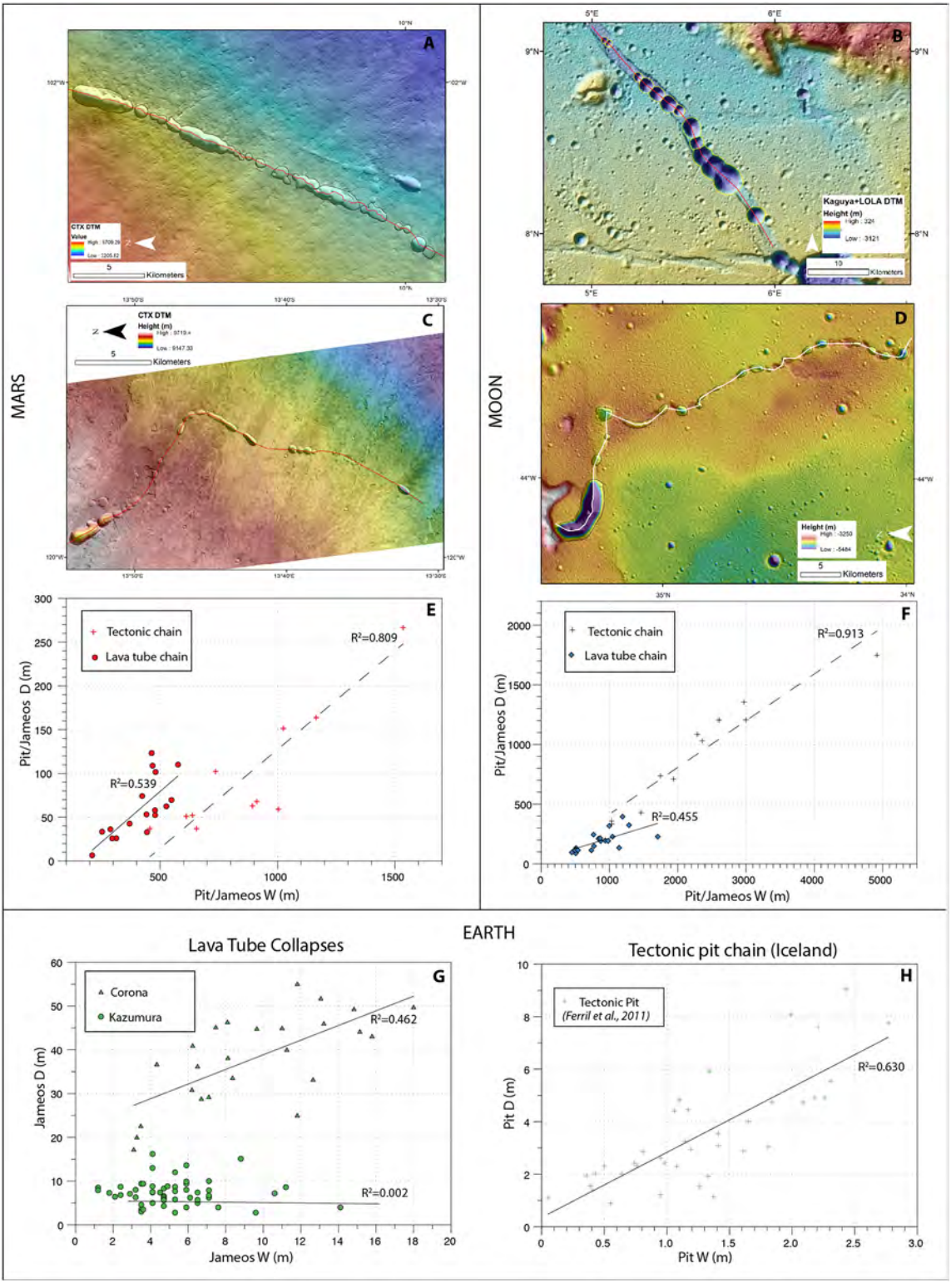
MARS
MOON
EARTH
A
B
C
D
E
F
G
H
CTX DTM
Kaguya+LOLA DTM
Kilometers
Tectonic chain
Lava tube chain
R²=0.809
R²=0.539
R²=0.913
R²=0.455
Pit/Jameos D (m)
Pit/Jameos W (m)
Lava Tube Collapses
Corona
Kazumura
R²=0.462
R²=0.002
Jameos D (m)
Jameos W (m)
Tectonic pit chain (Iceland)
Tectonic Pit
(Ferril et al., 2011)
R²=0.630
Pit D (m)
Pit W (m)

Figure 5

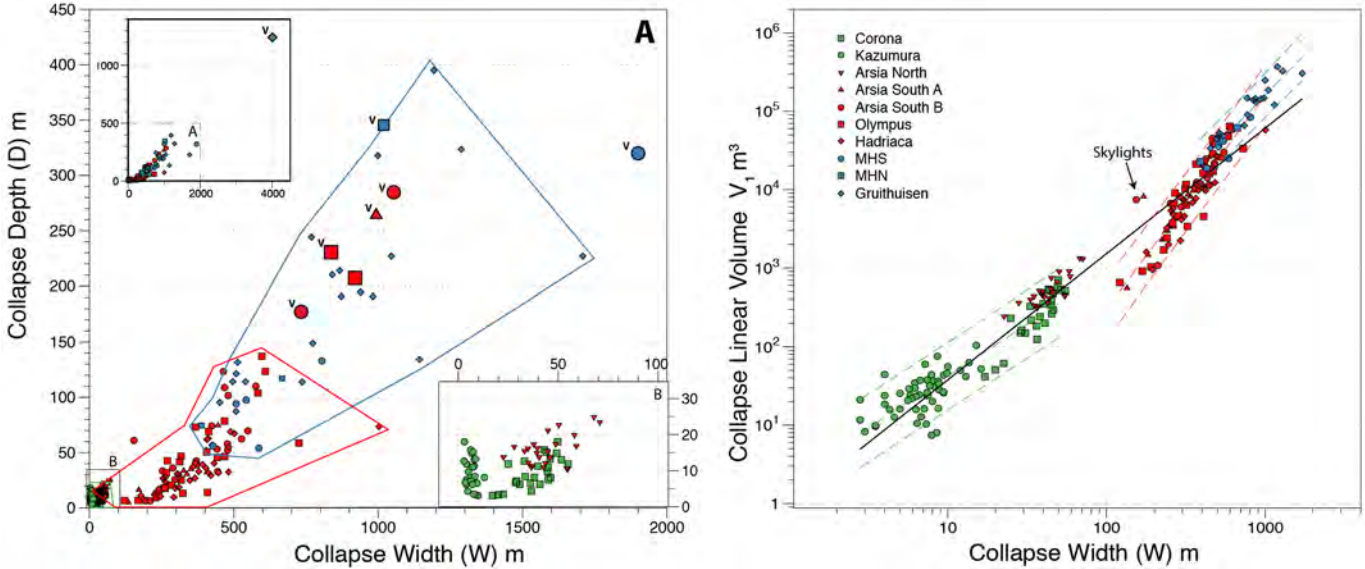
A
B
Collapse Depth (D) m
Collapse Width (W) m
Collapse Linear Volume V_1 m^3
Skylights
Corona
Kazumura
Arsia North
Arsia South A
Arsia South B
Olympus
Hadriaca
MHS
MHN
Gruithuisen

Figure 6

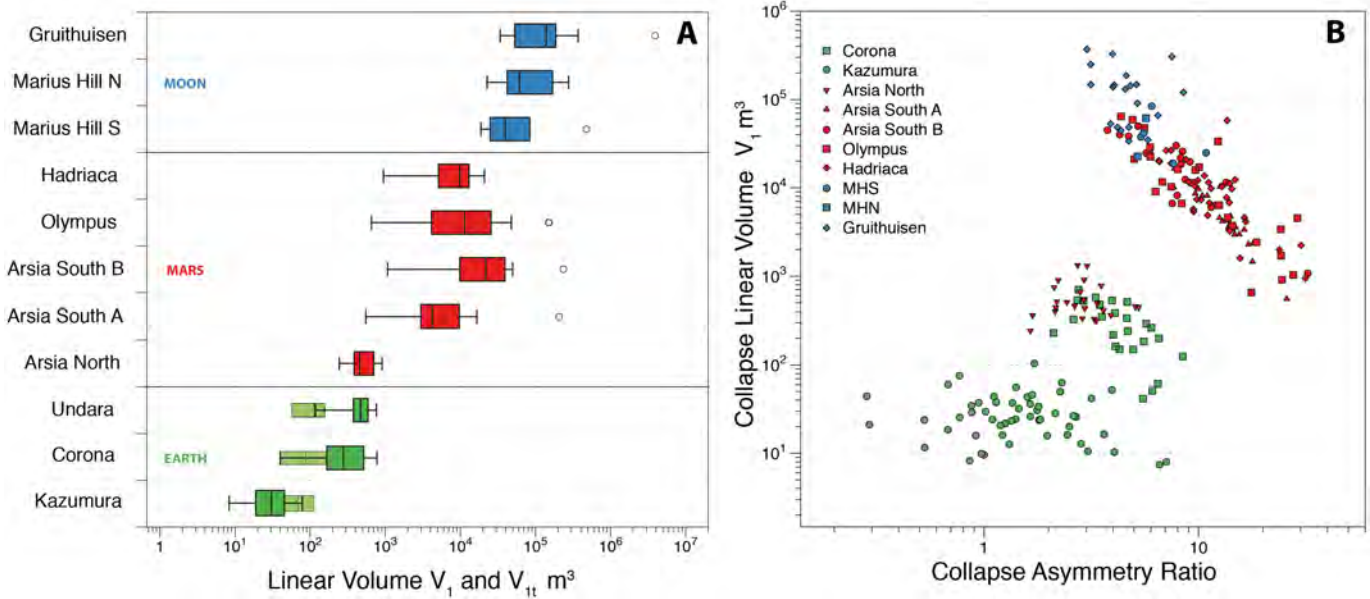
A
Gruithuisen
Marius Hill N
Marius Hill S
MOON
Hadriaca
Olympus
Arsia South B
Arsia South A
Arsia North
MARS
Undara
Corona
Kazumura
EARTH
1
10¹
10²
10³
10⁴
10⁵
10⁶
10⁷
Linear Volume V1 and V1t m³
B
Corona
Kazumura
Arsia North
Arsia South A
Arsia South B
Olympus
Hadriaca
MHS
MHN
Gruithuisen
Collapse Linear Volume V1 m³
10⁶
10⁵
10⁴
10³
10²
10¹
1
10
Collapse Asymmetry Ratio

Figure 7

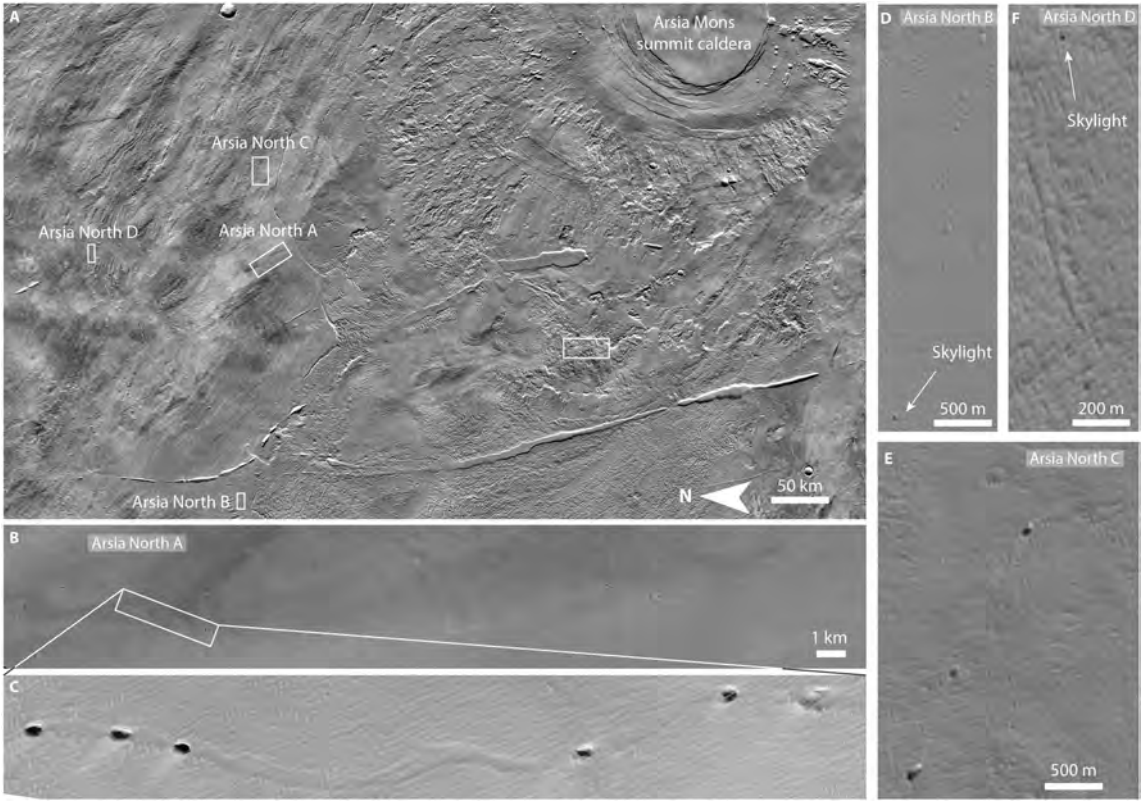
A
Arsia Mons
summit caldera
Arsia North C
Arsia North D
Arsia North A
Arsia North B
N
50 km
B
Arsia North A
1 km
C
D
Arsia North B
Skylight
500 m
F
Arsia North D
Skylight
200 m
E
Arsia North C
500 m

Figure 8

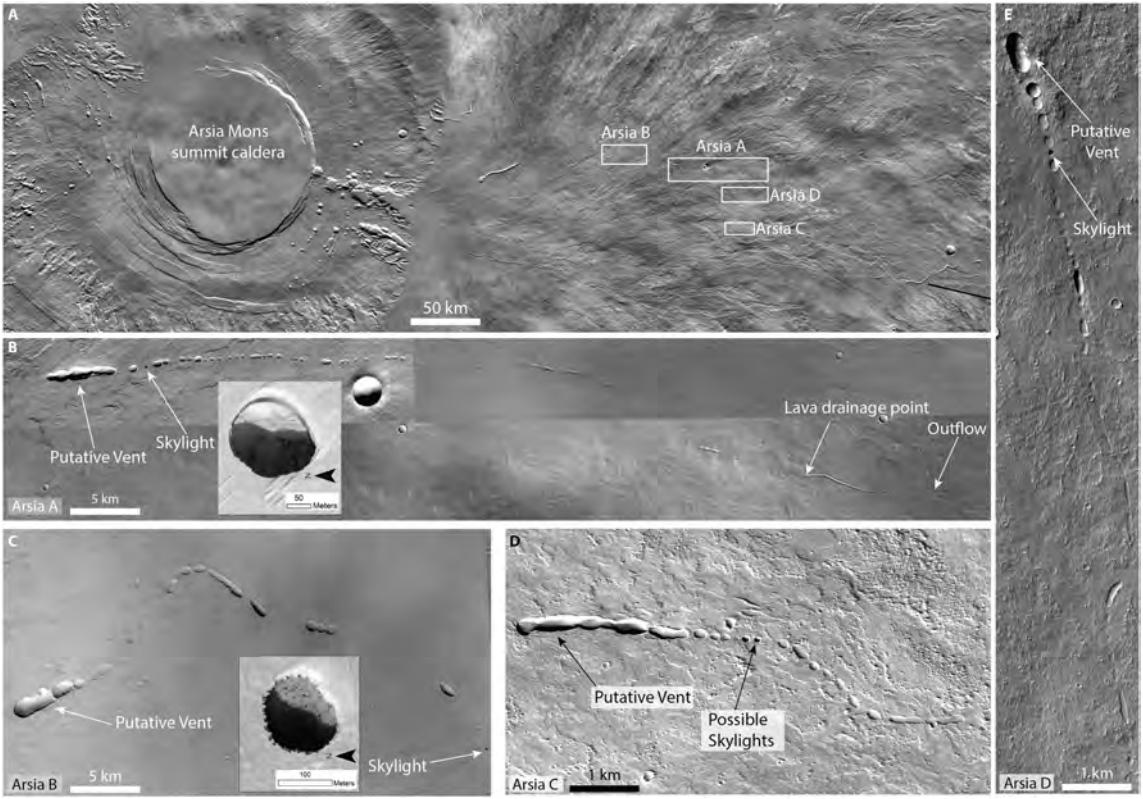
A
Arsia Mons
summit caldera
Arsia B
Arsia A
Arsia D
Arsia C
50 km
B
Putative Vent
Skylight
Arsia A
5 km
Lava drainage point
Outflow
C
Putative Vent
Skylight
Arsia B
5 km
D
Putative Vent
Possible
Skylights
Arsia C
1 km
E
Putative
Vent
Skylight
Arsia D
1 km

Figure 9

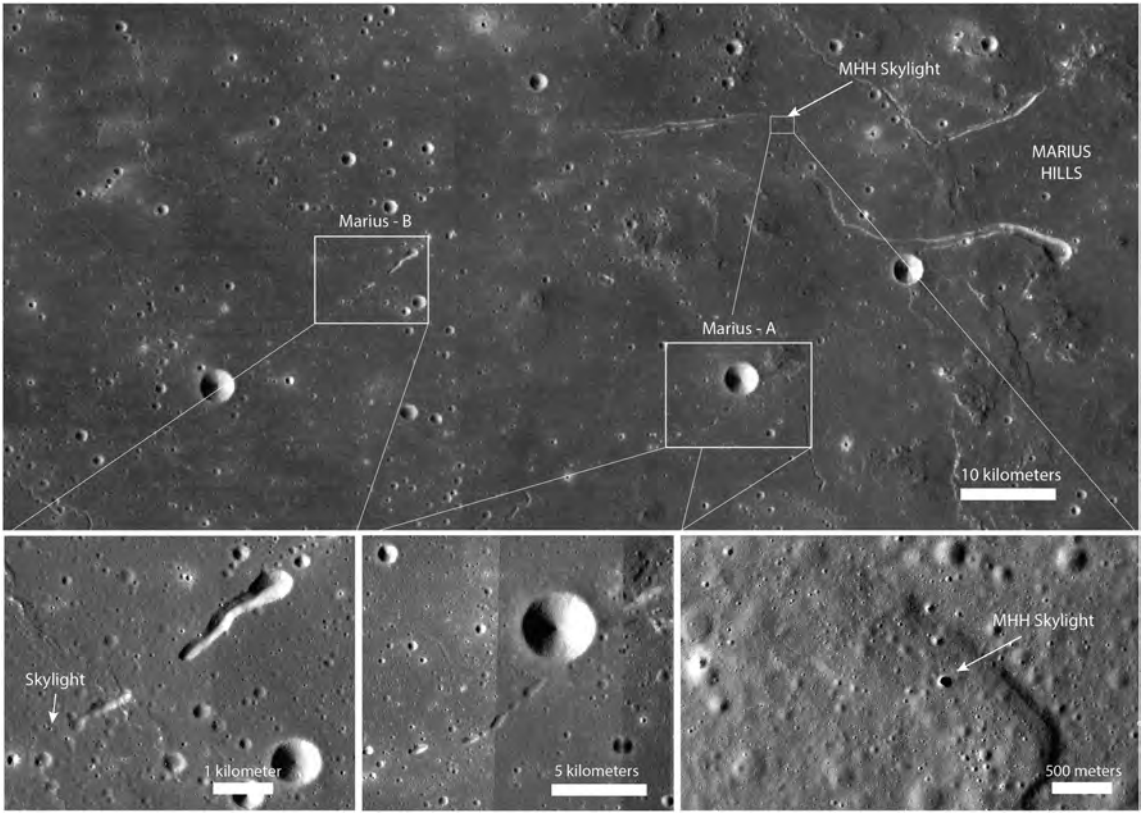
MHH Skylight
MARIUS
HILLS
Marius - B
Marius - A
10 kilometers
Skylight
1 kilometer
5 kilometers
MHH Skylight
500 meters

Figure 10

Lava tubes on Earth, Moon and Mars: a review on their size and morphology revealed by comparative planetology

Francesco Sauro[1,2], Riccardo Pozzobon[3]*, Matteo Massironi[3], Pierluigi De Berardinis[1], Tommaso Santagata[4], Jo De Waele[1]

1) Department of Biological, Geological and Environmental Sciences, Italian Institute of Speleology, University of Bologna, Via Zamboni 67, 40126, Bologna, Italy
2) European Space Agency, ESA PANGAEA program, European Astronaut Centre, Cologne, Germany
2) Department of Geosciences, University of Padova
3) Virtual Geographic Agency, Reggio Emilia, Italy
*Correspondence to: Riccardo Pozzobon, email riccardo.pozzobon@unipd.it

Abstract

Sinuous collapse chains and skylights in lunar and Martian volcanic regions have often been interpreted as collapsed lava tubes (also known as pyroducts). This hypothesis has fostered a forty years debate among planetary geologists trying to define if analogue volcano-speleogenetic processes acting on Earth could have created similar subsurface linear voids in extra-terrestrial volcanoes. On Earth lava tubes are well known thanks to speleological exploration and mapping in several shield volcanoes, with examples showing different genetic processes (inflation and overcrusting) and morphometric characters. On the Moon subsurface cavities have been inferred from several skylights in Maria smooth plains and corroborated using gravimetry and radar sounder, while on Mars several deep skylights have been identified on lava flows with striking similarities with terrestrial cases. Nonetheless, the literature on this topic is scattered and often presents inaccuracies in terminology and interpretation. A clear understanding of the potential morphologies and dimensions of Martian and lunar lava tubes remains elusive.

Although it is still impossible to gather direct information on the interior of Martian and lunar lava tube candidates, scientists have the possibility to investigate their surface expression through the analysis of collapses and skylight morphology, morphometry and

their arrangement, and compare these findings with terrestrial analogues. In this review the state of the art on terrestrial lava tubes is outlined in order to perform a morphological and morphometric comparison with lava tube candidate collapse chains on Mars and the Moon. By comparing literature and speleological data from terrestrial analogues and measuring lunar and Martian collapse chains on satellite images and digital terrain models (DTMs), this review sheds light on tube size, depth from surface, eccentricity and several other morphometric parameters among the three different planetary bodies. The dataset here presented indicates that Martian and lunar tubes are 1 to 3 orders of magnitude more voluminous than on Earth, and suggests that the same processes of inflation and overcrusting were active on Mars, while deep inflation and thermal entrenchment was the predominant mechanism of emplacement on the Moon. Even with these outstanding dimensions (with total volumes exceeding 1 billion of m^3), lunar tubes remain well within the roof stability threshold. The analysis shows that aside of collapses triggered by impacts/tectonics, most of the lunar tubes could be intact, making the Moon an extraordinary target for subsurface exploration and potential settlement in the wide protected and stable environments of lava tubes.

Keywords: lava tube; inflation; subsurface; comparative planetology; volcanospeleology

1. Introduction

The recent years have seen a rapid expansion of international participation in lunar and Martian exploration, with thousands of publications on planetary geology based on images and data obtained through satellites and rover missions (Burns, 2010). Comparative planetology allows the analysis and interpretation of geological features on different planets. The comparison can be applied both to morphologies and processes considering the differences in planetary parameters such as gravity, temperature, pressure, density and composition of the atmosphere, geological history and others (Chahine et al., 2010). However, while the surfaces of terrestrial planets of our solar system have been documented with high resolution, multispectral cameras, and even by rover missions, very little is known about the subsurface and the potential presence of underground voids.

Early in the seventies, planetary geologists had already identified peculiar collapse sinkhole-like morphologies in several volcanic areas of Mars and in the lunar Maria (Carr et al., 1977; Carr, 1973). These “sinkholes” are often referred to as “collapse” or “pit” chains when they are aligned (Fig. 1). Since these features lack the elevated crater rim and ejecta deposits that are typically associated with impact craters, they have been thought to represent collapses of underground cavities. Because most of these features are found on lava flows or along the sides of volcanic edifices, they were very early associated to the putative presence of “lava tubes”, also known as “pyroducts” (Kempe, 2012, 2019). Lava tubes are well known on terrestrial shield volcanoes thanks to volcanological and speleological research (Bunnell, 2008), even though also other processes could be accounted for the formation of pits and volcanic non-eruptive depressions (Halliday, 2004; Okubo and Martel, 1998). The lava tube collapse hypothesis was also proposed by several authors to explain the formation of sinuous lunar rills, that would represent collapsed tubes (Cruikshank and Wood, 1972; Greeley, 1971a; Oberbeck, 1969). Nonetheless, several authors have shown that also on Mars and the Moon not all sinkholes can be directly related to lava tubes and other volcanic and tectonic processes are most likely driving the formation of these features (Cushing, 2017; Wyrick et al., 2004). Hence, the potential presence of still intact lava tubes below the surface of the Moon and Mars is a matter of debate since more than fifty years.

In recent times, the availability of high resolution images of the surface of Mars from High Resolution Imaging Science Experiment camera (HiRISE, 0.25 m/pixel resolution) on board Mars Reconnaissance Orbiter (MRO) and the Moon from the Lunar Reconnaissance Orbiter Narrow Angle Camera Camera (LROC NAC, 0.5 m/pixel resolution) on board Lunar Reconnaissance Orbiter (LRO) has allowed identifying peculiar holes characterized by vertical or overhanging walls, named “skylights”, often proposed as “cave-entrance” candidates (Cushing, 2012; Haruyama et al., 2012). Until now, more than 300 of these potential cave entrances have been identified on the Moon (Wagner and Robinson, 2019) and more than 1000 on Mars (Cushing, 2017). Most of them are isolated features but several are associated with collapse chains on Mars or sinuous rilles on the Moon. While in sinkholes, detritus from the collapse could obstruct the access to the intact tube, skylight features represent direct ceiling accesses to underlying still intact lava tubes. The most

spectacular examples of these entrances are situated in the volcanic plateau of Marius Hills on the Moon (Haruyama et al., 2012), and on the lava plains of Arsia and Olympus volcanoes on Mars (Cushing et al., 2007). Robotic technologies, could allow to examine stratigraphic sections of lava flows from skylights allowing to collect new data on the formation of plateau basalts on the Moon and shield volcanoes on Mars (Kerber et al., 2018). Intact, open segments of lava tubes could provide stable shelters for human habitats shielded by cosmic radiation and micrometeorite impacts on the Moon (Haruyama et al., 2012). These voids could have dimensions suitable for housing a permanent base providing potential access to several resources, including volatiles and possibly water ice trapped in cave sediments (Blamont, 2014; Williams et al., 2010). In addition, skylights could provide direct access to the subsurface of Mars, which is considered one of the main targets for the search of past and present life traces on the red planet (Boston et al., 2001; Léveillé and Datta, 2010; Michalvsky et al., 2018).

Nonetheless, aside of identifying the presence of lava tube collapses and skylights, scientists have very few hints on the potential dimension and morphology of subterranean voids on these planetary bodies. On the Moon recent studies have attempted to evaluate the dimensions of intact lava tube fragments below the surface using the radar sounder system (Kaguya) (Kaku et al., 2017) and gravity mass deficit by Gravity Recovery and Interior Laboratory mission (GRAIL) (Chappaz et al., 2017), targeting pits and sinuous rilles regions. These studies seem to confirm that subsurface voids certainly exist, but the available limited resolution of the instruments have only allowed to retrieve partial information on their size, depth and shape. Finite element modelling of ceiling stability (Blair et al., 2017; Theinat et al., 2020) was used to estimate the sustainable potential dimensions of lunar and Martian lava tubes by iteratively varying roof thickness and strength of the material. However, this approach is limited to the stability range of these voids in the different planetary bodies without providing direct evidences of their real existence and any information on their genetic processes. Recently, tubular sinuous ridges hundred of meters wide and hundred of kilometers long on the lava plains of Southwest Tharsis on Mars have been proposed as undrained tubes based upon several morphological analogies with terrestrial examples (Zhao et al., 2017). Other studies in Noctis Labyrinthus on Mars have interpreted pit chains and linear depressions as collapses above hundred-

kilometers long lava tubes but have failed to provide any evidence of their subsurface development and dimensions (Leone, 2014).

On the other hand - on Earth - several morphological and genetical studies have been performed on lava tubes in terrestrial shield volcanoes (Kempe, 2012, 2019) with hundreds of kilometers of lava tubes and associated collapses and skylights mapped by speleological organizations. Detailed morphological descriptions and topographic surveys of kilometer-long tubes are available thanks to speleological explorations on Hawai'i (USA) (Bunnell, 2008; Greeley, 1971b; Kauahikaua et al., 1998; Peterson et al., 1994), the Canary Islands (Spain) (Sauro et al., 2019; Wilkens et al., 2009), Iceland (Hróarsson and Jónsson 1991), Northern Queensland (Australia) (Atkinson et al., 1975), Sicily (Italy) (Calvari and Pinkerton, 1999), Jeju Island (South Korea) (Woo et al., 2008), the Galapagos (Ecuador) (Jorda-Bordehore et al., 2016), and many other lava fields in the world (Kempe, 2012, 2019). This huge amount of data can be used for comparative planetology studies in order to infer lava tube dimensions and morphologies in the different planetary bodies of the inner solar system.

Although the morphological similarities of several collapse chains and skylights on Mars and the Moon with terrestrial lava tube features have been underlined by several authors (Cushing et al., 2007; Cushing, 2012; Léveillé and Datta, 2010), to date, a detailed morphological and morphometric comparison among the three planetary bodies has not yet been provided. Given the direct genetic relationship between the collapses, the skylights and the lava tubes, morphometric analysis can be used to estimate the dimension and general morphology of intact sections of the tube along the same collapse chain line.

In this review, we discuss the genetic mechanisms and related morphologies of lava tubes on Earth and we provide morphological evidences to recognize lava tube collapse chains and associated skylights on Mars and the Moon. We also define morphometric and morphological relationships between collapses and underlying intact segments of the tubes on Earth, allowing for morphological and volumetric estimation of the Martian and lunar cases.

To this aim, we have examined the most important morphometric parameters of collapse chains and skylights associated to lava tubes observed in satellite images and DTMs from Earth, the Moon and Mars. For the terrestrial lava tubes we can relate these measurements

with the dimensions of the still intact tube, which has been mapped through standard speleological surveys or laser scanner technologies and the relationship between surface and subsurface lava tube features can be extended to the other bodies.

This review and the associated comparative analysis provide, for the first time, direct evidence of the size, depth and morphology of lunar and Martian lava tube candidates in comparison with terrestrial ones, providing new clues on their genetic processes and implications on volcanology, habitability and astrobiology (Boston et al., 2004; Léveillé and Datta, 2010). These data constitute the basis for planning of future robotic and human exploration missions of these subsurface planetary features.

2. Lava tube genetic mechanisms and morphologies on Earth

A lava tube, also known as pyroduct (Kempe, 2012, 2019), is defined by Halliday (2004) as a "roofed conduit of flowing lava, either active, drained, or plugged". The lengths of lava tubes on Earth vary from a few meters up to tens of kilometers (Bunnell, 2008). Their width and height vary from 0.5 m up to 30 m, developing from few centimeters below the surface up to a depth of few tens of meters. Lava tubes are in most of the cases sub-parallel to the surface itself. Cross-sections of lava tubes are usually arched, round, oval, or alternatively keyhole shaped, due to accretion of lava to the sidewalls and downcutting by thermal and physical erosion (Allred and Allred, 1997; Fagents and Greeley, 2001; Greeley et al., 1998).

Lava tubes can present different patterns: a) single tubes, sinuous or rectilinear, b) braided tubes, with bifurcations and conjunctions c) multilevel tubes with different levels connected by lava falls and shafts, d) a combination of braided tubes on different levels. This range of morphologic variability is due to different genetic processes (Fig. 2) controlled mainly by the effusion rate, the slope of the land surface on which the lava flows, the underlying paleo-topography, and the composition and related rheology of the lava.

The first genetic observations of actively forming lava tubes are those of Peterson and Swanson (1974) and Peterson (1994) during long-lasting effusive eruptions at Kīlauea volcano in the Hawai'i. They observed most of the tubes forming by "overcrusting" of an open lava channel. This process is based on the principle that the outer surface of an active

lava flow chills quickly because of the temperature difference between the molten lava and the atmospheric air. The cooling surface becomes progressively more viscous and finally solidifies (Dragoni et al., 1995), insulating the molten lava below. The insulation slows the rate of cooling inside the closed tube helping to maintain heat and low viscosity over long distances and time. The overcrusting of the channel can happen through slightly different mechanisms, depending on the flow rate, turbulence and channel geometry (Fig. 2 A-B): 1) the growth of solidified rooted crusts from lava stream banks; 2) overflows and spatters accreted to form shelves and levees that progressively grow forming a roof across the stream; 3) plates and lithoclasts of solidified lava floating downstream welding together and forming a blocky roof. The three mechanisms are not mutually exclusively and frequently the channel is overcrusted through a combination of these three processes.

When the feeding source of the lava runs out, the flow slowly evacuates the conduit leaving an empty tube. Usually overcrusted tubes are limited to the width and depth of the channels where they originally formed, with roofed sections not exceeding few tens or maximum hundreds of meters in length and a few meters in diameter. The discharge rates of these tubes are often moderate, between 1 to 5 m^3 s^{-1}. If the lava flow reaches the sea, the chilled crust solidifies much more quickly forming "littoral" tubes that show characteristic features in association with pillows (Peterson et al., 1994). These tubes however are rarely drained and mostly plugged, and generally have limited extensions. Examples of overcrusted tubes, aerial and littoral, have been described in most of the terrestrial shield volcanoes (Rossi, 1997).

Another overwhelmingly more frequent genetic process forming lava tubes is shallow inflation and draining of inflated pahoehoe lobes (Fig. 2 C). This process has been widely described by Hon et al. (1994) and Peterson (1994): initially inflation acts within thin sheets of pahoehoe lava, but when the chilling crust is strong enough, the increasing internal pressure results in uniform uplift of the entire sheet flow lobe. As the flow advances, preferred pathways develop in the older portions of the liquid-cored flow; these pathways can evolve into elliptical lava tube systems that sometimes can be drained and leave an open tunnel (Cooper an Kauahikaua, 1992). In case of long-lasting eruptions several small tubes can merge focusing the flow along one main path. The focused flow has

stronger thermic erosion potential and can enlarge and entrench the conduit (Kempe, 2019).

Lava tubes formed by shallow inflation are usually characterized by a superficial bulge (due to the inflation) along its development, and by an original horizontal elliptical cross section that can be entrenched by thermal erosion. The most remarkable examples on Earth are on Hawai'i (Kempe, 2019), on the Canary Islands (Sauro et al., 2019) and on Iceland (Hróarsson and Jónsson, 1991) but they are in any case present in all major shield volcanoes on Earth.

Inflation can act also in long-lasting aa lava flows as described by Calvari and Pinkerton (1998) (Fig. 2 D). In this case the inflation acts mainly at the front where the flow stops, thickens and widens. Since lava continues to be supplied at a uniform rate but cannot reach further than the front, the internal pressure increases and inflation propagates from the front region backwards forming a tube network. When the pressure overcomes the tensile strength of the crust in the front area, tumuli or new ephemeral vents open and a new flow is fed by the upper tube system (Duncan et al., 2004). These peculiar lava tubes in aa flows are usually characterized by higher discharge rates compared to pahoehoe, in the order of 10-20 m^3 s^{-1}. Because of these peculiar genetic mechanisms, lava tubes in aa flows are usually bigger than in pahoehoe, but are more segmented into primary and secondary flows.

Tumuli hosting small chambers and short low-ceiling caves can also be associated to both aa and pahoehoe inflationary tubes s a result of lava being injected from below (Pedersen et al., 2017; Table 1).

In addition to overcrusted and shallow inflated lava tube morphotypes, few cases on Earth have been proposed as a very peculiar example of "deep inflated-entrenched" lava tubes (Fig. 2 E). These formed through inflation along deep inception horizons following previous lava flow boundaries where, after inflation, the conduit has been enlarged by downward thermic erosion and breakdown phenomena (Tonello, 2017; Kempe, 2019). These lava tubes are among the biggest in size on Earth, with the most famous examples being Corona Lava Tube in Lanzarote (Sauro et al., 2019) and the Undara Lava Tube in Queensland (Atkinson et al., 1975). In these cases, the flow discharge can reach values of over 50 m^3 s^{-1}.

Sometime the conduit can form also along fractures and eruptive fissures (Fig. 2 F), through processes described as ”evacuated dike tunnels” sensu Cushing et al. (2015). An example of a very deep plug pressure tube along a fracture is the Wood Valley Pit Crater in Hawai‘i (Favre, 1993). Here the thermal erosion created a lava tube conduit through plug flow along a fracture, at almost 90 meters of depth below the surface (Okubo and Martel, 1998). The fracture doesn’t reach the surface being probably sealed by younger flows on top. In this case, this peculiar lava tubes controlled by a fracture present vertical elliptical cross sections.

In all genetic cases, chains of collapses aligned along the tube development represent the surface expression of these conduits (Fig. 1 A-C). Collapses of the ceiling form during the genesis of the lava tube through flow overpressure (pseudo-vents), or, more commonly, by gravitational effects when the tube is finally drained, including block stoping transferring the void from deep conduits to the surface (Cushing et al., 2015). These collapses, called “*pukas*” in Hawai‘i or “*jameos*” in the Canary archipelagos (Fig. 1 A-C), typically form sinuous chains and are mostly elongated along the direction of the tube (Fig. 1 A-E). It is worth mentioning that in literature collapses associated to lava tubes are often confused with other volcanic vertical pit types - frequently named “pit craters” - that can be associated to other processes like tectonic or fissural magma flow (Halliday, 2004a; Cushing et al., 2015). In this review we will use the Canarian term “*jameos*” for the lava tube-associated terrestrial cases, as reported in the most updated edition of *Glossary of Geology* from the American Geological Institute (Jackson, 2005). *Jameos* is a genetic-specific term referred to a collapse that is certainly related to lava tube formation, while pit crater is a more general term, not necessarily due to lava tube collapse but potentially related also to other types of cavities (Okubo and Martel, 1998).

On Earth a collapse can represent different stages: 1) proper *jameos*, which are collapses that involve the whole tube width with vertical or steeply descending detrital slopes (Fig. 1 B-C), 2) skylights with vertical or overhanging walls where the opening is much smaller than the tube width below (Fig. 1D). *Jameos* are frequently filled by detritus, while skylights are just openings on the roof of the conduit. Between one *jameo*/skylight and the subsequent one the underground tunnel can be intact and accessible for exploration and mapping (Fig. 1A).

3. Collapses and skylights related to lava tube candidates on the Moon and Mars

The putative presence of lava tubes on planetary bodies such as Mars and the Moon has been proposed as early as in the sixties (Oberbeck, 1969) with their evidence expressed as sinuous rilles and sinkholes in volcanic terrains. The terms "collapse" or "pit" are commonly used in the planetary geology literature to define lunar or Martian morphologies characterized by sinking circular or elliptical topographic depressions that lack the elevated crater rim and ejecta deposits typical of impact craters. Several authors have associated collapse chains in planetary volcanic terrains to the breaking of lava tube ceilings, exactly like *jameos* on Earth (Cushing, 2012; Leone, 2014; Wagner and Robinson, 2014). Nonetheless, the direct relationship of these features and lava tubes cannot be inferred easily without direct exploration. Several other genetic processes have been proposed for collapse/pit chains such as dike intrusions, collapses of shallow magma chambers, dilational faults and voids created by tensional fractures (Cushing, 2012; Ferrill et al., 2004; Ferrill et al., 2011; Leone, 2014; Rubin, 1992; Scott and Wilson, 2002; Smart et al., 2011; Wilson and Head III, 2002; Wyrick et al., 2004).

Also skylights have been associated to lava tubes. Even so, other speleogenetic processes have been proposed as well, like hypogenic and sulfate karstification, tectonic caves and shallow magma chamber evacuation on Mars. The Mars Global Cave Candidate (MGC3) catalogue (Cushing, 2017) differentiates between: 1) lava tube candidate *jameos* along rilles, channels and collapse chains, 2) Atypical Pit Craters (APCs) usually isolated with peculiar morphological characteristics, 3) Small Rimless Pits (SRPs) along flow channels 4) Pinholes which are likely very small entrances and 5) lateral entrances on cliffs. Applying this classification only 1, and 3 can be directly associated with lava flows and can therefore be considered potential lava tubes entrances. Atypical pit craters instead remain controversial features with an unclear origin.

Likewise, on the Moon not all skylights formed in volcanic terrains, but also in impact melts, therefore in these cases other processes are probably responsible for their formation (Wagner and Robinson, 2014).

For these reasons, any study aiming to identify lava tube collapses and skylight candidates on the surface of these planetary bodies has to follow a rigorous approach based on a geomorphological comparison with terrestrial analogues.

As discussed by Wyrick et al. (2004), several pit chains on Mars are related to dilational faults that are distributed along the flanks of volcanic edifices of the Tharsis region and on flat-lying floors of broad basins, with striking similarities with terrestrial analogues on Iceland (Ferrill et al., 2011) and Hawai'i (Okubo and Martel, 1998). On the Moon, dilational pit chains are common within and around Mare basins, mainly related to tensional tectonic regions (Watters et al., 2012). Tectonic pit chains are often rectilinear or curvilinear and are mostly associated with tectonic lineaments or bounded within grabens (Pozzobon et al., 2015). Frequently, there are transitions along strike from visible faulting to faults and pits to pit chain alone (Mège et al., 2003). Tectonic pits are often coalescent depressions forming scalloped troughs and do not necessary follow the maximum slope.

Conversely, lava tube *jameos* on Earth (and by analogy lava tube associated collapses on Mars and Moon) present important morphological differences that make them easily discernible from tectonic counterparts (Tab. 1). The main characteristic, which makes them distinguishable from the tectonic chains, is their sinuosity (Cushing et al., 2007).

Additionally, also some remarkable morphological differences are expected between collapse chains related to overcrusted or inflated lava tubes (Dragoni et al., 1995; Kauahikaua et al., 1998; Kempe et al., 2010; Orr et al., 2015) (Tab. 1). Overcrusted tubes are formed mainly within lava channels and therefore their topographic expression can be followed from one collapse to the other along the channel benches (Dragoni et al., 1995; Kempe et al., 2010). Being the flow gravity-driven (Sakimoto et al., 1997), overcrusted tubes always follow the line of maximum steepness. An example of a putative overcrusted lava tube collapse chain on Mars is shown by Cushing (2012) on the lava plains to the north of Arsia Mons. This sinuous chain of *jameos*, with a total length of 40 km, shows clear bulges/benches that can be followed on the surface from one collapse to another (Fig. 1G). Conversely, inflated tubes usually do not present any linear evidence on the surface aside of collapses or wide bulged areas and tumuli (Orr et al., 2015). Because this genetic type of lava tube is pressure-plug driven (Sakimoto et al., 1997) with subsurface inflation able to follow prominent inception horizons (discontinuities like fractures or lava flow

boundaries), their directions can also slightly deviate from the steepest slope line. Typical examples of this type of collapse chains are those on the southern flanks of Arsia or Hadriaca on Mars and the Gruithuisen chain on the Moon (Fig. 1 I-O). Inflated can also be braided and develop on different levels as shown in several terrestrial examples, like Cueva del Viento on the island of Tenerife (Montoriol-Pous and de Mier, 1974). Examples of braided collapse chains have been identified on flanks of Olympus Mons (Fig. 1N), whereas no evidences of their presence have been detected on the Moon so far.

Lava tubes collapse chains can be discriminated from other genetic types also by the presence of a vent at the top of the chain. While on Earth, this is usually a volcanic cone and crater, there are evidences that in the shield volcanoes of Mars or in the fissural volcanic field of the Moon this is often represented by a deeper and wider depression which can represent their feeding vent. Smaller circular skylights with vertical or overhanging walls can be indeed found along lava tube collapse chains, usually with a smaller width compared to the collapses (Fig. 1D, 1H, 1L). All these characteristics are useful to properly distinguish lava tube collapse (*jameos*) chains on the Moon and Mars, however these criteria are solely based on the analogies with terrestrial lava tubes, while other unknown or slightly diverse emplacement mechanisms could be acting on different planetary bodies.

4. Morphology of collapses related to tube stability and emplacement mechanisms

Terrestrial examples can also help to define the morphometric relationship between collapse chains and intact lava tube segments on the Moon and Mars. In most terrestrial lava tubes, *jameos* appear in plan view as ellipses elongated along the conduit development direction and their width (*W*) approximates the underlying lava tube average width (*Wt*) of the intact sectors (Fig. 1A). However, in case of braided superposed branches, collapse chains follow the development of the shallowest part of the tube while other segments can remain stable and thus without any expression at the surface. *Jameos* can have vertical or high angle slope sidewalls when the ceiling is completely collapsed forming depressions elongated along the tube lateral limits (Fig. 1B). Skylights instead have vertical or overhanging walls forming smaller circular depressions (Fig. 1C-D). Indeed, skylights on the ceiling have a smaller width *W* compared to the tube *Wt* (Fig. 1D). In all surveyed

terrestrial lava tube chains, skylights are by definition much smaller than *jameos* (Bunnell, 2008). Their circular shape is guaranteed by the uniform horizontal stress field on the ceiling (i.e., being σ1 vertical, and σ2 = σ3) when tube sidewalls confinement is not yet reached transforming the skylight into an elongated *jameos.* Thus even the collapse planar ellipticity can be used as a distinctive character among lava tube openings.

The scaling factor *f=W/Wt* between *jameos* and intact tube segments is shown in Fig. 3 for three different terrestrial examples. In the case of a braided multilevel tube like Kazumura in Hawai'i (Allred and Allred, 1997) *f* is slightly smaller than 1, with most of the collapses still with vertical walls. The width of the tube is not changing in proximity of the *jameos*. Conversely, *jameos* in the deep-inflated Corona lava tube in Lanzarote are situated in areas where the conduit was wider in average. These larger areas are mainly located where the lava tube changes its direction, and the lateral enlargement was probably due to flow overpressure and lateral thermal erosion. The transition from an $f<1$ to an $f>1$ is related to the predominance of a gravity-driven flow or of a pressure-driven flow in the tube, respectively (Sakimoto et al., 1997).

The pressure-driven flow is even more evident in the inflated tube of Undara in Queensland (Atkinson and Atkinson, 1995) where *jameos* are much wider than the intact tube *Wt* (f=5.3). In some cases, collapses seems even unrelated to the tube development, being interpreted as lateral pressure overflows forming local lava ponds that afterwards drained back into the lava tube (Atkinson, 1991).

These different scaling factors are clearly controlled by different emplacement mechanisms. Therefore in order to provide estimates of lava tube dimensions based on associated collapse morphometry on the Moon and Mars, it is necessary to consider the different genetic hypotheses by carefully investigating the morphological characteristics able to discern overcrusted from shallow/deep inflated cases (Table 1).

5. Morphometry: materials and methods

5.1 Lava tube and related jameo*/sinkhole morphometric parameters*

In the last years morphometry has been used as a tool for comparing genetically related features on different planetary bodies (Ansan and Mangold, 2013; De Toffoli et al., 2019;

Plescia, 2004; Pozzobon et al., 2019). Using DTMs we extracted profiles along the chains and a wide range of comprehensive morphometric parameters of lava tube collapses on Earth, Mars and the Moon, including volumes (Table 2). For each *jameo*/skylight along a chain the following parameters have been extracted: length (*L*), width (*W*, considered as the minor axis of elliptical collapses), depth (*D*), collapse total volume (*V*), linear volume (V_1, the average volume of 1-m-long cross-sections), asymmetry ratio (*AR*, the ratio between width and depth). For the whole collapse chain it is possible to measure the following parameters: total length (*Ctl*), collapse chain sinuosity (*Si*), and slope (*S*). In the case of Earth, thanks to speleological exploration, terrestrial laser scanning, and topographic surveys, it is possible to directly acquire the width (*Wt)*, height (*Ht*) and linear volume (V_1t) of the intact tube between collapses, as well as the total length of the underground void (*Ttl*).

Finally, the expected intact tube length (*Tutl*) is given by the difference between the chain total length (*Ctl*) and the sum of all collapse lengths (*L*).

5.2 Case studies and dataset generation

5.2.1 Earth

The terrestrial examples analyzed are Corona (Lanzarote, Spain), among the most voluminous tubes known on Earth (Carracedo et al., 2003), Kazumura (Hawai'i, USA), the longest terrestrial lava tube (Allred et al., 1997), and the Undara lava tube in North Queensland (Australia) (Whitehead, 2010). In total, we gathered a dataset of 120 *jameos* and skylights measured in the three sites. These three examples have been chosen as terrestrial maximum size end-members in terms of dimension, being considered among the most voluminous lava tubes on Earth (Allred and Allred, 1997; Atkinson and Atkinson, 1995; Sauro et al., 2019). A detailed description of each lava tube and associated *jameos*/skylights is provided in the Suppl. Mat.

The 6.5 km long Corona lava tube system (Supplementary Fig. 1) above the sea-level was entirely mapped together with its *jameos* during three different survey campaigns in 2017 using a combination of Terrestrial Laser Scanning (TLS) and Mobile Mapping (MM). The final result is one of the longest 3D surveys of terrestrial lava tubes to date (Santagata et al., 2018; Sauro et al., 2019). The main path of the entire cave system was mapped with an

unprecedented resolution of 6 mm point spacing on average. The laser scanner surveys within the caves were georeferenced on the surface through differential GPS and using DTMs derived from regional airborne Light Detection and Ranging data (LIDAR, 2.5 m point spacing from Spanish Geological Survey) and Unmanned Aerial Vehicles (UAVs) photogrammetric surveys of the *jameos* and surrounding terrains. All the morphometric parameters of Corona lava tube were thus retrieved using this high-resolution dataset.

The morphometric data for *jameos*/skylights in Kazumura and Undara were obtained through existing speleological maps and databases. The measurements of Kazumura have been performed with the aid of the Kazumura Atlas (Allred et al., 2002) providing plan views and profiles of the entire tube length, including *jameos* and skylights (Supplementary Fig. 2). The measurements of morphometric parameters on the digitalized maps where performed in a Geographic Information System (GIS) environment. For Undara we relied on existing data from previous publications (Atkinson, 1991; Atkinson and Atkinson, 1995) and speleological maps, including average measurement of conduit *Wt* and *Ht* (Supplementary Fig. 3).

5.2.2 Mars

On Mars, a total of 122 collapses related to five lava tube candidate chains were examined on Arsia, Olympus and Hadriaca volcanoes (Table 3, Fig. 2, Supplementary Figures 4-8). The analysis was extended for comparison also to a typical graben-bounded tectonic pit chain in Ascraeus Mons (Wyrick et al., 2004) (Supplementary Figure 9). This was achieved through high-resolution stereo DTMs (18 m of grid size) generated from Context camera images (CTX, 6 m/pixel on board MRO)(Malin et al., 2007). CTX images present indeed a good compromise between resolution (~5.5 m/pixel) and areal extent (swath width of 30 km and length variable between 50 and 300 km) providing broad coverage and sufficient resolution for mapping and morphometric analyses. By contrast, the high resolution stereo pairs provided by the HiRISE camera (0.25 m/pixel, with associated DTMs with 1 m of grid spacing) have a small field of view (6x12 km in the RED channel) and an extremely limited coverage on the areas of our interest and thus could not provide the needed areal extent to carry out our analysis

The best overlapping CTX images were selected using the Planetary Image Locator Tool (PILOT) stereo analyzer for targeted regions (Bailen et al., 2015) which is able to compute the stereo angles of the image pairs and the expected vertical precision of the final output (Supplementary Table 1).

All the stereo pairs were pre-processed with Integrated Software for Imagers and Spectrometers (ISIS3) suite from USGS (United States Geological Survey) (Gaddis et al., 1997; Torson and Becker, 1997). The bundle adjustment of the stereo pairs and stereo matching was performed with Ames Stereo Pipeline (ASP, Beyer et al., 2014; Moratto et al., 2010; Shean et al., 2016). The point clouds were aligned with the Mars Orbiter Laser Altimeter Precision Experiment Data Records (MOLA PEDR) for absolute height reference and the DTM was gridded with a resolution of 18 m. The associated ortho-images at 6m/pixel resolution were also produced for each site.

5.2.3 Moon

On the Moon a total of 27 collapses putatively related to lava tubes were analyzed in three different collapse chains in Marius Hills and Gruithuisen (Table 3, Fig. 2, Supplementary Figures 10-12) using the Kaguya/LOLA merged DTMs (59 m of grid spacing, Barker et al., 2016). In both cases, we have carefully selected the collapse chains that for their morphological characteristics (Table 1) can be differentiated from tectonic pit chains (Wyrick et al., 2004) on LROC NAC image mosaics. In addition, the same DTM approach has been performed for comparison on the graben bounded tectonic pit chain of Hyginus Rill (Wilson et al., 2011) (Supplementary Fig. 13).

Lunar lava tube traces and collapses were mapped on LROC NAC images (Supplementary Table 2) that, with ISIS 3, were calibrated, destriped, attached to the spacecraft navigation and pointing kernels (SPICE) and exported as 32bit geotiffs allowing to perform contrast stretch during the mapping and analysis of the collapses.

5.3 Topographic profiles and extraction of collapse maximum depth (D)

We traced the profiles of the collapses on Mars and the Moon by calculating the second derivative of the DTM (Wood, 1996). This variable produces a line along the collapse chain perpendicular to the direction of the maximum slope, visually providing the trace of the

deepest path from which the topographic profiles were extracted (Supplementary Fig. 14). This was achieved using the *r.param.scale* GRASS GIS module with a kernel size of analysis of 11x11 pixels (Wood, 1996).

The problem of no-data areas in correspondence of shadowed regions is particularly relevant for some collapses (~30%) on Mars where LiDAR data by MOLA did not reach a sufficient resolution to merge them with stereo DTMs. On the Moon the DTM dataset used is a combination of LOLA laser altimeter able to map shaded areas merged with stereo photogrammetry from Selene-Kaguya images. On Mars the areas presenting hard shadows in the images typically do not converge in the stereo matching and most softwares apply a hole-filling technique during the post-processing to mitigate this effect. In some cases, like in Arsia's largest collapse chains, almost one third of the depression is shadowed. In order to keep the information as much similar to the ground truth we did not use any hole filling technique. Indeed, the region interested by such hard shadows is typically one side wall of the deepest collapses, whereas the profile line matches the bottom floor which is covered by DTM.

The absolute maximum depth of each collapse was obtained by subtracting from the height values of the topographic profile, the profile traced on a DTM where holes were "filled" with synthetic surfaces (Supplementary Fig. 15). For this purpose we used a technique based on the creation of a synthetic surface constrained to the collapse edges in order to approximate the original topography before collapses and creating a DTM where holes are filled as shown in Pozzobon et al. (2018) and Pozzobon et al. (*in press*). This is obtained by digitizing the edges of the collapses on a combination of optical images and maximum profile curvature extracted from the DTM using the *r.param.scale* GRASS module (Wood, 1996) and with the aid of an overlaid ortho-image in transparency. The nodes of the polygon retracing the collapse edges were used to triangulate the synthetic surface, that was subsequently merged with the DTM obtaining a "filled" surface best approximating the pristine pre-collapse condition. The two stacked profiles and the absolute depth are presented in supplementary figures for each collapse chain (Supplementary Materials).

To be sure to extract the actual local maximum depth in each of the collapses we treated the obtained absolute depth data as a waveform and performed a peak analysis in MATLAB

environment extracting local peaks within the collapses and hence identifying univocally the greatest depth value.

For the smaller *jameos* of Arsia North and the skylights along all collapse chains, the very high contrast between the shaded areas and the surroundings bear no information usable for stereo correlation. However, knowing the azimuth and incidence angle of the light source on the ground from image metadata and by measuring the shadow it is possible to derive the depth of each *jameo*/skylight. The depths where extracted by using the *shadow height* tool in the *qview* program of the ISIS3 software suite. For each *jameo*/skylight we measured 10 profiles parallel to the illumination direction extracting maximum and average depth.

5.4 Collapse and conduit volume extraction

To correctly perform a volume calculation of collapses based on DTMs on all three planetary bodies it is necessary to take into account the high variability of the surrounding terrain as well as its general steepness, slope and roughness. In this case, opposite to the profile extraction phase, we applied a hole-filling technique of the shadows/no data areas in the DTMs in order to obtain a closed surface. A simple volume estimation based on average height of the collapse is thus not possible. The volumes enclosed between the reference synthetic surface and the real one were calculated with the *surface difference* in the 3D analyst toolbox of ArcGIS obtaining an estimate in cubic meters. It is worth to emphasize that the calculated volumes correspond to the minimum volume of the collapse, since some mass wasting from the walls and aeolian infilling is to be expected.

The terrestrial laser scan model of the Corona lava tube served as a starting point to build on comparative planetology and as a reference to check the performance and reliability of morphometric calculations based on DTMs. In particular, to validate the methodology of volumes extraction from DTMs described above, we compared the volumes obtained from TLS of the Corona collapses (Supplementary Fig. 16), with the same ones extracted using the airborne LiDAR data at 5 m resolution. The results gave an almost perfect match (R^2=0.9989) with volumes obtained through terrestrial laser scanning slightly higher than those extracted from the LIDAR DTM; this is most probably due to sporadic lateral overhanging walls that cannot be resolved by airborne LiDAR surveys.

By using the point cloud of the terrestrial laser scan model of the Corona lava tube we also derived the volumes of the intact sections of the tube together with the collapsed ones (Supplementary Movie 1). This operation was carried out by importing the aligned point clouds in Auto-Cad 2017 and extracting vertical cross-sections orthogonal to the tube path using 5 m interval for the intact tube and 1 m for the collapses (*jameos*) (Supplementary Figure 16, Supplementary Movie 1).

All of the lava tube cross-sections were digitized in 2D cad polylines subsequently cut into 1 m thick discrete slices (also referred to as linear volumes V_1 for *jameos* sections and V_1t for intact tube sections). The total volumes of the *jameos* were instead closed at the surface by interpolating their edges and laterally by interpolating the margin of their openings towards the intact conduit.

In the cases of Kazumura and Undara where 3D models and high resolution DTMs were not available, because of the two-dimensional nature of the cave maps such as (plan and profile views), we approximated the collapse volumes through the simple equation $[(D*W)/2]*\pi$, where D is the average depth and W the width of the tube. Tube linear volumes V_1t were instead approximated assuming an elliptical cross-section of the conduits following the equation $(Ht/2)*(Wt/2)*\pi$ where Ht is the height of the conduit and Wt is the width of the conduit. The same equations have been used for the dataset of the collapse chain of Arsia North on Mars, where the average depths (D) of collapses have been calculated through the shadow method and used to calculate V_1 of the collapses.

6. Results

6.1 Morphometry of terrestrial cases

Lava tube *jameos* measured on terrestrial shield volcanoes have an elliptical plan shape with the long axis parallel to the direction of subsurface tube development (Fig. 1A). Along the same chain, the minor axes of the *jameos* (perpendicular to the subsurface tube development) show comparable W, which is representative of the width of the underlying lava tube (Fig. 1A, Fig. 3, Fig. 4). Morphometric data are reported in Table 4. In the case of Kazumura, the mean collapse W is 7.3 m (σ=2.9), with the main portions of the intact tube characterized by a comparable Wt of 10.5 m (σ=4.7). Bigger dimensions can be found in the

Corona lava tube where the mean collapse *W* is 37.6 m (σ=12.1) while the intact tube departing from the collapses shows slightly smaller dimensions with *Wt* between 7 to 27 m with an average *Wt*=13.7 m (σ=5). According to Atkinson (1991) similar dimensions can be found also in the Undara lava tube with a *Wt* of 15-20 m, but here the related collapses can reach up to 50-60 meters in *W*. The depth *D* of the collapses is more homogeneous in the four cases (respectively in average 5.2, 9.8, and 10.0 for Kazumura, Corona and Undara) and is well comparable to the heights *Ht* of the intact tube sections (respectively in average 8.1, 9.7, and 6.5). Following the increase of *W* in the three cases while maintaining similar *D*, the asymmetry ratio (*AR*) of the collapses is growing from Kazumura (1.4) to Corona (3.8) and Undara (5 to 12). Linear volumes (volume along a 1 m thick cross-section) have also been measured in the three cases, both along the collapses (V_1) and along the intact tube sections (V_1t). The average linear volume represents an estimation of the collapse/conduit size independently from their asymmetry ratio and allows to calculate a volumetric conversion factor (*f*) between the intact tube and the collapse, as $f=V_1/V_1t$ resulting in 0.4, 2.9 and 5.2 respectively for Kazumura, Corona and Undara. In Kazumura the tube is intact along 97 % of the collapse chain, while in Corona and Undara the intact portions cover 73-74 % of the chain but they are not always accessible due to rockfall and infillings.

Few skylights of the cave ceiling show a much smaller *W* along the chains (Fig. 2). These skylight outliers in each chain dataset are usually rounded (*L*=*W*) and present peculiar morphologies with overhanging walls opening on the conduit roof. Skylights are common in Kazumura, but they characterize also some parts of Corona.

6.2 Morphometry of lava tube collapse chains on Mars

Similar morphological characteristics can be found in the four lava tube candidates measured on Mars (Fig. 1 G-O). The chains here show a higher density of collapses compared to Earth, with only from 20 to 40 % of intact portions along the whole chain (Table 5). An exception to this range is the chain of Arsia North, where the pristine lava tube parts reach 95%. In all cases collapses are elongated along the sinuous chain development. In the chains of Arsia South-A, Arsia South-B and Arsia North smaller outliers

where *L*=*W* have been identified as overhanging skylights, similar to those observed in terrestrial examples (Fig. 1H and 1L, Supplementary Figures 4-5-6).

Arsia North collapses have the smallest average *W* of 44 m (σ=11) and depth *D* of 16 m (σ=4), while the other cases show much bigger dimensions. The collapse chain of Arsia South-A shows an average *W* of 283 m (σ=84) and depth *D* of 25 m (σ=17). Slightly bigger dimensions are found in Arsia South-B (*W*=415 m, σ=108; *D*=60 m, σ=34), and in the chains analyzed in Hadriaca (*W*=374 m, σ=144; *D*=35 m, σ=18) and Olympus (*W*=366 m, σ=149 m; *D*=45 m, σ=36). The ratio between width and depth *AR* of the collapses is comparable to Earth only for Arsia North (2.8), while it is much higher for the other cases (11.2 and 6.9 for Arsia South-A and Arsia South-B, 10.8 in Hadriaca, 8.1 for Olympus). Most of the collapses show an important infilling of windborne deposits, that could be responsible for the high asymmetry ratio.

The two smaller and rounded skylights along Arsia South A and B appear to be filled with more aeolian sediment than the bigger depressions. Arsia South-A skylight is 58.8 meters deep on average and presents a maximum depth of 64.7 meters, whereas Arsia South-B is 49.6 meters deep on average with a maximum depth of 61.4 meters. Both present a slight infilling of unconsolidated aeolian material bulging towards the center, and some boulders resulted from the roof collapse with an average width of 10 m and protruding from the aeolian deposits for about 2 m of height.

Both the Arsia South and the Olympus cases show at the upstream termination of the chain one or two much deeper and wider depressions possibly representing the original tube-feeding vent (Fig. 2 I-N, Fig. 4). These show a depth of over 250 m in Arsia South-A (versus a *jameos* mean depth of 25 m) and, 210-230 m in Arsia South-B and Olympus (versus a *jameos* mean depth of 60 and 45 m, respectively). In Hadriaca the vent has not been identified, most probably because the initial part of the chain has been eroded by the nearby Dao Vallis. However, the area of Hadriaca is characterized by other three putative lava tube chains departing from a rounded caldera (Fig. 1 O).

6.3 Morphometry of lava tube collapse chains on the Moon

Collapse chains are less common on the Moon than on Mars, while continuous rills are dominant morphologies in several areas of the Maria (Hurwitz et al., 2013; McCall, 1970). Steep pits are usually isolated and in few cases associated to rill features (Robinson et al., 2012; Wagner and Robinson, 2014). Nonetheless, it was possible to identify and analyze three collapse chains that share very similar characteristics with the Martian and terrestrial ones (Fig. 1 P-R; Supplementary Figures 10-12). We informally called them Marius Hills A, Marius Hills B and Gruithuisen chains. As on Mars the percent of intact portions along the tube is around 40% of the chain (Table 5). All chains start with a deeper depression possibly representing the tube-feeding vent (respectively 320, 345, and 1240 m deep; Fig. 4). Aside of this initial depression they continue with a series of smaller collapses sharing comparable *W* and *D*, two or three times bigger than the Martian ones. More in detail, in Marius Hills A the collapses show an average *W*=574 m (σ=141), and *D*=87 (σ=33), very similar to Marius Hills B (*W*=527 m, σ=197; *D*=96, σ=30). These values are only slightly lower than those of Gruithuisen, which show an average *W*=858 m (σ=322) and an average *D*=190 m (σ=84). In general, the ratio between width and depth *AR* is similar or slightly smaller than on Mars, with a mean value of 6.6 for Marius Hills A, 5.5 for Marius Hills B and 4.5 for Gruithuisen. In the short chain of Marius Hills B it was also possible to identify a roundish skylight with much smaller dimension compared to the other collapses, and with debris material at the bottom (Fig. 1S).

6.4 Morphometric differences between tectonic pits and lava tube collapses

The data obtained from lava tube candidate collapse chains on Earth, Mars and the Moon can be compared to tectonic examples, as shown in Fig. 5. For Earth we compared the *jameos* of Corona and Kazumura with the tectonic pits measured in Iceland by Ferrill et al. (2011), while for Mars and the Moon we chose very typical graben-bounded chains. The profile distribution of collapses is much more regular and homogenous in the putative lava tube candidates compared to the tectonic ones (Fig. 4 and Supplementary Figures 13 and 9). Also, the tectonic chains present clearly more coalescent pits while the lava tube ones show a more regular depth and are often separated from each other (Fig. 4, Supplementary Figures 9 and 13). The initial larger and deeper depression (interpreted as potential lava

tube vent) is also typical of lava tube chains and not present on tectonic pit chains. In terms of morphometric statistics, tectonic pit chains present a stronger positive correlation between the width (*W*) and depth (*D*) of the collapse (Fig. 5 E-H). This is not the case of lava tube candidates, where this correlation is weaker or absent. These results show that morphometry can differentiate between different collapse genetic mechanisms. All the examples shown in this review from Mars and the Moon are within the morphometric constrains that exclude a potential tectonic origin, favoring the lava tube emplacement as the main process forming the subsurface voids creating the chain.

7. Discussion

The morphometric characteristics of a collapse chain are the expression of the main processes and parameters controlling the tube emplacement. These are the effusion rate, slope, rheology and driving forces like gravity or plug pressure (Sakimoto et al., 1997). Nonetheless, it is known from terrestrial examples that important morphological differences arise between channel overcrusting or shallow/deep inflation lava tubes (Dragoni et al., 1995; Kauahikaua et al., 1998; Kempe et al., 2010). Hence size estimations of Martian and lunar tubes remain mainly speculative if these different genetic processes are not taken into account.

Indeed, looking exclusively at morphologies, the lava tube collapse chains on Earth share several common characteristics with those proposed here as potential candidates on Mars and the Moon (Fig. 1), among them: a) most of the collapse chains here analyzed are sinuous and not related to tectonic lineaments; b) the minor axes *W* and depths *D* of the collapses are comparable along each chain, with *W* perpendicular to the tube development line; c) in most cases the deeper depression at the beginning of the chain could represent the feeding source of the tube; d) the presence of steeper overhanging and roundish skylights in the Martian chain in the Arsia examples and in Marius Hills B on the Moon indicates that between one collapse and the other there should be an intact portion of the lava tube. All these morphological and morphometric characteristics suggest that these collapse chains are genetically related and clearly different from pit chains formed along

tectonic dilational faults, grabens and dike swarms (e.g. Ferrill et al., 2004; Wyrick et al., 2004) (Fig. 4).

However, while morphologies and elevation profiles (Fig. 4) are strikingly similar, the morphometric range is mainly homogeneous in each planetary body, but significantly differs among Earth, Mars, and the Moon (Fig. 6). The minor axis *W* of the collapses shows a relevant increasing trend from Earth (maximum few tens of m), to Mars (from 40 to 400 m), and to the Moon (500-900 m) (Fig. 6A). The average linear volume of the collapses follows the same trend in all three planetary bodies, being up to 80 times bigger on Mars than on Earth, and with the greatest magnitude on the Moon, which presents collapses from 300 to 700 times bigger than on Earth (Fig. 6B; Table 4).

Aside from the dimensions, drastically increasing from Earth to Mars and to the Moon, also width/depth ratio *AR* varies considerably (Fig. 7B). This parameter provides information on the expected eccentricity of the conduit, which in turn is related to its genetic mechanisms. On Earth the variation in *AR* from Kazumura, Corona and Undara (respectively 1.4, 3.9 and 5 to 6; Table 4), are certainly related to different processes of tube emplacement (overcrusting versus inflation) and effusion rates (Kauahikaua et al., 1998; Kempe et al., 2010; Orr et al., 2015). The different volumetric factor *f* between collapses and intact tube linear volumes (V_1t) in the three examples is also an expression of the emplacement process. Surely there is a difference not only in effusion rates but also in the speleogenesis of the three terrestrial examples: Kazumura was formed through a combination of overcrusting of small channels and shallow inflation evolving in a master tube (Allred and Allred, 1997) entrenched by thermal erosion (emplacement driven by gravity flow), the formation of the other considered terrestrial tubes, Corona and Undara, is related to deeper and more persistent inflation processes (Tonello, 2017; Whitehead, 2010) (emplacement driven by pressure flow). In these two latter cases, the difference in dimensions between the still intact tube and the wider collapses is related to flow overpressure and lateral thermic erosion in specific sections of the tube forming wider areas that have collapsed as soon as the internal pressure decreased (Fig. 3). Undara represents an extreme example where tube pressure overflow filled lava lakes within the collapses, draining back inside the tube at the end of the eruption (Atkinson, 1991; Whitehead, 2010). Therefore, for analogy with the terrestrial cases, also on Mars and the

Moon *f* is expected to be close or minor to 1 in the case of channelized overcrusted tubes, and greater than 1 with the predominance of inflation processes.

Also on Mars the variability of width/depth ratio *AR* (Table 4) found in the different examples could be related to different lava tube genetic processes. Arsia North presents clear channel benches along its development and shows smaller dimensions and *AR* (2.8) compared to the other cases (Fig. 1G, 7B, Table 4), being comparable to the biggest terrestrial cases. The morphological characters point to an overcrusted origin of this tube, with smaller collapse chains with the same characteristics also in other areas of the northern flank of Arsia (Cushing 2012; for example the channels and associated collapses and skylights at -2.098/-122.150, -2.577°/-127.110, -0.467°/-123.606, Fig. 8). Small skylights along Arsia North could provide an easy access to the still intact segments of the tube (Fig. 1H).

On the other hand, the collapse chains along the lava flows of Arsia South, Olympus and Hadriaca do not show any surface expression aside of collapses and skylights (Fig. 1 I-M, Fig. 9), and have a range of *AR* (from 6 to 11) suggesting that the underlying lava tube might present a high degree of eccentricity in cross-section. Because of these characteristics this type of collapse chains are most probably related to a predominance of deep inflation controlled by the boundaries between pre-existing lava flows (Tonello, 2017). This hypothesis can be tested looking specifically at the collapse chain profile examined in Arsia South-A (Fig. 1I; Fig. 4). Here the depth of the original conduit is expected to follow the maximum depth of the collapses, which regularly decreases from the vent (70-50 m) to the distal part of the chain (30-20 m). This depth of emplacement is in agreement with lava flow thickness measured on the flanks of Arsia Mons (Mouginis-Mark and Rowland, 2008), suggesting that the lava tube is confined within lava flow boundaries. In addition, inflation is pressure-driven and therefore has the ability to inject the tube mainly along the existing most favorable inception horizons and not necessarily along the steepest slope, as can be observed in the lower part of Arsia South-B (Supplementary Figure 6). In Arsia these morphological characteristics seem to be repeated not only in Arsia South-A and Arsia South-B, but also in at least other two cases with starting vents and skylights to the southwest of the Arsia edifice (Fig. 9; at coordinates -14.876/-120.212, -14.949/-120.609). In addition the lava flows in this area present other 75 skylights,

Atypical Pit Craters, or cave entrance candidates registered in the MGC3 (Cushing, 2017). The average depth of the 37 skylights reported in MG3 that can be measured with the shadow method is 65 meters, supporting the hypothesis that a network of inflated tubes probably exists at these depths since this value represents the typical lava flow thickness on Arsia Mons (Mouginis-Mark and Rowland 2008). The morphologies of these collapse chains imply that on the southern apron of Arsia the emplacement of lava tubes was frequent and acting mainly in the subsurface through deep inflation.

Nonetheless, the high width/depth ratio *AR* of these Martian chains might be overestimated because of the partial infilling of the depressions with aeolian sediments (decreasing collapse depths), which appear to be ubiquitous from HiRISE images both in Arsia (Fig. 1L), Olympus and Hadriaca.

Looking to the skylights at Arsia North, most of these are occupied by aeolian sediment cones with heights of 10-20 meters in some places (Fig. 1H). Considering a similar thickness of the sediment infilling, the original *AR* is probably in the order of 1 or 2 instead of the observed 3, as happens in overcrusted terrestrial cases. Similarly, looking at the outcropping part of boulders from the collapsed roofs partially buried by aeolian sediments at the bottom of the two skylights in Arsia South-A and Arsia South-B (in average 10 m in diameter and protruding 2 m out of the sediments) it is possible to estimate the thickness of these deposits in the order of 5-10 meters. This value could be even higher for the more open collapses, suggesting that the original pre-infilling *AR* could be around 5-8 instead of 7-10, and thus more comparable to terrestrial deep inflated cases.

The collapse chain analyzed in Olympus presents similar characteristics to those in Arsia, but here the chain is splitting into two branches showing a braided pattern (Fig. 1N), which is typical of several terrestrial examples including some portions of Kazumura and Corona. On Hadriaca the chain also shares very similar characteristics (Fig. 1O) but the frequency of the collapses is much higher with a limited spacing between them. This means that most of the tube has collapsed and that erosion and weathering agents have partially obliterated its course, as described in general for the Hadriaca edifice (Williams et al., 2007).

As observed on inflated examples on Earth, intact tube dimension on Mars could be characterized by a scaling factor compared to the related collapses (Fig. 3). The volumetric scaling factor f is unknown for the Martian case but, considering by analogy f=1 for

overcrusted examples, we can estimate a linear tube volume of V_l $6*10^2$ for Arsia North (Fig. 7A), with conduit width *Wt* from 20 up to 70 m and heights *Ht* of the lava tube from 10 to 25 meters. If we apply a *f*=1 also for the other cases (Arsia South, Hadriaca and Olympus) we can estimate a linear tube volume range of V_l $6\text{-}21*10^3$ (Fig. 7A), with conduit width *Wt* from 100 up to 450 m (Fig. 6). Quite low heights of the lava tubes passages (*Ht*) are expected due to the high width/depth ratio *AR*, in the range of a few tens of meters. However, because inflation is prevailing, as in the inflation cases analyzed on Earth, an *f*>1 is a more realistic value, therefore these tubes could have linear volumes from three to six times smaller than the previous values.

These morphometric outcomes are in agreement with those found in sinuous ridges interpreted as shallow, only partially drained inflated tubes on Syria Planum (Zhao et al., 2017), showing typical width *W* of 300-500 m and low height of the inflated bulge of 10-20 m. This also confirms the typically high asymmetry ratio of the Martian lava tubes due to the predominant inflation process.

On the Moon the examined lava tube collapse chains are among the very few detected on lunar volcanic regions (Hurwitz et al., 2013). The collapse chains present the same morphological characteristics observed on Mars, but with volumes one order of magnitude greater (Table 3, Fig. 6 A-B-C). In addition, the width/depth ratios *AR* are lower than on Mars but still comparable to inflated examples on Earth (Fig. 7B). Lower *AR* are not surprising on the Moon because the higher effusion rates and the stronger thermal erosion (Williams et al., 2000; Wilson and Head III, 1983) facilitate the evolution of inflated tubes to entrenched conduits with lower eccentricity. Considering an *f*=1 it is possible to estimate a maximum linear lava tube volume V_lt of $4\text{-}14*10^4$ m^3, with tube width *Wt* ranging between 500 and 800 m and its height *Ht* of 80-190 m (Fig. 6-7). The *Ht* value is indeed confirmed by the Lunar Radar Sounder analysis of Kaguya in the Marius Hills region (Kaku et al., 2017), showing a comparable putative depth of the tube between 75 and 150 m. However, as explained in the case of Mars, also on the Moon *f* could have a slightly higher value if inflation processes are predominant, and the conduits could be from a half to one-third smaller than the above reported estimation.

All these lunar values for the collapses fit into the stability range as calculated by Blair et al. (2017) and Theinat et al. (2020) even considering roof thickness of few tens of meters and

conduits with an asymmetry ratio between 4 and 7. This could explain why collapse chains are not common on the Moon compared to Mars and we should expect the presence of several still intact conduits lying below the smooth Maria plains. Indeed collapse chains on the Moon are unlikely generated by gravitational instabilities and should require collapse triggers such as meteorite impacts (Martellato et al., 2013) or tectonic events. Indeed, all the lunar chains analyzed in this study are characterized by a non-gravity related collapse trigger candidate (Fig. 10): in Marius Hills A an important impact crater superposes and partially obliterates the chain (Figures 1Q, 10A), while in Marius Hills B and Gruithuisen a wrinkle ridge partially follows or crosses the collapse chains (Fig. 1P-R; see also Supplementary figures 10-11-12). It is hence possible that those chains formed during the tectonic activity of those structures. In addition an impact has also been proven as collapse trigger for the Marius Hills skylight studied by Robinson et al. (Fig. 10D)(Martellato et al., 2013; Robinson et al., 2012). Hence, our results suggest that below the main rilles of the Marius Hills plateau there could be intact tubes with dimensions comparable to those estimated for the collapse chains of Marius Hills A and B. Recent studies on the morphology and genesis of Rima Rilles have shown the high probability that this feature could also be related to the continuous collapse of a lava tube (Roberts and Tracy, 2019). Dimensions (*W* and *H*) are comparable to our results, in the hypothesis that the ceiling was not thick enough to remain stable after the draining. In this specific case, Sakimoto and Gregg (2019) modelled the thermal erosion and flow showing that in order to create such feature a closed ceiling tunnel is much more effective thermally than an open channel. All these data suggest that some deeper lunar rills could represent original tubes that collapsed right after the draining and other shallower ones, like in Marius Hills, could represent the still intact ceiling of intact tubes.

Considering together the percentage of intact tube segments along the chains and the linear volume estimations (Table 5), we can calculate that below the overcrusted example examined on Mars there could be almost $3*10^7$ cubic meters of intact voids. In inflated Martian cases this value rises to a maximum of $10*10^7$. The volume value increases even by one order of magnitude for the lunar cases, reaching up to $12*10^8$ cubic meters for the Gruithuisen case. If we consider the possible existence of lava tubes still intact all along their full development below the surface of the Moon and thus with length and V_1

comparable to the Gruithuisen case, accessible tunnel-like voids on Moon Maria might easily reach up to 8-10 billions of cubic meters opening new intriguing scenarios for future exploration and utilization.

8. Future space missions for lava tube detection and exploration

The comparative analysis and the morphological similarities presented in this review show a great potential for exploration of enormous intact lava tubes on the Moon and, on a less extent, Mars. However these outcomes are mainly based on comparison with terrestrial cases, while direct evidences are still limited. Aside of the radar signals reported by Kaku et al. (2017), and the gravity anomalies detected by GRAIL (Chappaz et al., 2017), we do not have yet a clear understanding on the lava tube extent and genetic processes underneath Moon Maria. The same applies for Mars, where the Shallow Radar (SHARAD on board MRO) sections have not yet proven the presence of subsurface lava tubes because of an inappropriate resolution and coverage (Perry et al., 2019; Bardabelias et al., 2020).

In the last two decades, several scientists have proposed mission scenarios to access candidate lava tube entrances to verify the presence of subsurface caves (Blamont, 2014). On the Moon most of the attention has been focused on the pits of Marius Hills and Mare Tranquillitatis (Wagner and Robinson, 2014), following scientific objectives driven mainly by the uniqueness of the outcrop exposure along the pit walls, rather than for their potential of accessing much bigger underground voids (Kerber et al., 2018). On Mars, a robotic mission to these features is still problematic, because of the time delay in operations, the required autonomy in navigation and problems related to landing in the high volcanic plateaus of the Tharsis volcanic region.

This review emphasizes the need of specific remote sensing and ground truth data to finally assess the existence of lava tubes and their genetic processes on the different planetary bodies. The morphometric data provided here could be the starting point for dedicated missions aiming to detect and measure dimensions - depth and width at the least - of intact sections of lava tubes on the Moon and Mars.

In this regard, several new specific satellite mission approaches have been recently proposed: ground penetrating radar from orbiters (Sood et al., 2016; Carrer et al., 2018)

small satellites arrays for multi-frequency radar sounding (Carrer et al 2019), and the very promising use of passive sounding through radio emissions from Sun and Jupiter (Romero-Wolf et al., 2020). Also the deployment of surface rover missions dedicated to subsurface analysis, with specific geophysical instruments, could provide definitive proofs of the existence of these voids and information on their subsurface development (Caroll et al., 2015). On the other hand, robotic missions devoted to the direct exploration of skylights could only confirm the existence of the tubular cavities, but probably their capability of accessing relevant parts of the cave would still be very limited. A roadmap for subsurface exploration of the Moon and Mars is strongly needed, and should involve ground penetrating remote sensing before carrying out robotic approaches below ground.

9. Conclusions

In conclusion, this review and the morphometric study show that terrestrial lava tube collapse chains present striking morphological similarities with those proposed here as candidates on Mars and the Moon. However, dimensions and morphometric parameters like width/depth ratio *AR* have peculiar ranges each pertaining a different planetary body. Volumes of collapses and related conduits show increasing orders of magnitude from Earth, to Mars and to the Moon (Fig. 7). The minor axis *W* of the collapses shows a relevant increasing trend from Earth (maximum 20-30 m), to Mars (from 40 to 400 m), and to the Moon (500-900 m) (Fig. 6). The average linear volume of the collapses follows the same trend in all three planetary bodies, being almost 80 times bigger on Mars than on Earth, and with the greatest magnitude on the Moon, which presents collapses from 300 to 700 times bigger than on Earth (Tab. 4). This increasing trend of lava tube size from Earth to Mars and the Moon can be correlated to the different gravity parameters of each planetary body. Lower gravity bodies present higher effusion rates and longer and thicker lava flows, favoring the emplacement of flood basalts where pressure flow prevails over gravity flow (Wilson and Head III). Also lower gravity allows the emplacement of wider conduits within the stability threshold also favoring the emplacement of lava tubes instead of open lava channels.

AR values suggest that both overcrusted and inflation cases are present on Mars, while on the Moon deep inflation is probably predominant but thermal erosion could have favored a lower eccentricity because of the higher effusion rates and longer duration of the eruptions (Wilson and Head III, 1983). The size estimation indicates that on the Moon, the typical volume $V_l t$ and *AR* of lava tubes with ceiling thickness of some tens of meters are not high enough to reach the roof instability threshold and cause collapse, as often happens on Earth and Mars. Indeed, on Mars intact portions of lava tubes surely exist, especially in overcrusted examples, but in most cases the biggest deep inflated tubes present more frequent collapses due to the higher width/depth ratio *AR* although aeolian dusts could have partially filled them.

Therefore, among the three planetary bodies, the Moon presents the highest potential for lava tube development and conservation. Most of its tubes are probably intact and stable along their full length exceeding a total volume of some billions of cubic meters each, but with few accessible entrances from the surface. These impressive volumetric values clearly show how future space missions devoted to the investigation of these voids could open a promising era of subsurface lunar and Martian exploration and a completely new perspective in planetary exploration.

Acknowledgments

We would like to thank Kevin Allred, Doug Medville, Peter Bannink and the Hawai'i Speleological Survey for providing the Kazumura Atlas for this study. Our gratitude goes to the Leica and VIGEA for the support provided in the realization of the TLS survey of the Corona lava tube, together with the survey operators Marta Lazzaroni, Umberto Del Vecchio, Norma Damiano, Ivana Guidone, , Farouk Kadded, Raphael Goudard and Marco Camorani. Our gratitude goes also to all ESA staff organizing and supporting the ESA PANGAEA-X program in whose framework part of the TLS survey has been performed. We would also like to thank Austin Jackson, Robbie Shone and Armstrong Osborne for providing photographs of different lava tubes on Earth. Thanks also to Samuel Payler for reviewing the text and to Prof. Jay Melosh and one other anonymous reviewer for the positive comments that allowed for further improvements of the final manuscript. Author contributions: FS contributed in concept, data elaboration, writing of the original draft, and

figure elaboration; RP contributed in concept, methodology, formal analysis, writing and figure elaboration; MM contributed with data interpretation and writing; PdB contributed with data acquisition and elaboration; TS contributed in the TLS surveys, methods, data and figures elaboration; JdW contributed with concept development and writing; Competing interests: Authors declare no competing interests; Data and materials availability: All data are available in the main text or in the Supplementary material.

References

Allred, K. and Allred, C., 1997. Development and morphology of Kazumura cave, Hawaii. Journal of Caves and Karst Studies, 59: 67-80.

Allred, K., Allred, C. and Richards, R., 1997. Kazumura Cave Atlas, Island of Hawai ʻi. Special Publication Hawai ʻi Speleological Survey, National Speleological Society, Huntsville, AL, 81.

Allred, K., Allred, C. and Richards, R., 2002. Kazumura Cave Atlas, Island of Hawai ʻi. Special Publication of the Hawaii Speleological Survey.

Ansan, V. and Mangold, N., 2013. 3D morphometry of valley networks on Mars from HRSC/MEX DEMs: Implications for climatic evolution through time. Journal of Geophysical Research: Planets, 118(9): 1873-1894.

Atkinson, A., 1991. The Undara lava tube system, North Queensland, Australia: Updated data and notes on mode of formation and possible lunar analogue, Proc. 6th Intern. Symp Volcanospeleol., Hilo, pp. 95-120.

Atkinson, A. and Atkinson, V., 1995. Undara Volcano and its lava tubes: a geological wonder of Australia in Undara Volcanic National Park, North Queensland. Vernon and Anne Atkinson.

Atkinson, A., Griffin, T. and Stephenson, P., 1975. A major lava tube system from Undara Volcano, North Queensland. Bulletin Volcanologique, 39(2): 266-293.

Bailen, M., Herkenhoff, K., Howington-Kraus, A. and Becker, K., 2015. Finding stereo pairs with the Pds planetary image locator tool (Pilot), Second Planetary Data Workshop.

Bardabelias, N.M., Holt, J.W. and Christoffersen, M.S., 2020. Potential Detection of martian Lava Tubes from Mars Global Cave Candidate Catalog Skylight Locations Using SHARAD. LPICo, 2197, p.1068.

Barker, M., Mazarico, E., Neumann, G., Zuber, M., Haruyama, J. and Smith, D., 2016. A new lunar digital elevation model from the Lunar Orbiter Laser Altimeter and SELENE Terrain Camera. Icarus, 273: 346-355.

Beyer, R., Alexandrov, O. and Moratto, Z., 2014. Aligning terrain model and laser altimeter point clouds with the Ames Stereo Pipeline, Lunar and Planetary Science Conference, pp. 2902.

Blair, D.M., Chappaz, L., Sood, R., Milbury, C., Bobet, A., Melosh, H.J., Howell, K.C. and Freed, A.M., 2017. The structural stability of lunar lava tubes. Icarus, 282: 47-55.

Blamont, J., 2014. A roadmap to cave dwelling on the Moon and Mars. Advances in Space Research, 54(10): 2140-2149.

Boston, P., Frederick, R., Welch, S., Werker, J., Meyer, T., Sprungman, B., Hildreth-Werker, V. and Thompson, S., 2004. Extraterrestrial subsurface technology test bed: Human use and scientific value of martian caves, AIP Conference Proceedings. American Institute of Physics, pp. 1007-1018.

Boston, P., Spilde, M., Northup, D., Melim, L., Soroka, D., Kleina, L., Lavoie, K., Hose, L., Mallory, L. and Dahm, C., 2001. Cave biosignature suites: microbes, minerals, and Mars. Astrobiology, 1(1): 25-55.

Bunnell, D., 2008. Caves of Fire: Inside America's Lava Tubes. National Speleological Society.

Burns, J.A., 2010. The four hundred years of planetary science since Galileo and Kepler. Nature, 466(7306): 575.

Calvari, S., Pinkerton, H., 1998. Formation of lava tubes and extensive flow field during the 1991-1993 eruption of Mount Etna. Journal of Geophysical Researches. 103: 27291-27301.

Calvari, S. and Pinkerton, H., 1999. Lava tube morphology on Etna and evidence for lava flow emplacement mechanisms. Journal of Volcanology and Geothermal Research, 90(3-4): 263-280.

Carr, M., Greeley, R., Blasius, K., Guest, J. and Murray, J., 1977. Some martian volcanic features as viewed from the Viking orbiters. Journal of Geophysical Research, 82(28): 3985-4015.

Carr, M.H., 1973. Volcanism on mars. Journal of Geophysical Research, 78(20): 4049-4062.

Carracedo, J., Singer, B., Jicha, B., Guillou, H., Badiola, E.R., Meco, J., Torrado, F.P., Gimeno, D., Socorro, S. and Láinez, A., 2003. La erupción y el tubo volcánico del Volcán Corona (Lanzarote, Islas Canarias). Estudios Geológicos, 59(5-6): 277-302.

Carrer, L., Gerekos, C. and Bruzzone, L., 2018. A multi-frequency radar sounder for lava tubes detection on the Moon: Design, performance assessment and simulations. Planetary and Space Science, 152, pp.1-17.

Carrer, L., Gerekos, C., Bovolo, F. and Bruzzone, L., 2019. Distributed Radar Sounder: A Novel Concept for Subsurface Investigations Using Sensors in Formation Flight. IEEE Transactions on Geoscience and Remote Sensing, *57*(12), pp.9791-9809.

Carroll, K.A., Hatch, D., Ghent, R., Stanley, S., Urbancic, N., Williamson, M.C., Garry, W.B. Talwani, M., 2015, March. Exploring Subsurface Lunar Voids Using Surface Gravimetry. In Lunar and Planetary Science Conference, Vol. 46, p. 1746.

Chahine, M.T., A'Hearn, M.F., Rahe, J., Solomon, P. and Nickle, N.L., 2010. Comparative Planetology with an Earth Perspective. Springer.

Chappaz, L., Sood, R., Melosh, H.J., Howell, K.C., Blair, D.M., Milbury, C. and Zuber, M.T., 2017. Evidence of large empty lava tubes on the Moon using GRAIL gravity. Geophysical Research Letters, 44(1): 105-112.

Cooper. K.M., Kauahikaua, J.P., 1992. Morphology of extinct lava tubes and the implications for tube evolution, Chain of Craters Road, Hawaii Volcanoes National Park, Hawaii. US Geol Surv Open-File Report 92-352, pp 1-44.

Cruikshank, D. and Wood, C., 1972. Lunar rilles and Hawaiian volcanic features: Possible analogues. The Moon, 3(4): 412-447.

Cushing, G.E., 2012. Candidate cave entrances on Mars. Journal of Cave and Karst Studies, 74(1): 33-47.

Cushing, G.E., 2017. Mars Global Cave Candidate Catalog (MGC3), Astrobiology Science Conference (LPI Contrib. No. 1965).

Cushing, G.E., Titus, T., Wynne, J. and Christensen, P., 2007. THEMIS observes possible cave skylights on Mars. Geophysical Research Letters, 34(17).

Cushing, G.E., Okubo, C.H. and Titus, T.N., 2015. Atypical pit craters on Mars: New insights from THEMIS, CTX, and HiRISE observations. Journal of Geophysical Research: Planets, 120(6):1023-1043.

De Toffoli, B., Pozzobon, R., Massironi, M., Mazzarini, F., Conway, S. and Cremonese, G., 2019. surface expressions of subsurface sediment Mobilization Rooted into a Gas Hydrate-Rich Cryosphere on Mars. Scientific reports, 9(1), pp.1-9.

Dragoni, M., Piombo, A. and Tallarico, A., 1995. A model for the formation of lava tubes by roofing over a channel. Journal of Geophysical Research: Solid Earth, 100(B5): 8435-8447.

Duncan, A.M., Guest, J.E., Stofan, E.R., Anderson, S.W., Pinkerton, H. and Calvari, S., 2004. Development of tumuli in the medial portion of the 1983 aa flow-field, Mount Etna, Sicily. Journal of Volcanology and Geothermal Research, 132: 173-187.

Fagents, S.A. and Greeley, R., 2001. Factors influencing lava-substrate heat transfer and implications for thermomechanical erosion. Bulletin of Volcanology, 62(8): 519-532.

Favre, G., 1993. Some observations of Hawaiian pit craters and relations with lava tubes, Proceedings of the 3rd International Symposium on Vulcanospeleology. International Speleological Foundation Seattle, Wash, pp. 37-41.

Ferrill, D.A., Wyrick, D.Y., Morris, A.P., Sims, D.W. and Franklin, N.M., 2004. Dilational fault slip and pit chain formation on Mars. GsA Today, 14(10): 4-12.

Ferrill, D.A., Wyrick, D.Y. and Smart, K.J., 2011. Coseismic, dilational-fault and extension-fracture related pit chain formation in Iceland: Analog for pit chains on Mars. Lithosphere, 3(2): 133-142.

Gaddis, L., Anderson, J., Becker, K., Becker, T., Cook, D., Edwards, K., Eliason, E., Hare, T., Kieffer, H. and Lee, E., 1997. An overview of the integrated software for imaging spectrometers (ISIS), Lunar and Planetary Science Conference, pp. 387.

Greeley, R., 1971a. Lava tubes and channels in the lunar Marius Hills. The Moon, 3(3): 289-314.

Greeley, R., 1971b. Observations of actively forming lava tubes and associated structures, Hawaii.

Greeley, R., Fagents, S.A., Harris, R.S., Kadel, S.D., Williams, D.A. and Guest, J.E., 1998. Erosion by flowing lava: Field evidence. Journal of Geophysical Research: Solid Earth, 103(B11): 27325-27345.

Halliday, W., 2004. Volcanic caves. Encyclopedia of Caves and Karst Science. Fitzroy Dearborn, New York, 760: 764.

Haruyama, J., Morota, T., Kobayashi, S., Sawai, S., Lucey, P.G., Shirao, M. and Nishino, M.N., 2012. Lunar holes and lava tubes as resources for lunar science and exploration, Moon. Springer, pp. 139-163.

Hon, K.E.N., Kauahikaua, J.I.M., Denlinger, R. and Mackay, K., 1994. Emplacement and inflation of pahoehoe sheet flows: Observations and measurements of active lava flows on Kilauea Volcano, Hawaii. Geological Society of America Bulletin, *106*(3): 351-370.

Hróarsson, B., & Jónsson, S. S., 1991. Lava Caves in the Hallmundarhraun Lava Flow, Western Iceland. In *Proceedings of the 6 th International Symposium on Vulcanospeleology*, pp. 85-88.

Hurwitz, D.M., Head, J.W. and Hiesinger, H., 2013. Lunar sinuous rilles: distribution, characteristics, and implications for their origin. Planetary and Space Science, 79: 1-38.

Jackson, J.A., 2005. Glossary of Geology, by JA Jackson. 2005 Approx. 900 p. 5th revised and enlarged ed. ISBN 3-540-27951-2. Berlin: Springer, 2005.: 5th.

Jorda-Bordehore, L., Toulkeridis, T., Romero-Crespo, P. L., Jordá-Bordehore, R., & García-Garizabal, I. (2016). Stability assessment of volcanic lava tubes in the Galápagos using engineering rock mass classifications and an empirical approach. *International Journal of Rock Mechanics and Mining Sciences*, *89*, 55-67.

Kaku, T., Haruyama, J., Miyake, W., Kumamoto, A., Ishiyama, K., Nishibori, T., Yamamoto, K., Crites, S.T., Michikami, T. and Yokota, Y., 2017. Detection of intact lava tubes at marius hills on the moon by selene (kaguya) lunar radar sounder. Geophysical Research Letters, 44(20).

Kauahikaua, J., Cashman, K.V., Mattox, T.N., Heliker, C.C., Hon, K.A., Mangan, M.T. and Thornber, C.R., 1998. Observations on basaltic lava streams in tubes from Kilauea Volcano, island of Hawai'i. Journal of Geophysical Research: Solid Earth, 103(B11): 27303-27323.

Kempe, S., 2012. Volcanic rock caves, Encyclopedia of Caves (Second Edition). Elsevier, pp. 865-873.

Kempe, S., 2019. Volcanic rock caves, Encyclopedia of Caves (Third edition). Academic Press, pp. 1118-1127.

Kempe, S., Bauer, I., Bosted, P., Coons, D. and Elhard, R., 2010. Inflationary versus crusted-over roofs of pyroducts (lava tunnels), Proceedings 14th International Symposium on Vulcanospeleology, pp. 93.

Kerber, L., Nesnas, I., Keszthelyi, L., Head, J., Denevi, B., Hayne, P., Mitchell, K., Ashley, J., Whitten, J. and Stickle, A., 2018. Moon diver: A discovery mission concept for understanding the history of the mare basalts through the exploration of a lunar mare pit, New Views of the Moon 2-Asia.

Leone, G., 2014. A network of lava tubes as the origin of Labyrinthus Noctis and Valles Marineris on Mars. Journal of Volcanology and Geothermal Research, 277: 1-8.

Léveillé, R.J. and Datta, S., 2010. Lava tubes and basaltic caves as astrobiological targets on Earth and Mars: a review. Planetary and Space Science, 58(4): 592-598.

Malin, M.C., Bell, J.F., Cantor, B.A., Caplinger, M.A., Calvin, W.M., Clancy, R.T., Edgett, K.S., Edwards, L., Haberle, R.M. and James, P.B., 2007. Context camera investigation on board the Mars Reconnaissance Orbiter. Journal of Geophysical Research: Planets, 112(E5).

Martellato, E., Foing, B. and Benkhoff, J., 2013. Numerical modelling of impact crater formation associated with isolated lunar skylight candidates on lava tubes. Planetary and Space Science, 86: 33-44.

McCall, G., 1970. Lunar rilles and a possible terrestrial analogue. Nature, 225(5234): 714-716.

Mège, D., Cook, A.C., Garel, E., Lagabrielle, Y. and Cormier, M.H., 2003. Volcanic rifting at martian grabens. Journal of Geophysical Research: Planets, 108(E5).

Michalski, J.R., Onstott, T.C., Mojzsis, S.J., Mustard, J., Chan, Q.H., Niles, P.B. and Johnson, S.S., 2018. The martian subsurface as a potential window into the origin of life. Nature Geoscience, *11*(1), pp.21-26.

Montoriol-Pous, J. and de Mier, J., 1974. Estudio vulcanoespeleológico de la Cueva del Viento (Icod de los Vinos, Isla de Tenerife, Canarias). Speleon, 21: 5-24.

Moratto, Z., Broxton, M., Beyer, R., Lundy, M. and Husmann, K., 2010. Ames Stereo Pipeline, NASA's open source automated stereogrammetry software, Lunar and Planetary Science Conference, pp. 2364.

Mouginis-Mark, P.J. and Rowland, S.K., 2008. Lava flows at Arsia Mons, Mars: Insights from a graben imaged by HiRISE. Icarus, 198(1): 27-36.

Oberbeck, V.R., 1969. On the origin of lunar sinuous rilles. Modern Geology, 1: 75.

Okubo, C.H. and Martel, S.J., 1998. Pit crater formation on Kilauea volcano, Hawaii. Journal of Volcanology and Geothermal Research, 86(1-4): 1-18.

Orr, T.R., Bleacher, J.E., Patrick, M.R. and Wooten, K.M., 2015. A sinuous tumulus over an active lava tube at Kīlauea Volcano: Evolution, analogs, and hazard forecasts. Journal of Volcanology and Geothermal Research, 291: 35-48.

Pedersen, G.B.M., Höskuldsson, A., Dürig, T., Thordarson, T., Jonsdottir, I., Riishuus, M.S., Óskarsson, B.V., Dumont, S., Magnússon, E., Gudmundsson, M.T. and Sigmundsson, F., 2017. Lava field evolution and emplacement dynamics of the 2014–2015 basaltic fissure eruption at Holuhraun, Iceland. Journal of Volcanology and Geothermal Research, *340*, pp.155-169.

Perry, M.R., Bain, Z.M., Crown, D.A., Scheidt, S.P. and Nunes, D.E., 2019. Detection and characterization of intact lava tubes on the western flank of Alba Mons in Mars Reconnaissance Orbiter Shallow Radar (SHARAD) Data. LPI Contributions, *2089*, p.6405.

Peterson, D.W., Swanson, D.A., 1974, Observed formation of lava tubes during 1970-71 at Kilauea Volcano, Hawaii. Studies in Speleology 2: 209-222

Peterson, D.W., Holcomb, R.T., Tilling, R.I. and Christiansen, R.L., 1994. Development of lava tubes in the light of observations at Mauna Ulu, Kilauea Volcano, Hawaii. Bulletin of Volcanology, 56(5): 343-360.

Plescia, J., 2004. Morphometric properties of martian volcanoes. Journal of Geophysical Research: Planets, 109(E3).

Pozzobon, R., Mazzarini, F., Massironi, M. and Marinangeli, L., 2015. Self-similar clustering distribution of structural features on Ascraeus Mons (Mars): implications for magma chamber depth. Geological Society, London, Special Publications, *401*(1), pp.203-218.

Pozzobon, R., Salvini, S., Mazzoli, C., Massironi, M. and Sauro, F., 2018. A DTM-based volume extraction approach: from micro-scale weathering forms to planetary lava tubes, EGU General Assembly 2018, Vienna, pp. EGU2018-8843.

Pozzobon, R., Mazzarini, F., Massironi, M., Rossi, A.P., Pondrelli, M., Cremonese, G. and Marinangeli, L., 2019. Fluids mobilization in Arabia Terra, Mars: Depth of pressurized reservoir from mounds self-similar clustering. *Icarus*, *321*, pp.938-959.

Pozzobon, R., Mazzoli, C., Salvini, S., Sauro, F., Massironi, M., Santagata, T., 2020. A DTM-based volume extraction approach: from micro-scale weathering forms to planetary lava tubes". 3D digital geological models: from terrestrial outcrops to planetary surfaces, AGU books, in press.

Roberts, C. E., Gregg T. K.P., 2019. Rima Marius, the Moon: Formation of lunar sinuous rilles by constructional and erosional processes. Icarus, 317: 682-688.

Robinson, M., Ashley, J., Boyd, A., Wagner, R., Speyerer, E., Hawke, B.R., Hiesinger, H. and Van Der Bogert, C., 2012. Confirmation of sublunarean voids and thin layering in mare deposits. Planetary and Space Science, 69(1): 18-27.

Robinson, M., Brylow, S., Tschimmel, M., Humm, D., Lawrence, S., Thomas, P., Denevi, B., Bowman-Cisneros, E., Zerr, J. and Ravine, M., 2010. Lunar reconnaissance orbiter camera (LROC) instrument overview. Space science reviews, 150(1-4): 81-124.

Rossi, M.J., 1997. Morphology of the 1984 open-channel lava flow at Krafla volcano, northern Iceland. Geomorphology, 20(1-2): 95-112.

Rubin, A.M., 1992. Dike - induced faulting and graben subsidence in volcanic rift zones. Journal of Geophysical Research: Solid Earth, 97(B2): 1839-1858.

Sakimoto, S.E., Crisp, J. and Baloga, S.M., 1997. Eruption constraints on tube - fed planetary lava flows. Journal of Geophysical Research: Planets, 102(E3): 6597-6613.

Sakimoto, S. E. H., Gregg, T. K. P., 2019, March. On the Formation of Lunar Sinuous Rilles: Insights from Multiphysics Modeling Techniques. Lunar and Planetary Science Conference (50).

Santagata, T., Sauro, F., Massironi, M., Pozzobon, R., Del Vecchio, U., Lazzaroni, M., Damiano, N., Tonello, M., Tomasi, I., Martínez-Frìas, J. and Mateo Medero, E., 2018. Subsurface laser scanning and photogrammetry in the Corona Lava Tube System, Lanzarote, Spain, EGU General Assembly 2018, pp. EGU2018-5290.

Sauro, F., Pozzobon, R., Santagata, T., Tomasi, I., Tonello, M., Martínez-Frías, J., Smets, L.M.J., Gómez, G.D.S. and Massironi, M., 2019. Volcanic Caves of Lanzarote: A Natural Laboratory for Understanding Volcano-Speleogenetic Processes and Planetary Caves, Lanzarote and Chinijo Islands Geopark: From Earth to Space. Springer, pp. 125-142.

Scott, E.D. and Wilson, L., 2002. Plinian eruptions and passive collapse events as mechanisms of formation for martian pit chain craters. Journal of Geophysical Research: Planets, 107(E4).

Shean, D.E., Alexandrov, O., Moratto, Z.M., Smith, B.E., Joughin, I.R., Porter, C. and Morin, P., 2016. An automated, open-source pipeline for mass production of digital elevation models (DEMs) from very-high-resolution commercial stereo satellite imagery. ISPRS Journal of Photogrammetry and Remote Sensing, 116: 101-117.

Smart, K.J., Wyrick, D.Y. and Ferrill, D.A., 2011. Discrete element modeling of martian pit crater formation in response to extensional fracturing and dilational normal faulting. Journal of Geophysical Research: Planets, 116(E4).

Sood, R., Melosh, H.J. and Howell, K., 2016. Lunar advanced radar orbiter for subsurface sounding (LAROSS): Lava tube exploration mission. In AAS/AIAA 26th Space Flight Mechanics Meeting.

Theinat, A.K., Modiriasari, A., Bobet, A., Melosh, H.J., Dyke, S.J., Ramirez, J., Maghareh, A. and Gomez, D., 2020. Lunar lava tubes: Morphology to structural stability. Icarus, 338: 113442.

Tonello, M., 2017. Origin and evolution of an inflated lava tube between the Mio-Pliocene volcanic complex of Famara and the Quaternary lava flows of La Corona in Lanzarote. , University of Padova, 111 pp.

Torson, J. and Becker, K., 1997. ISIS-A software architecture for processing planetary images, Lunar and Planetary Science Conference, pp. 1443.

Wagner, R. and Robinson, M., 2019. 3D Modeling of Lunar Pit Walls from Stereo Images, Lunar and Planetary Science Conference.

Wagner, R.V. and Robinson, M.S., 2014. Distribution, formation mechanisms, and significance of lunar pits. Icarus, 237: 52-60.

Watters, T.R., Robinson, M.S., Banks, M.E., Tran, T. and Denevi, B.W., 2012. Recent extensional tectonics on the Moon revealed by the Lunar Reconnaissance Orbiter Camera. Nature Geoscience, 5(3): 181.

Whitehead, P.W., 2010. The regional context of the McBride Basalt Province and the formation of the Undara Lava flows, tubes, rises and depressions. Organising Group, 14th International Symposium on Vulcanospeleology.

Wilkens, H., Iliffe, T.M., Oromí, P., Martínez, A., Tysall, T.N. and Koenemann, S., 2009. The Corona lava tube, Lanzarote: geology, habitat diversity and biogeography. Marine Biodiversity, 39(3): 155-167.

Williams, D.A., Fagents, S.A. and Greeley, R., 2000. A reassessment of the emplacement and erosional potential of turbulent, low - viscosity lavas on the Moon. Journal of Geophysical Research: Planets, 105(E8): 20189-20205.

Williams, D.A., Greeley, R., Zuschneid, W., Werner, S.C., Neukum, G., Crown, D.A., Gregg, T.K., Gwinner, K. and Raitala, J., 2007. Hadriaca Patera: insights into its volcanic history from Mars express high resolution stereo camera. Journal of Geophysical Research: Planets, 112(E10).

Williams, K., McKay, C.P., Toon, O. and Head, J.W., 2010. Do ice caves exist on Mars? Icarus, 209(2): 358-368.

Wilson, L., Hawke, B.R., Giguere, T.A. and Petrycki, E.R., 2011. An igneous origin for Rima Hyginus and Hyginus crater on the Moon. Icarus, 215(2): 584-595.

Wilson, L. and Head III, J.W., 1983. A comparison of volcanic eruption processes on Earth, Moon, Mars, Io and Venus. Nature, 302(5910): 663.

Wilson, L. and Head III, J.W., 2002. Tharsis - radial graben systems as the surface manifestation of plume - related dike intrusion complexes: Models and implications. Journal of Geophysical Research: Planets, 107(E8): 1-1-1-24.

Wood, J., 1996. The geomorphological characterisation of digital elevation models, University of Leicester, Leicester.

Wyrick, D., Ferrill, D.A., Morris, A.P., Colton, S.L. and Sims, D.W., 2004. Distribution, morphology, and origins of martian pit crater chains. Journal of Geophysical Research: Planets, 109(E6).

Zhao, J., Huang, J., Kraft, M.D., Xiao, L. and Jiang, Y., 2017. Ridge-like lava tube systems in southeast Tharsis, Mars. Geomorphology, 295: 831-839.

Figures

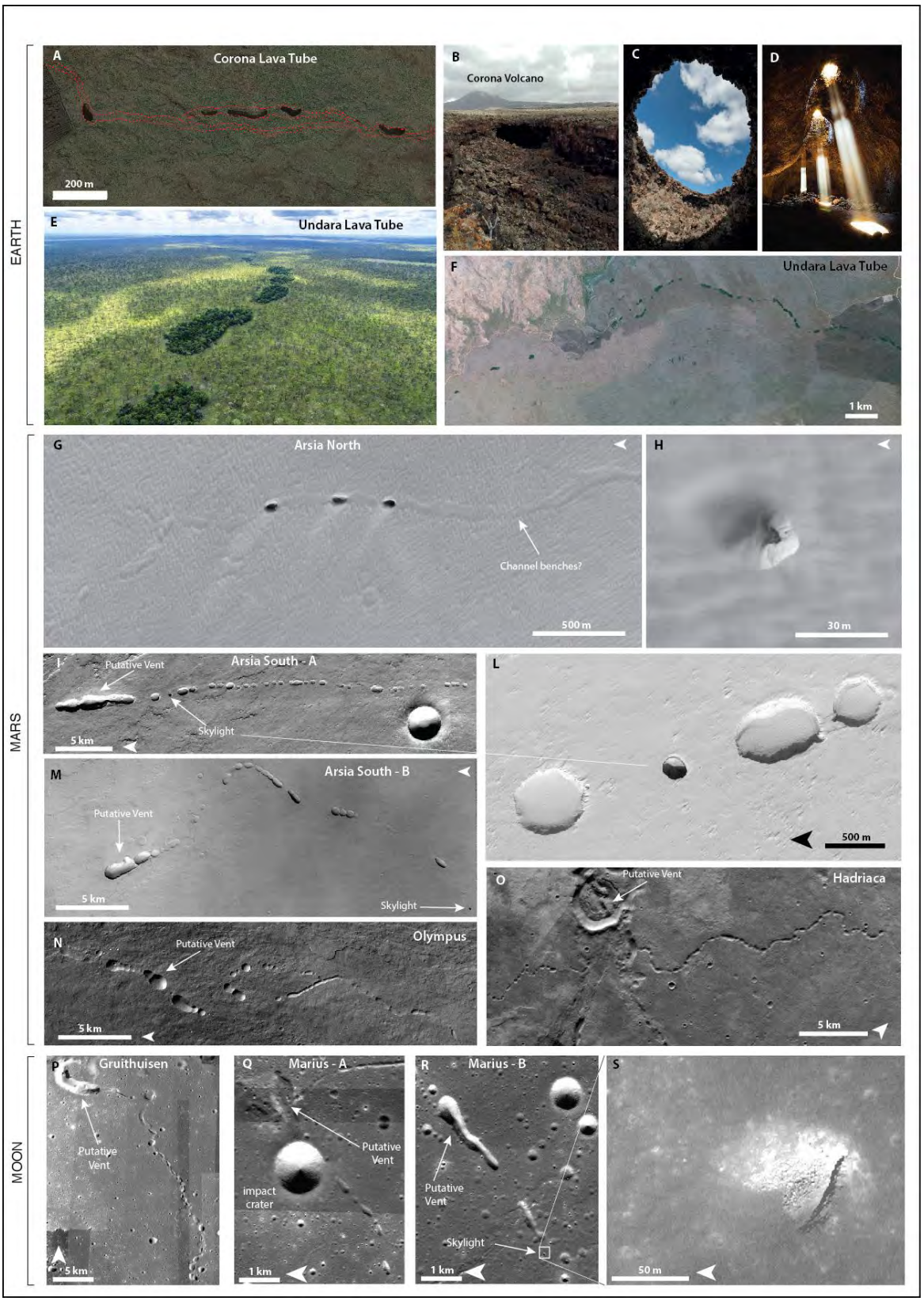
EARTH
MARS
MOON
A
Corona Lava Tube
200 m
B
Corona Volcano
C
D
E
Undara Lava Tube
F
Undara Lava Tube
1 km
G
Arsia North
Channel benches?
500 m
H
30 m
I
Putative Vent
Arsia South - A
Skylight
5 km
L
500 m
M
Arsia South - B
Putative Vent
5 km
Skylight
O
Putative Vent
Hadriaca
5 km
N
Putative Vent
Olympus
5 km
P
Gruithuisen
Putative Vent
5 km
Q
Marius - A
Putative Vent
impact crater
1 km
R
Marius - B
Putative Vent
Skylight
1 km
S
50 m

Fig. 1. Morphologies of lava tube collapse chains on Earth, Mars and the Moon. A) Satellite image of the collapse chains of the Corona lava tube showing the relationships between the subsurface tube development and collapses (red dotted lines represent the sidewalls of the tube surveyed with laser scanner). B) The *Jameo de la Puerta Falsa* (Corona lava tube) represents a typical elongated collapse with steep side slopes and overhanging walls at the two entrances to the intact lava tube. C) The *Jameo de La Gente* (Corona lava tube) shows vertical walls, steep slopes at the bottom and a less elongated shape in plan view. D) A series of three aligned skylights in the "Skylight Lava Tube" in Oregon (USA, photo A. Jackson): these holes in the ceiling of the conduit present a much smaller width compared to the intact tube. E-F) Collapse of the Undara Lava Tube are easily recognizable from air and satellite images because of the different vegetation. G-O) Examples of Martian lava tube candidate collapse chains in Arsia and Olympus Mons; H) A skylight showing a potential access to the tube along the Arsia North chain; L) A typical rounded skylight with overhanging walls along the collapse chain of Arsia-A; P-R) Examples of lunar lava tube candidate collapse chains in Gruithuisen and Marius Hills; S) A smaller collapse characterized by fallen boulders and vertical walls is a probable incipient skylight in the chain of Marius-B.

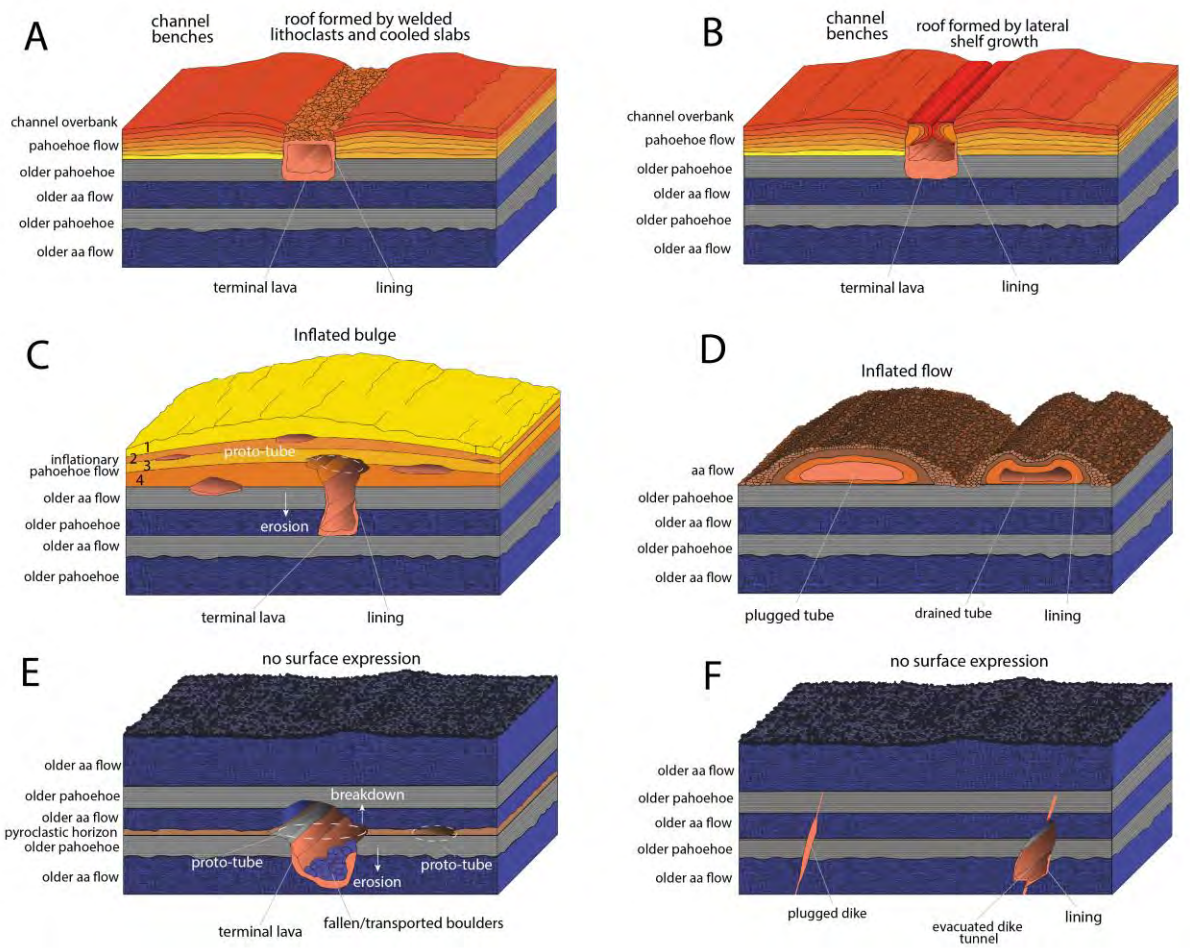

Fig. 2. Lava tube genetic processes (modified and integrated from Kempe et al., 2012): A) Lava tube formed by the crusting-over of channels by floating solidified slabs and lithoclasts welded together; B) Lava tube within a channel formed by lateral shelf accretion and consecutive closure; C) Lava tube formed by shallow inflation of pahoehoe sheets and later downward erosion; D) Lava tube formed by inflation and draining of aa flow nucleus; E) Lava tube formed by deep inflation along pre-existing lava flows boundaries or intra-flow pyroclastic deposits (inception horizons) enlarged by thermal erosion and breakdown; F) Tube formed through draining of a conduit formed by thermal erosion along a sealed fracture (eruptive fissure). .

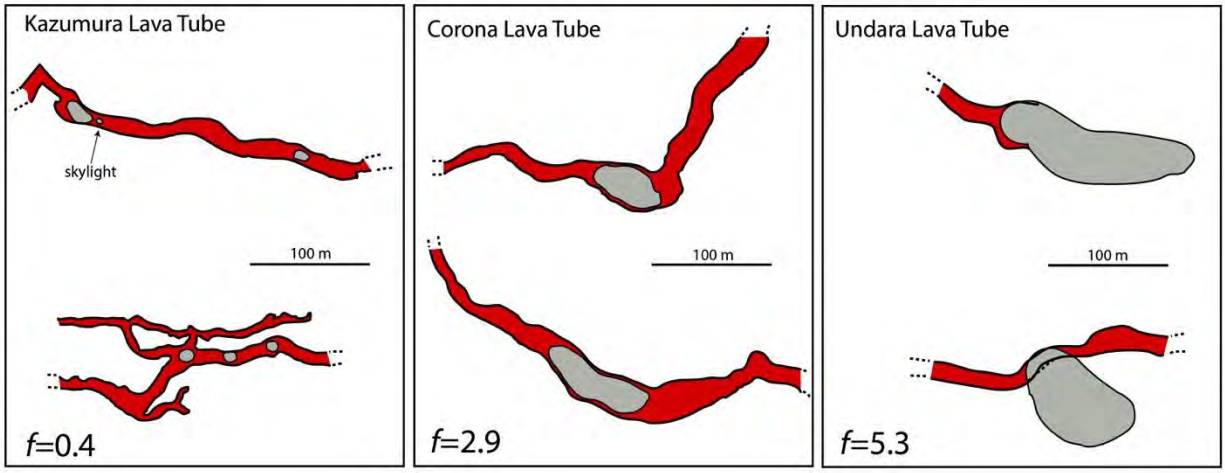

Fig. 3. Plan view maps of lava tubes showing different scaling factors *f* between collapses and intact tube segments. The two examples from Kazumura are from page 58a and 74 of the Kazumura Atlas. The Corona examples are derived from laser scanner mapping (above *Jameo de la Gente,* below *Jameo de la Puerta Falsa*). The Undara examples are from a modified figure in Atkinson et al. (1975).

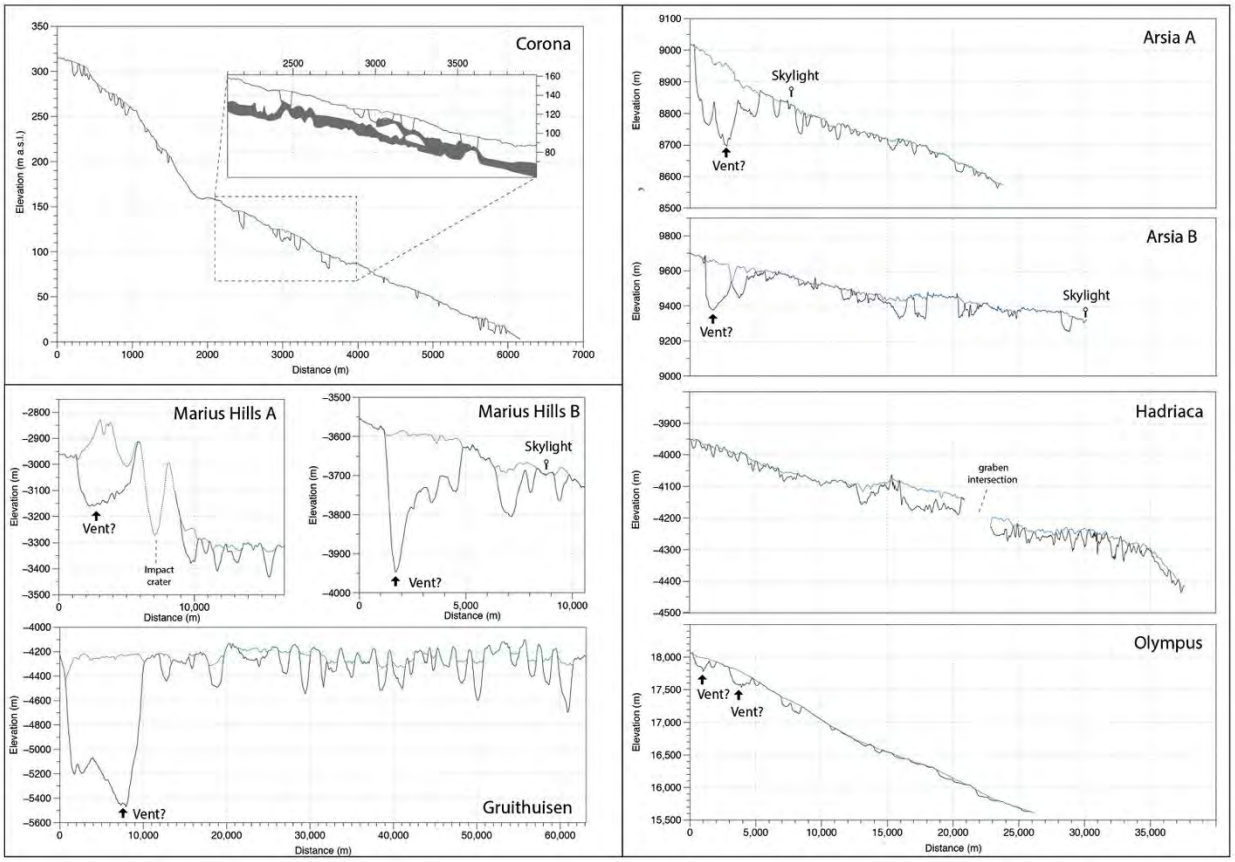

Fig. 4. Profiles of tube collapse pit chains (black lines) with superposed the extrapolated intact topography on Earth, Mars and the Moon. For the Corona terrestrial lava tube the inset shows the relationship between the collapses and the tube surveyed with laser scanner.

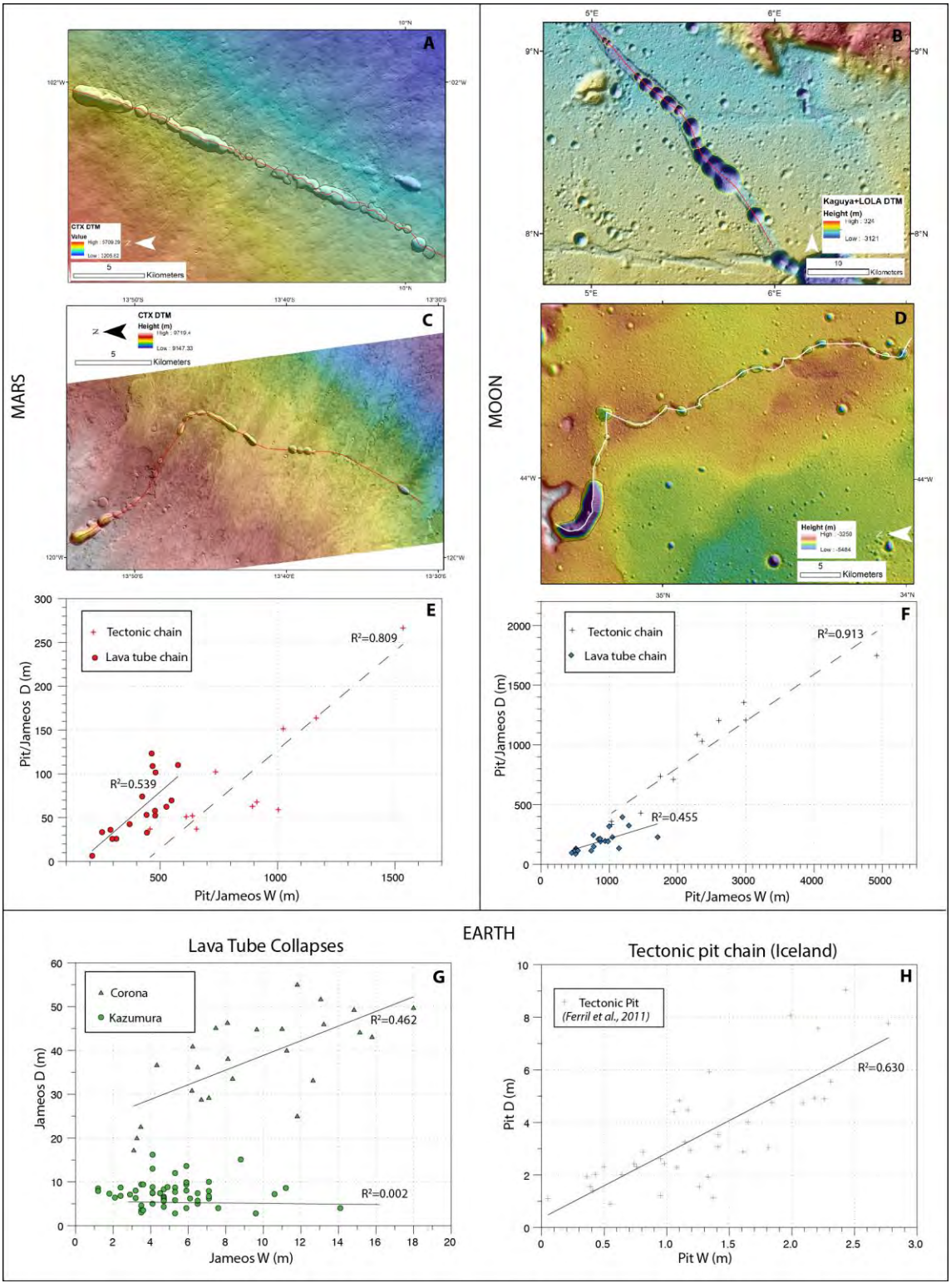

Fig. 5. Main morphological and morphometric characters of tectonic pit chains and lava tube collapse chains: Tectonic pit chains on Mars (A) and on the Moon (B) are characterized by coalescent pits and bounding grabens. Their development is rectilinear

and in the case of Mars (A) perpendicular to the steepest slope. Lava tube collapse chains on Mars (C) and on the Moon (D) are characterized by non-coalescent depressions and sinuous development. They often start with an initial deeper depression interpreted as the putative tube feeding vent. Width *W* and Depth *D* morphometric relationships of the three genetic cases, on Mars (E), the Moon (F), terrestrial lava tubes (G) and terrestrial tectonic pits in Iceland (H) from Ferril et al. (2011).

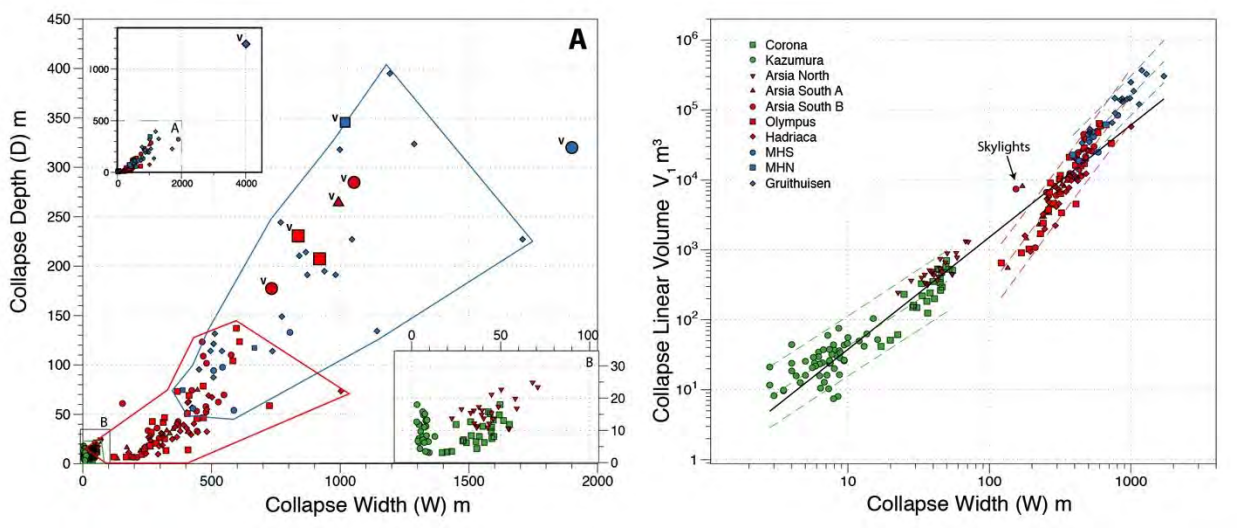

Fig. 6. Collapse chain morphometric parameter plots. A) The complete dataset showing the distribution of collapses width *W* and depth *D* (Earth in green, Mars in red, Moon in blue; legend for symbols is shown in D). Different line colors define the morphometric range for each planetary body. Bigger and deeper outliers are interpreted as putative vents (v in A) at the beginning of each chain (Gruithuisen vent shown in the upper left inset because of its exceptionally large size). The lower-right inset shows the partial overlap of terrestrial cases with putative overcrusted tubes in Arsia North on Mars. B) Collapse width *W* versus linear volume V_1 expressed in a logarithmic plot (putative vent outliers excluded); power laws trend lines for each planetary body and for the whole dataset (black line) are shown.

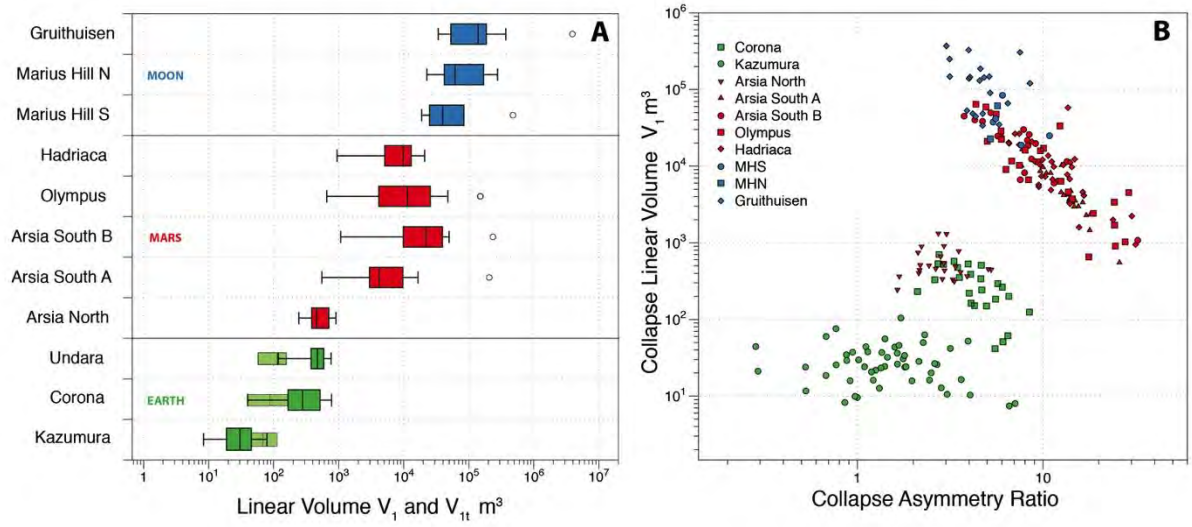

Fig. 7. A) Boxplot showing the quartiles, minimum and maximum distribution for V_1 of collapse chains analyzed in the three planetary bodies; outliers are the putative vents; for Earth the smaller and light green boxes show the quartile distribution of the intact tube V_1t in each chain (the data for Undara are derived from literature). B) Collapse asymmetry ratio versus V_1 in a logarithmic plot.

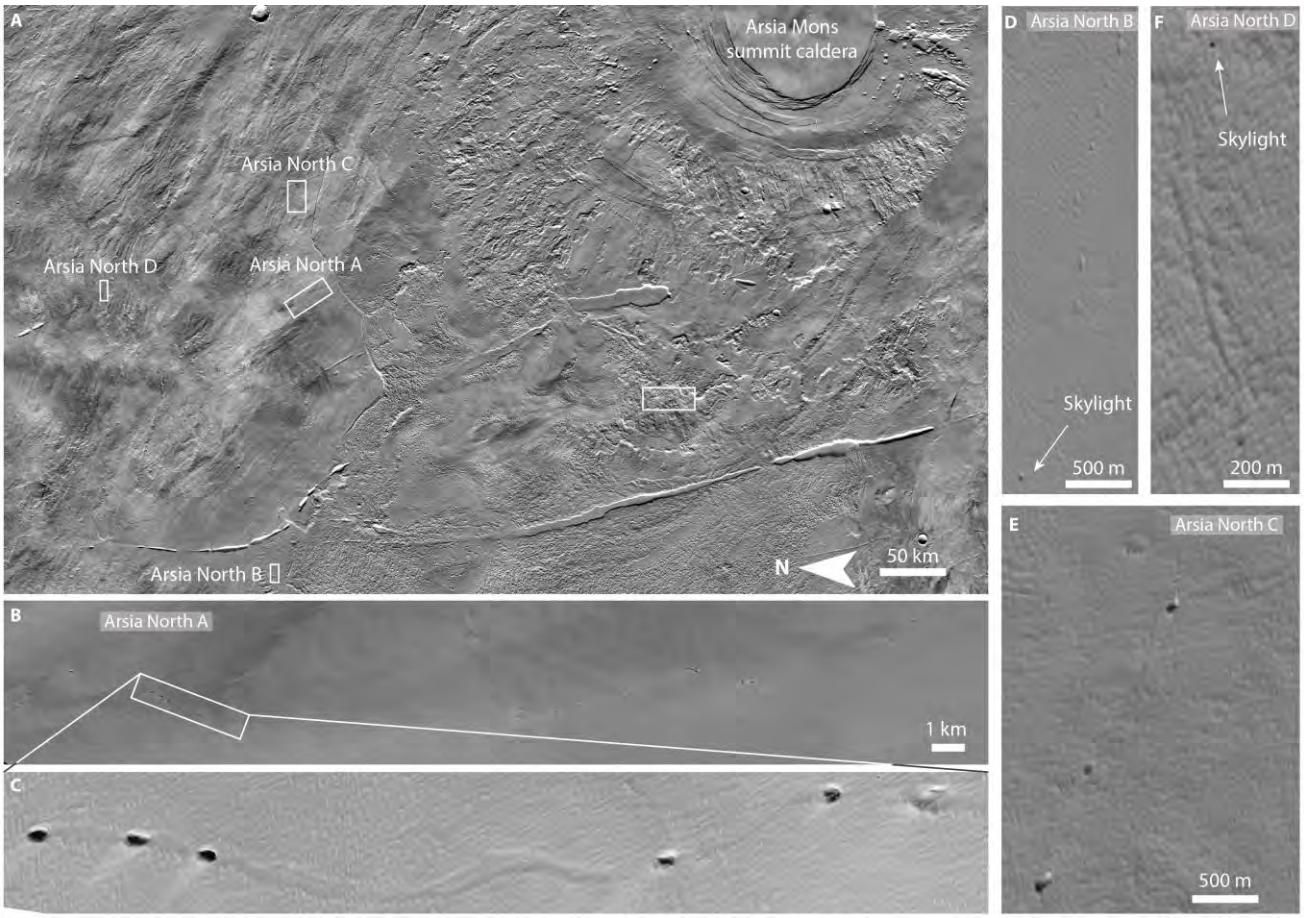

Fig. 8. Panel showing collapse chains with similar characteristics on the lava plains to the north of Arsia Mons (A). B-C) The collapse chain Arsia North measured in this study. D) A similar chain with skylights named Arsia North B. F) Two skylights with channel benches among them in the collapse chain named Arsia North D. E) A series of collapses connected by clear channel benches along Arsia North C.

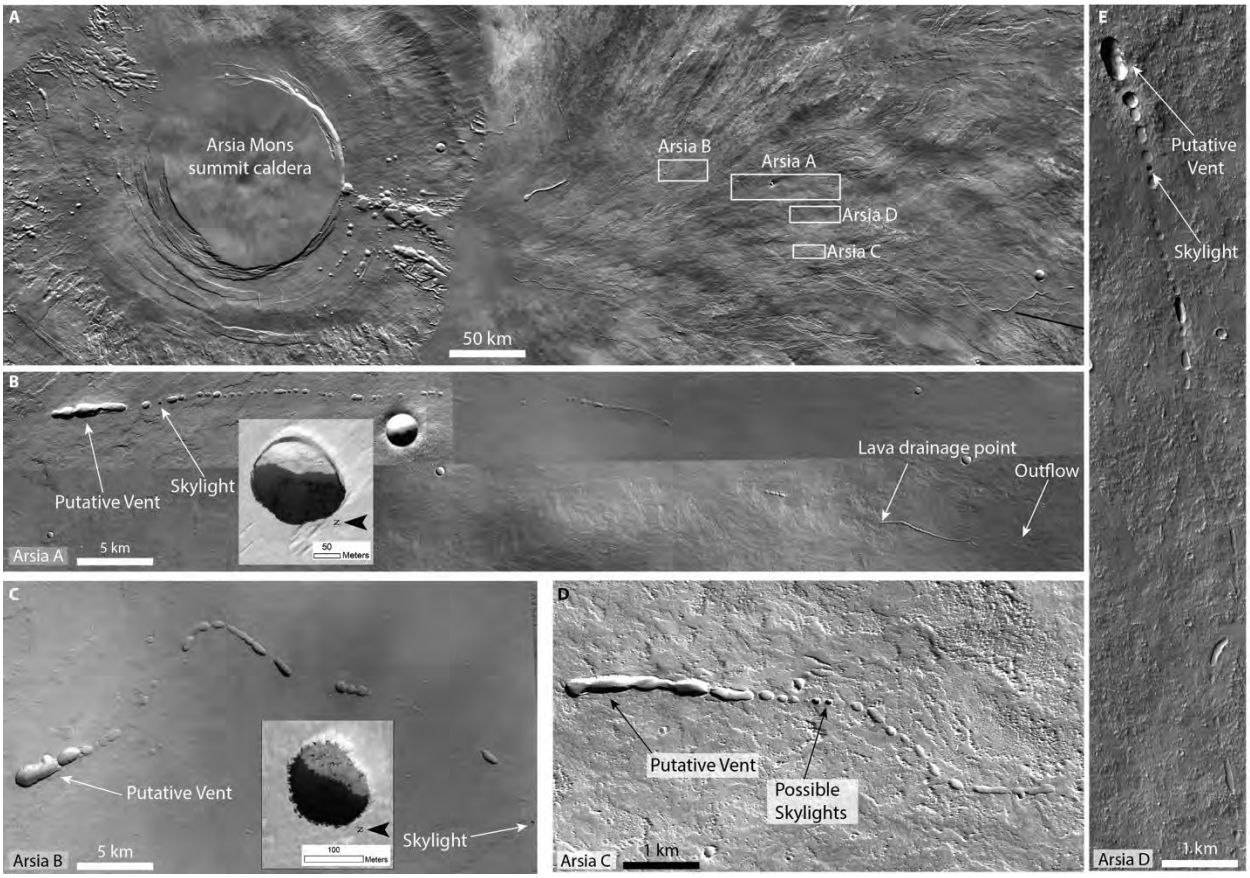

Fig. 9. Panel showing collapse chains with similar characteristics on the southern flank of Arsia Mons.

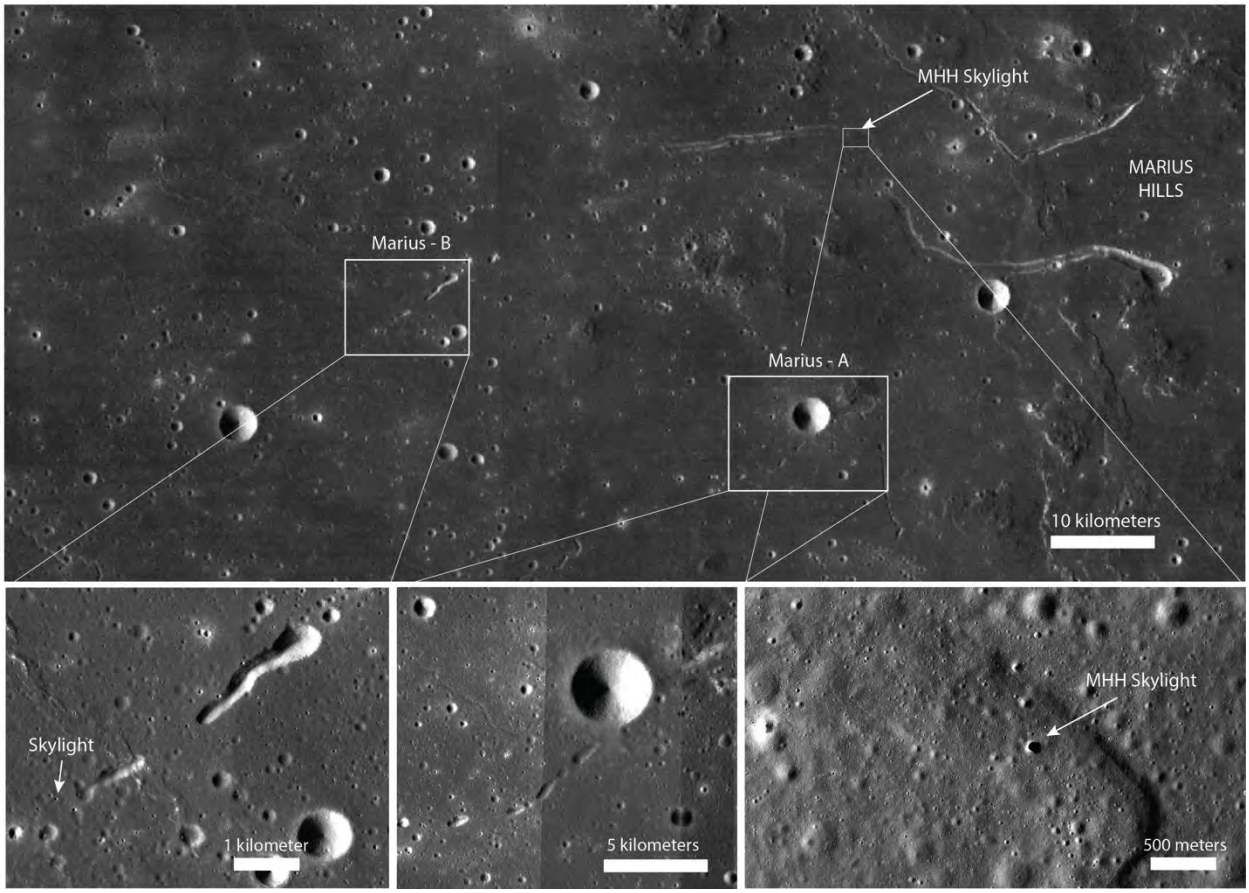

Fig. 10. Localization of collapse chains and skylights in the Marius Hills dome.

Chain morphological characters	Overcrusted	Shallow Inflated in pahoehoe	Shallow Inflated in aa	Deep inflated inception horizon	Deep inflated in Eruptive fissure	Tectonic
Rectilinear (R), curvilinear (C), Sinuous (S)	S	S	S, R along flow axes	S, rarely R	R, C	R, C
Braided	Rarely	Often	Rarely	Often	No	No
Collapse width (W) variability along the chain	Low	High	Low	Low	High	High
Coalescent pits	No	No	No	No	No	Yes
Following steepest slope line	Yes	Mostly but not always	Mostly but not always	Mostly but not always	Mostly but not always	No
Skylights	Common	Common	Common	Rare	Very rare	Rare
Initial vent on top of the chain	Yes	Yes, but not always	Also secondary vents	Yes	Yes, but not always	No
Within graben	No	No	No	No, or rarely	No	Yes
Within lava channels, sinuous rilles	Always	No, central part of the flow	No	Not always	No	No
Along one single lava flows	Always	Not always	Yes	Not always	No	No
Bulges or lateral benches between collapses	Often	Possible wide bulge/ridge, no benches,	Wide Bulge	No surface expression	No	No
Possible presence of other volcanic features	Lava falls, welded slabs and boulders in channel	Inflation clefts, tumuli and hornitos, degassing tracks	Inflation clefts, tumuli and hornitos, degassing tracks	Secondary vents	Deep pit craters like Wood Valley (Cushing et al. 2015)	No
Collapse asymmetry ratio	1 or <1	>1 (if not entrenched)	>1 (if not entrenched)	>1 (if not entrenched)	1 or <1	1

Table 1. Typical morphological characteristics of lava tube collapse chains (overcrusted/shallow inflated/deep inflated/eruptive fissures) compared to non-volcanic tectonic pit chains.

	Morphometric Parameters	Acronym	Source	Notes
Collapse (*jameos*/skylights) chain (Earth, Mars, Moon)	**Total Length**	*Ctl* (km)	Ortho-rectified and georeferenced satellite images	/
	Sinuosity Index	Si	*Sinuous AB path/Linear AB distance*	/
	V (Vertical Range)	*Vr* (m)	Total vertical topographic range from the highest to the lower collapse *height of A – height of B*	/
	Slope (steepness)	*CS* (°)	Average slope of the pit chain *Sin(CS)=Ctl/Vr*	/
Collapses (*jameos*/skylights) (Earth, Mars, Moon)	**Collapse Length**	*L* (m)	Major axis of the minimum bounding rectangle	/
	Collapse Width	*W* (m)	Minor axis of the minimum bounding rectangle	/
	Collapse Depth	*D* (m)	Maximum depth of the collapse	/
	Collapse Volume	*V* (m^3)	Surface difference *Synthetic Surface-DTM*	Calculated also from TLS for the Corona collapses
	Collapse Linear Volume	V_1 (m^3)	*The volume per 1 m thick cross section* $[(D*W)/2]*\pi$	
	Collapse Asymmetry Ratio	*AR*	*W/D*	Provide indications on the tube eccentricity
	Collapse Azimuth	*CA* (°)	Azimuth of the major axis of the minimum bounding rectangle	
Intact tube (Earth)	**Intact Tube Width**	*Wt* (m)	Width of the tube perpendicular to the tube development in a given cross section	In Corona and Kazumura *Wt* has been extracted from cross sections with 5 m spacing
	Intact Tube Height	*Ht* (m)	Maximum tube height in a given cross section	In Corona and Kazumura *Ht* has been extracted from cross sections with 5 m spacing
	Intact Tube linear volume	V_1t (m^3)	<u>For Corona</u> Direct measurement of the surface area of a given cross section of the 3D survey obtained with TLS <u>For Kazumura and Undara</u> $[(Ht*Wt)/2]*\pi$	
	Total tube length	*Ttl* (km)	Surveyed length of the whole intact tube sections	
	Tube collapse scaling factor	*f*	Average linear volume of the collapses divided per the average linear volume of the intact conduit V_1/V_1t	
Total conduit volumes (Earth, Mars, Moon)	**Total uncollapsed tube length**	*Tutl (m)*	The total length of the chain minus the total sum of collapses lengths *Ctl - Sum(L)*	Provide an estimation of the total length of intact sections
	Percent of uncollapsed sections along the chain	*Tutl (%)*	Same as above but in %	Provide an estimation of the percentage of intact sections
	Total volume of uncollapsed tube segments and total volume of the original tube	*TtV* (m^3) *TtoV* (m^3)	For Moon and Mars *Tutl* multiplied to the linear volume (of tube V_1t for the terrestrial cases, of collapse V_1 For the terrestrial cases, *Ttl* multiplied to the linear volume (of tube V_1t, of collapse V_1 for Moon and Mars)	Provide an estimate of the total volume of the intact tube sections without considering secondary infilling

Table 2. Morphometric parameters of collapse chains, individual collapses and intact tube sections provided in this study.

	Location	Coordinates	Data source and analysis method	Morphotype
Earth	Kazumura	19.412° -155.237°	Kazumura Atlas cave maps (Allred et al., 2002)	Overcrusted, entrenched, multilevel
	Corona	29.165° - 13.455°	Lidar DTMs (Spanish Geological Survey), Laser scans (Santagata et al., 2018)	Deep inflation along inception horizon, multilevel, partly braided
	Undara	-18.220° 144.628°	Cave maps (Atkinson, 1991; Atkinson and Atkinson, 1995)	Inflation and pressure overflow
Mars	Arsia North	-3.062° -123.930°	CTX, HiRiSe, shadow/height tool	Sinuous chain with continuous channel benches, collapses and skylights
	Arsia South-A	-14.377° -119.949°	CTX stereo-pairs DTM HiRiSe shadow/height tool (for skylights)	No surface expression aside of collapses, 1 skylight, deeper and wider depression at the beginning of the chain (vent?)
	Arsia South-B	-13.632° -119.869°	CTX stereo-pairs DTM HiRiSe shadow/height tool (for skylights)	Sinuous, no surface expression aside of collapses and 1 skylight, deeper and wider depression at the beginning of the chain (vent?)
	Olympus	19.456° -133.399°	CTX stereo-pairs DTM	Sinuous, braided, no surface expression aside of collapses and wider depression at the beginning of the chain (vent?)
	Hadriaca	-36.668° 89.394°	CTX stereo-pairs DTM	Sinuous, no surface expression aside of collapses, highly eroded
	Ascraeus Tectonic	10.123° -102.098°	CTX stereo-pairs DTM	Graben-bounded tectonic pit chain
Moon	Marius -A	13.096° -57.056°	LRO-NAC Kaguya/LRO LOLA DTMs	Sinuous, no surface expression aside of collapses, wider depression at the beginning of the chain (vent?)
	Marius-B	13.603° -58.047°	LRO-NAC Kaguya/LRO LOLA DTMs	No surface expression aside of collapses, 1 skylight, wider depression at the beginning of the chain (vent?)
	Gruithuisen	34.618° -43.467°	LRO-NAC Kaguya/LRO LOLA DTMs	Sinuous collapse chain, with some lava overflows and intersected by a wrinkle ridge, wider and much deeper depression at the beginning of the chain (vent?)
	Hyginus Rill Tectonic	8.384°, 5.630°	LRO-NAC Kaguya/LRO LOLA DTMs	Graben-bounded tectonic pit chain

Table 3. Lava tubes on Earth and candidate lava tube collapse chains on the Moon and Mars studied in this review for the morphometric analysis.

Collapse chain parameters

	Lava tube	N° Collapses	N° Skylight	Vent	Ctl (km)	Si	S	Vertical Range
Earth	Kazumura	53	29	Yes	32.1	1.3	1.9	1102
	Corona	25	2	Yes	6.5	1.1	2.91	240
	Undara*	>40	/	Yes	41	1.24	0,7-1,4	377
Mars	Arsia North	22	2	Yes	42	1.12	0.5	277
	Arsia South A	23	1	No	56	1.01	1.1	1094
	Arsia South B	17	1	Yes	30	1.23	0.9	315
	Olympus	25	0	Yes	29	1.1	5.2	2704
	Hadriaca	32	0	No	75.7	1.1	0.7	630
Moon	Marius Hill South	5	0	Yes	16.9	1	1.2	210
	Marius Hill North	2	1	Yes	8.5	1	0.01	60
	Gruithuisen	20	0	Yes	41	1.2	0.02	40

Collapses morphometry

	Lava tube	Av. L	σ L	Av. W	σ W	Av. D	σ D	Av. V	σ V	Av. V1	σ V1	Av. AR
Earth	Kazumura	13.9	7.3	7.4	2.9	5.2	2.5	/	/	29	18	1.4
	Corona	62.2	32.8	37.6	12.1	9.8	4.4	10263	9084	316	177	3.9
	Undara*	250	/	68	/	5-25	/	/	/	/	/	5-6
Mars	Arsia North	64	25	44.5	11.7	15.7	4,2	/	/	569	289	2.8
	Arsia South A	369.1	164.4	283.3	83.7	25.3	16.7	1410732	2181775	6740	6330	11.2
	Arsia South B	759.7	506.2	415.2	107.8	59.8	34	7324819	7079975	21514	14909	6.9
	Olympus	737.7	560.4	366.2	148.8	45	36.2	4549680	5714013	14970	17710	8.1
	Hadriaca	888.9	743.77	374.3	143.8	34.7	18.2	4648559	9511566	11700	10855	10.8
Moon	Marius Hill South	1070.3	374.5	573.9	141.5	87	32.9	16482675	13802402	41388	25543	6.6
	Marius Hill North	1358	802.6	527.4	197	95.8	30.2	21733653	22293270	42039	27341	5.5
	Gruithuisen	1333.7	629.4	858.5	322	189.9	83.54	81715413	78192450	141601	100929	4.5

Subsurface tube morphometry

	Lava tube	Ttl (km)	Av. Wt	σ Wt	Av. Ht	σ Ht	Av. V1t	σ V1t	*f*
Earth	Kazumura	41,8 (65,6)	10.5	4.7	8.11	3.44	69.21	37.4	0.4
	Corona	7.5	13.7	5.1	9.7	3.7	104	69	2.9
	Undara*	/	15-20	/	6.5	/	76-102	/	5.3

Tab. 4. Main morphometric parameters of collapse chains (for Earth, Mars and Moon) and of related intact tube sections (Earth). *Data for Undara are derived from existing literature and cave maps (Atkinson, 1991). Morphometric parameters acronyms are: *Ctl* – Chain total length; *Si* – Sinuosity index; *S* – Slope; *Vr* – Vertical range; *Av. L* – Average length of the collapses (major axis); σL - standard deviation of *L*; *Av. W* – Average width of the collapses (minor axis); σW - σ standard deviation of *W*; Av. D – Average depth of the collapses; σD -

standard deviation of D; Av. V – Average volume of the collapses; σV - standard deviation of *V*; *Av.Vl* – Average linear volume (along 1 meter thick cross section) of the collapses; σV_1 - standard deviation of V_1; *Av AR* – Average asymmetry Ratio; *Ttl* – Total tube length; *Av. Wt* – Average tube width; σWt - standard deviation of *Wt*; *Av. Ht* – Average height of the tube passages; σHt standard deviation of *Ht*; A*v. V_1t* – Average linear volume of the tube passages; $\sigma V_1 t$ - standard deviation of $V_1 t$; *f* - conversion factor collapse/tube.

Estimated total volumes

	Lava tube	Tutl (m)	Tutl (%)	TtV (m3) (*f*=1)	TtV (m3) (*f*=3)	TtoV (m3)
Earth	Kazumura	31281	97.44859813	2164645.2	/	2221320
	Corona	4538	73.71669916	471952	/	640224
	Undara*	29999	73.16829268	2699910	/	3690000
Mars	Arsia North	23359	94.04162808	13291271	4430423.667	14133391
	Arsia South A	9683	40.87551184	65263420	21754473.33	159663860
	Arsia South B	13615	45.12910604	292913110	97637703.33	649055866
	Olympus	20372	47.85304895	304968840	101656280	637302840
	Hadriaca	7193	20.18407835	84158100	28052700	416952900
Moon	Marius Hill A	6402	38.43659942	264965976	88321992	689358528
	Marius Hill B	4137	39.10947249	173915343	57971781	444688542
	Gruithuisen	27244	43.17591125	3857777644	1285925881	8935023100

Tab. 5. Estimation of total tube parameters: *Tutl* – total uncollapsed tube length; *TtV* – total uncollapsed tube volume (two scenarios: with *f*=1 and *f*=3); *TtoV* total original tube volume before collapses.

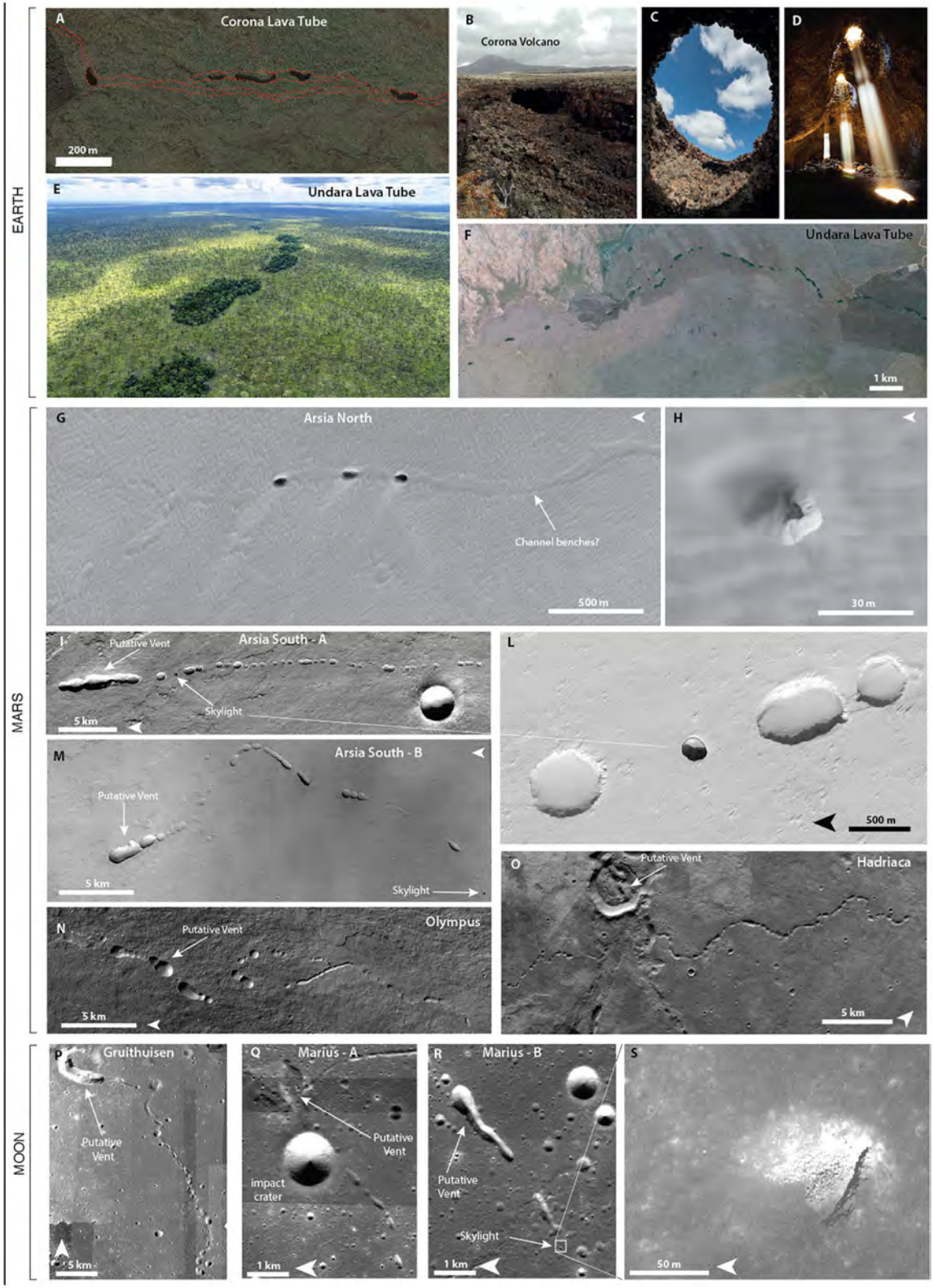
EARTH
A
Corona Lava Tube
200 m
B
Corona Volcano
C
D
E
Undara Lava Tube
F
Undara Lava Tube
1 km
MARS
G
Arsia North
Channel benches?
500 m
H
30 m
I
Putative Vent
Arsia South - A
Skylight
5 km
L
500 m
M
Arsia South - B
Putative Vent
5 km
Skylight
O
Putative Vent
Hadriaca
5 km
N
Putative Vent
Olympus
5 km
MOON
P
Gruithuisen
Putative Vent
5 km
Q
Marius - A
Putative Vent
impact crater
1 km
R
Marius - B
Putative Vent
Skylight
1 km
S
50 m

Figure 1

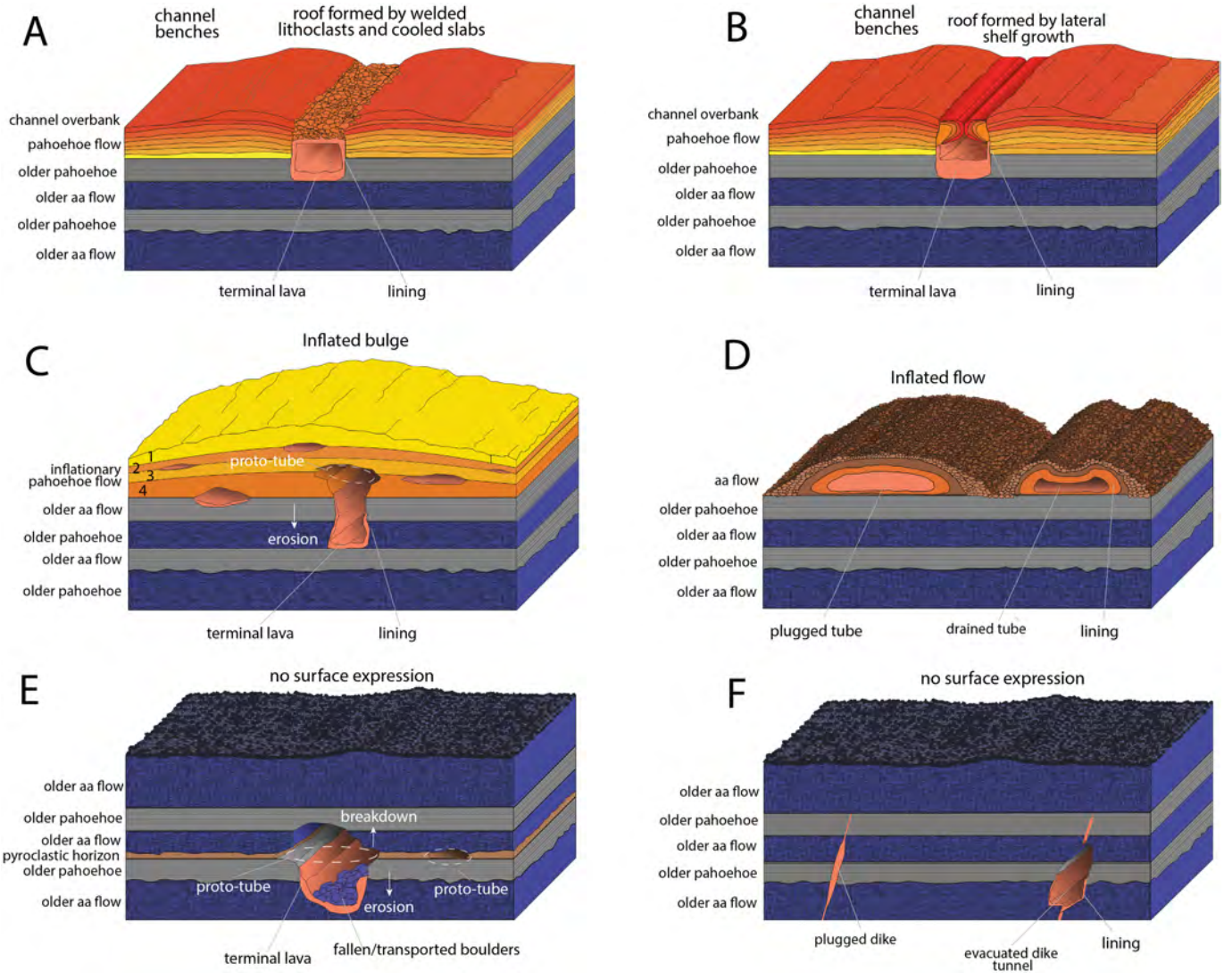
A
channel benches
roof formed by welded lithoclasts and cooled slabs
channel overbank
pahoehoe flow
older pahoehoe
older aa flow
older pahoehoe
older aa flow
terminal lava
lining
B
channel benches
roof formed by lateral shelf growth
channel overbank
pahoehoe flow
older pahoehoe
older aa flow
older pahoehoe
older aa flow
terminal lava
lining
C
Inflated bulge
inflationary pahoehoe flow
1
2
3
4
proto-tube
older aa flow
older pahoehoe
older aa flow
older pahoehoe
erosion
terminal lava
lining
D
Inflated flow
aa flow
older pahoehoe
older aa flow
older pahoehoe
older aa flow
plugged tube
drained tube
lining
E
no surface expression
older aa flow
older pahoehoe
older aa flow
pyroclastic horizon
older pahoehoe
older aa flow
breakdown
proto-tube
proto-tube
erosion
terminal lava
fallen/transported boulders
F
no surface expression
older aa flow
older pahoehoe
older aa flow
older pahoehoe
older aa flow
plugged dike
evacuated dike tunnel
lining

Figure 2

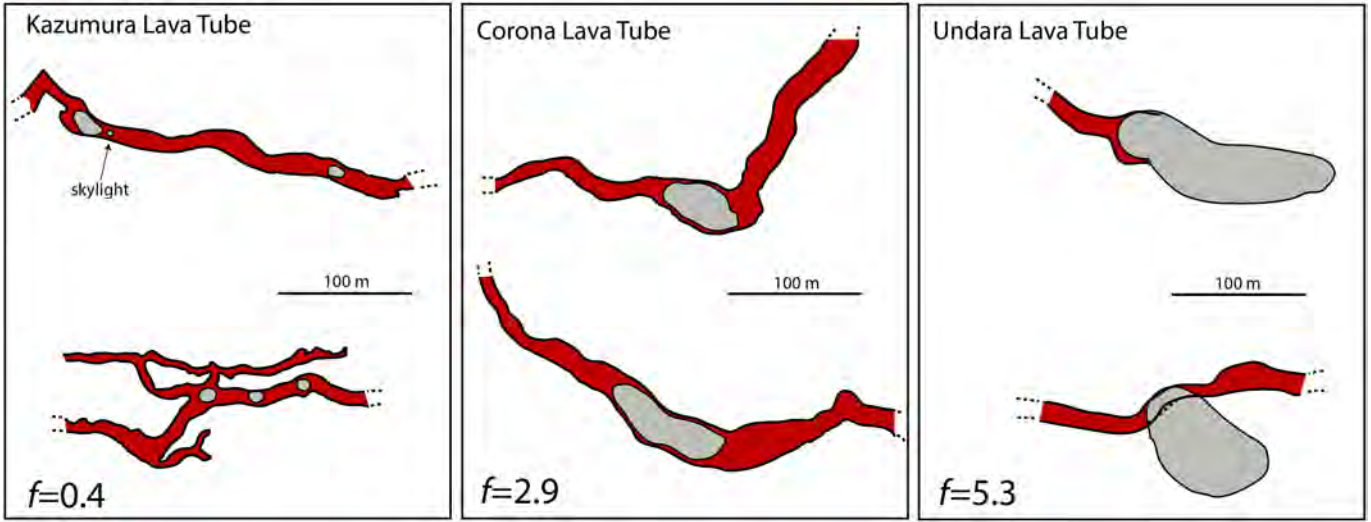
Kazumura Lava Tube
skylight
100 m
f=0.4
Corona Lava Tube
100 m
f=2.9
Undara Lava Tube
100 m
f=5.3

Figure 3

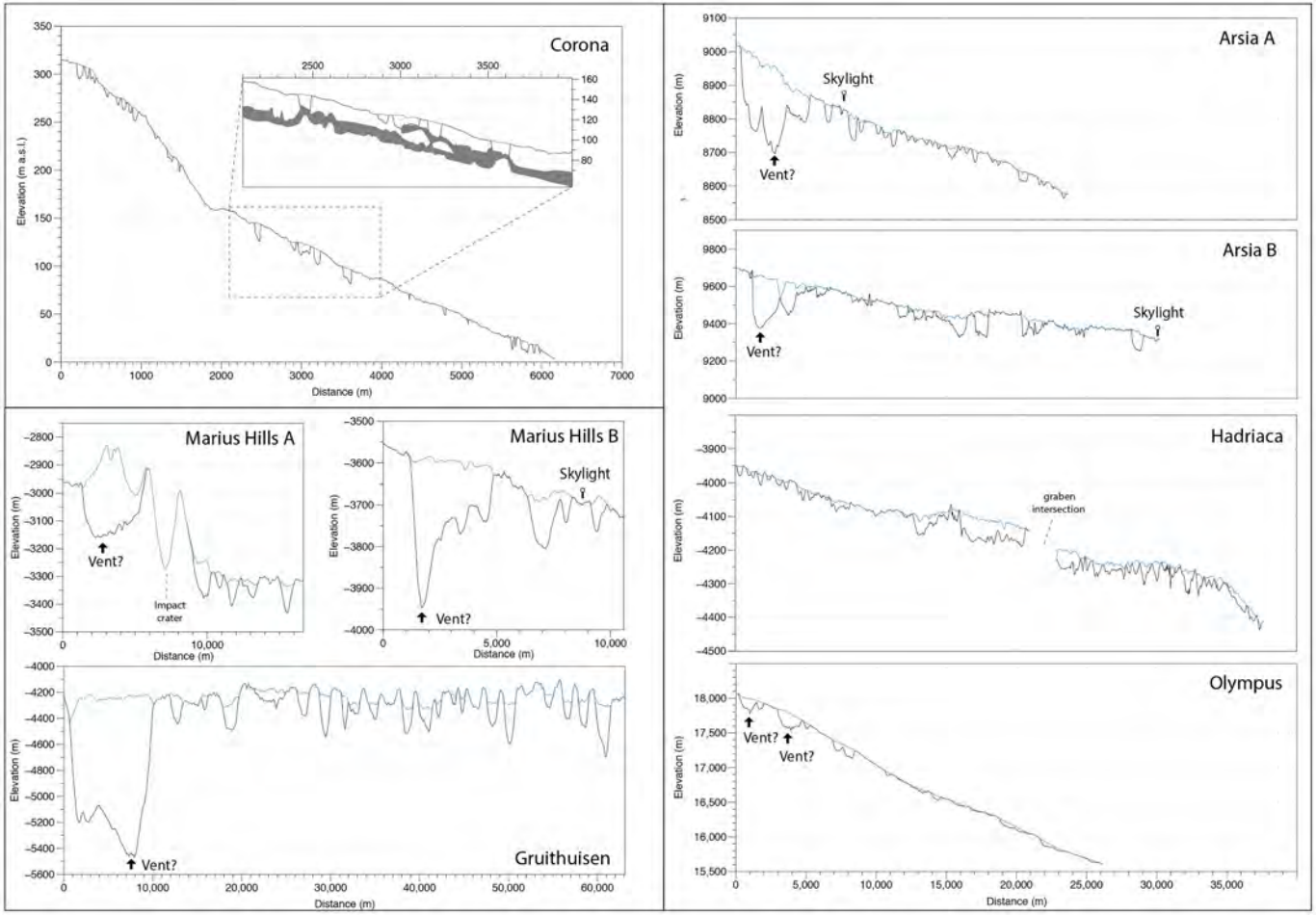
Corona
Elevation (m a.s.l.)
Distance (m)
Marius Hills A
Vent?
Impact crater
Marius Hills B
Skylight
Vent?
Gruithuisen
Vent?
Arsia A
Skylight
Vent?
Arsia B
Skylight
Vent?
Hadriaca
graben intersection
Olympus
Vent?
Vent?

Figure 4

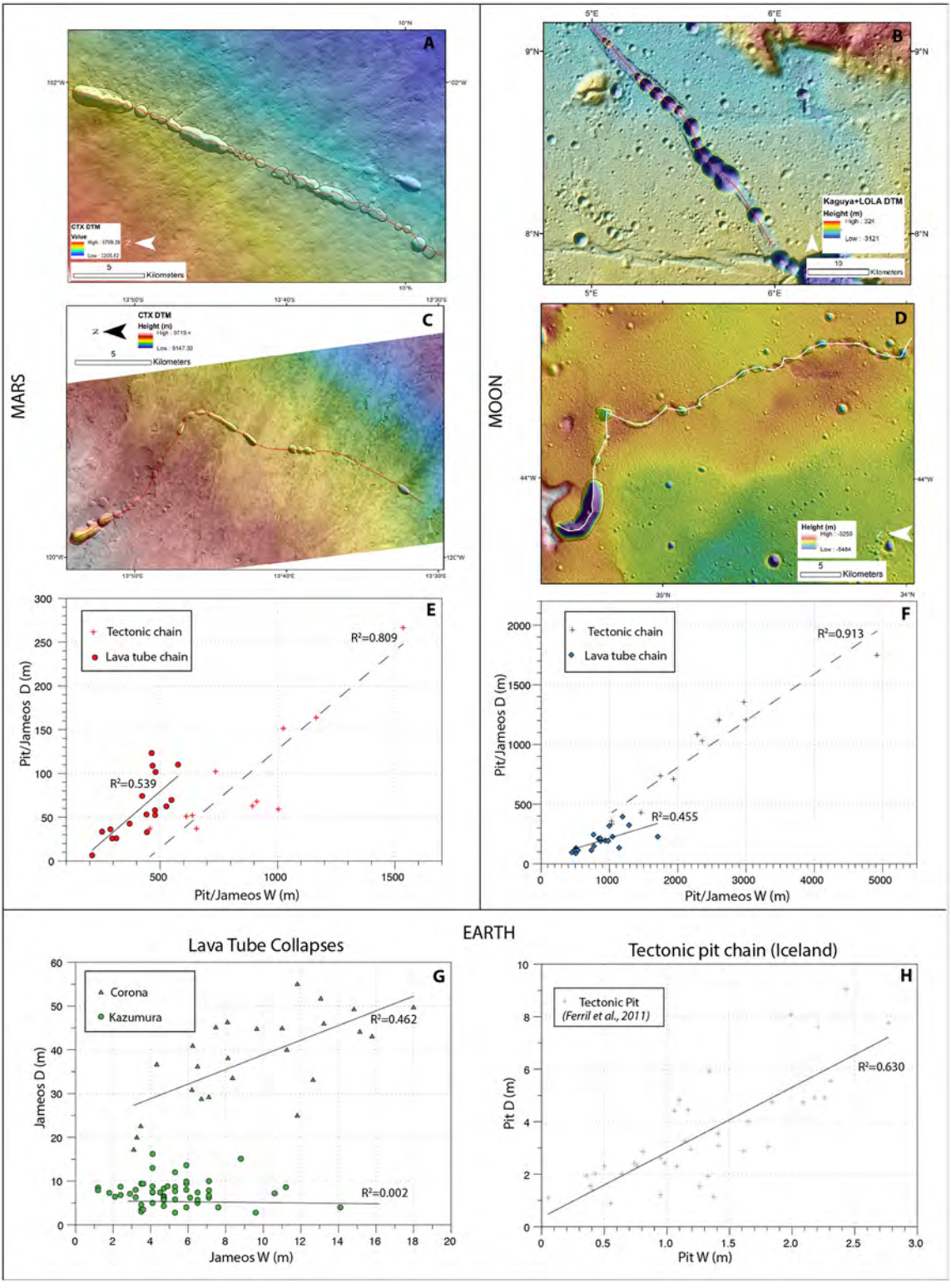
MARS
MOON
EARTH
A
B
C
D
E
F
G
H
CTX DTM
Kaguya+LOLA DTM
Kilometers
Tectonic chain
Lava tube chain
R²=0.809
R²=0.539
R²=0.913
R²=0.455
Pit/Jameos D (m)
Pit/Jameos W (m)
Lava Tube Collapses
Corona
Kazumura
R²=0.462
R²=0.002
Jameos D (m)
Jameos W (m)
Tectonic pit chain (Iceland)
Tectonic Pit
(Ferril et al., 2011)
R²=0.630
Pit D (m)
Pit W (m)

Figure 5

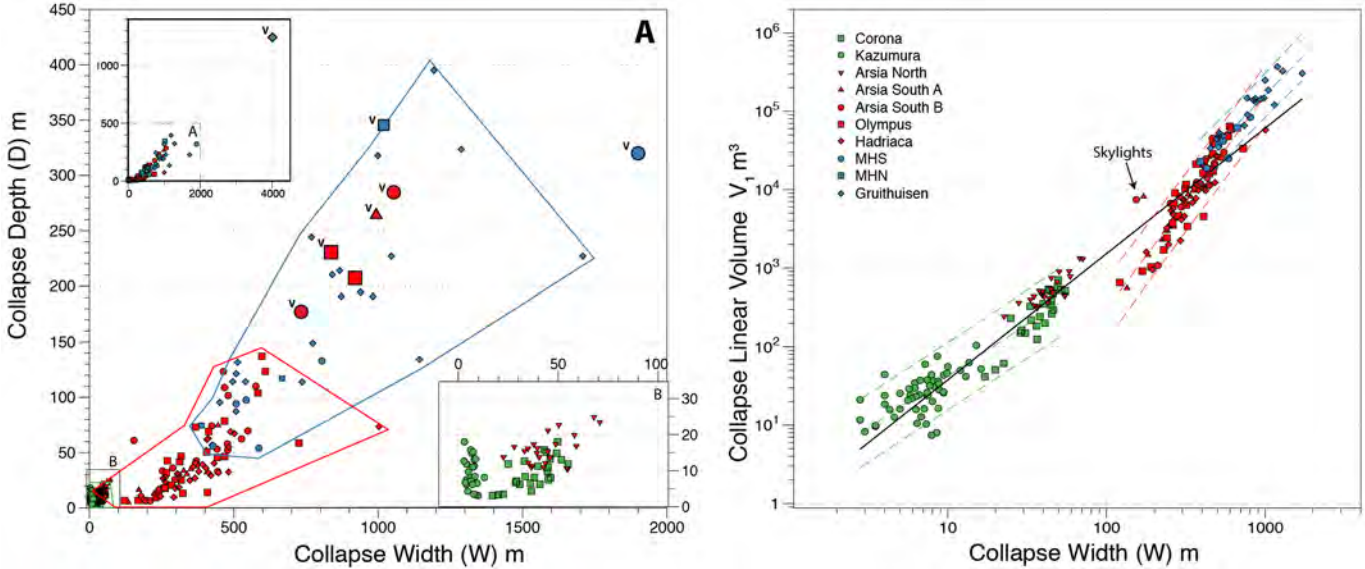
A
B
Collapse Depth (D) m
Collapse Width (W) m
Collapse Linear Volume V_1 m^3
Skylights
Corona
Kazumura
Arsia North
Arsia South A
Arsia South B
Olympus
Hadriaca
MHS
MHN
Gruithuisen

Figure 6

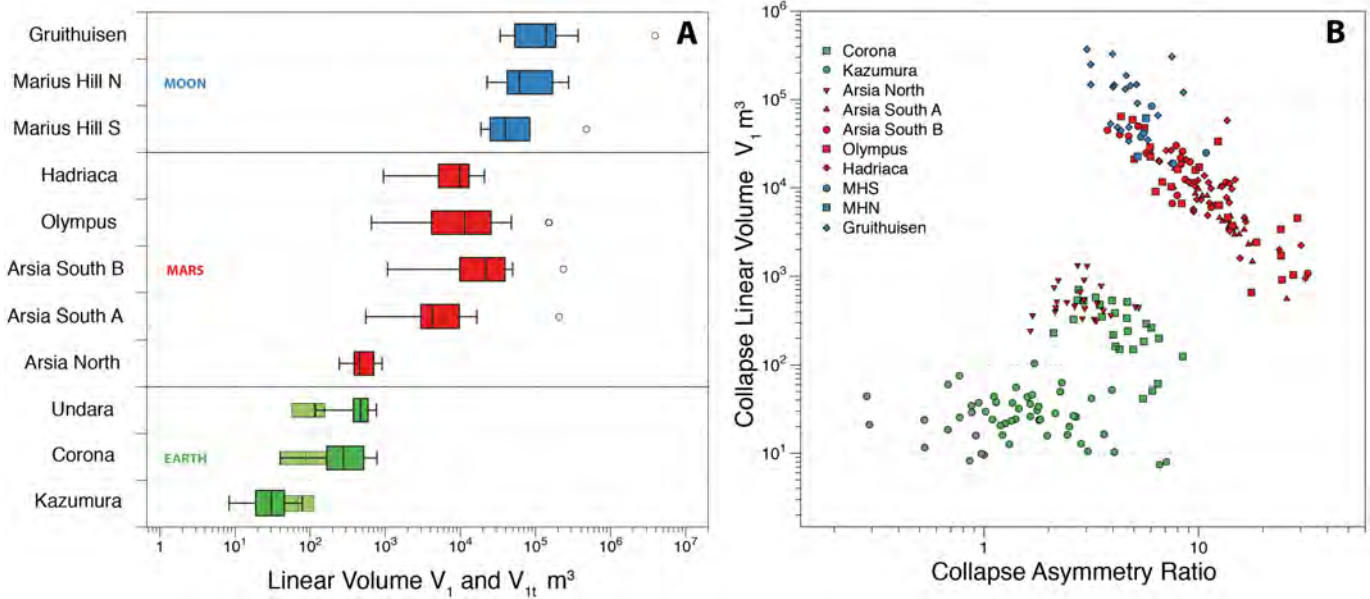
A
Gruithuisen
Marius Hill N
Marius Hill S
MOON
Hadriaca
Olympus
Arsia South B
Arsia South A
Arsia North
MARS
Undara
Corona
Kazumura
EARTH
1
10¹
10²
10³
10⁴
10⁵
10⁶
10⁷
Linear Volume V1 and V1t m³
B
Corona
Kazumura
Arsia North
Arsia South A
Arsia South B
Olympus
Hadriaca
MHS
MHN
Gruithuisen
Collapse Linear Volume V1 m³
10⁶
10⁵
10⁴
10³
10²
10¹
1
10
Collapse Asymmetry Ratio

Figure 7

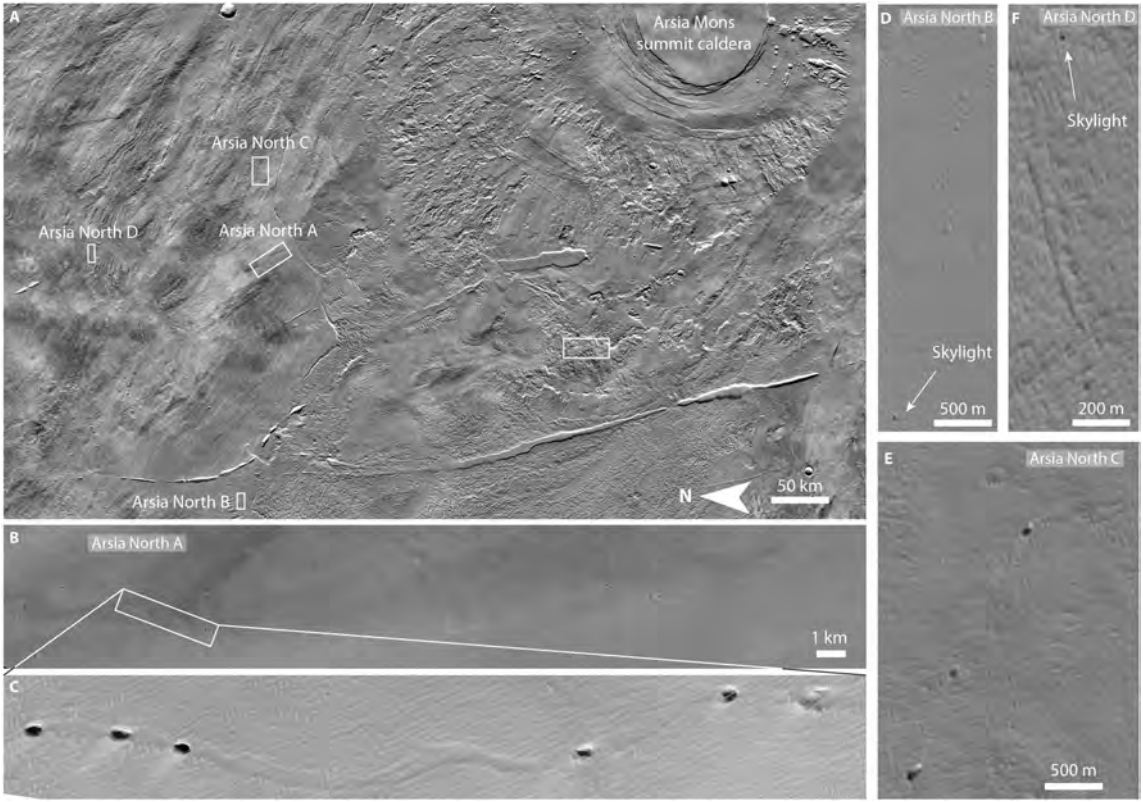
A
Arsia Mons
summit caldera
Arsia North C
Arsia North D
Arsia North A
Arsia North B
N
50 km
B
Arsia North A
1 km
C
D
Arsia North B
Skylight
500 m
F
Arsia North D
Skylight
200 m
E
Arsia North C
500 m

Figure 8

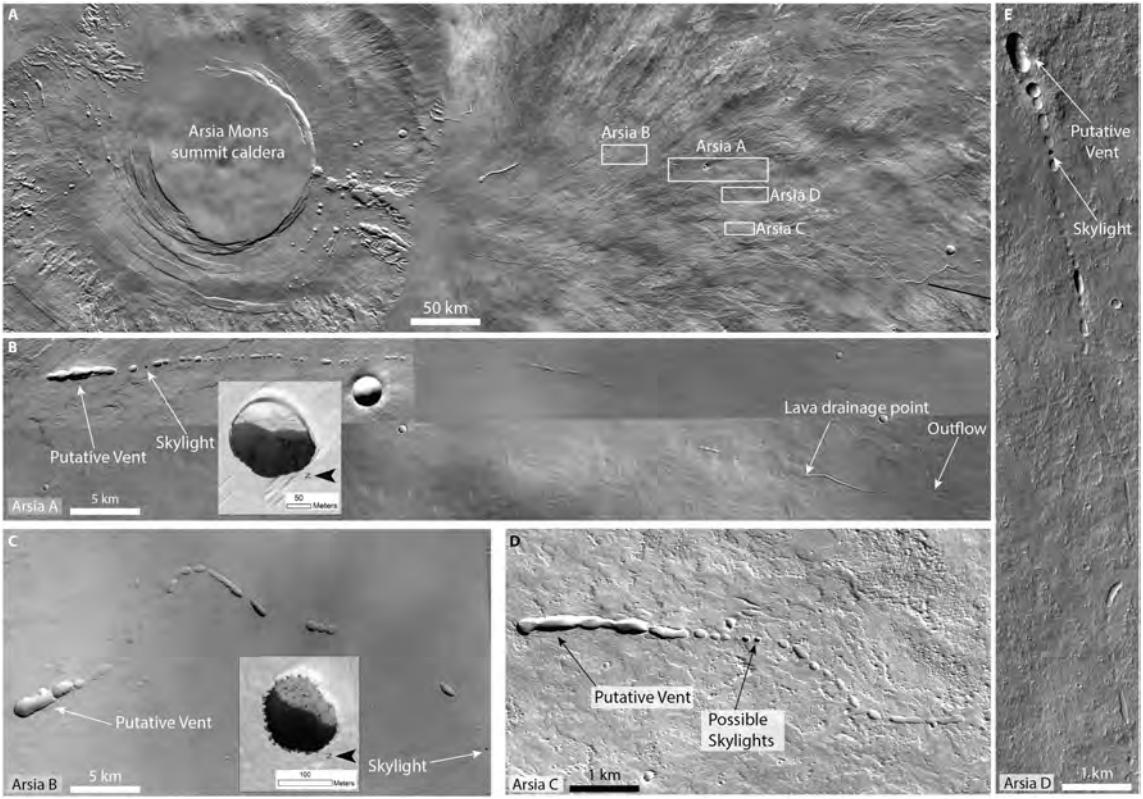
A
Arsia Mons
summit caldera
Arsia B
Arsia A
Arsia D
Arsia C
50 km
B
Putative Vent
Skylight
Arsia A
5 km
Lava drainage point
Outflow
C
Putative Vent
Skylight
Arsia B
5 km
D
Putative Vent
Possible
Skylights
Arsia C
1 km
E
Putative
Vent
Skylight
Arsia D
1 km

Figure 9

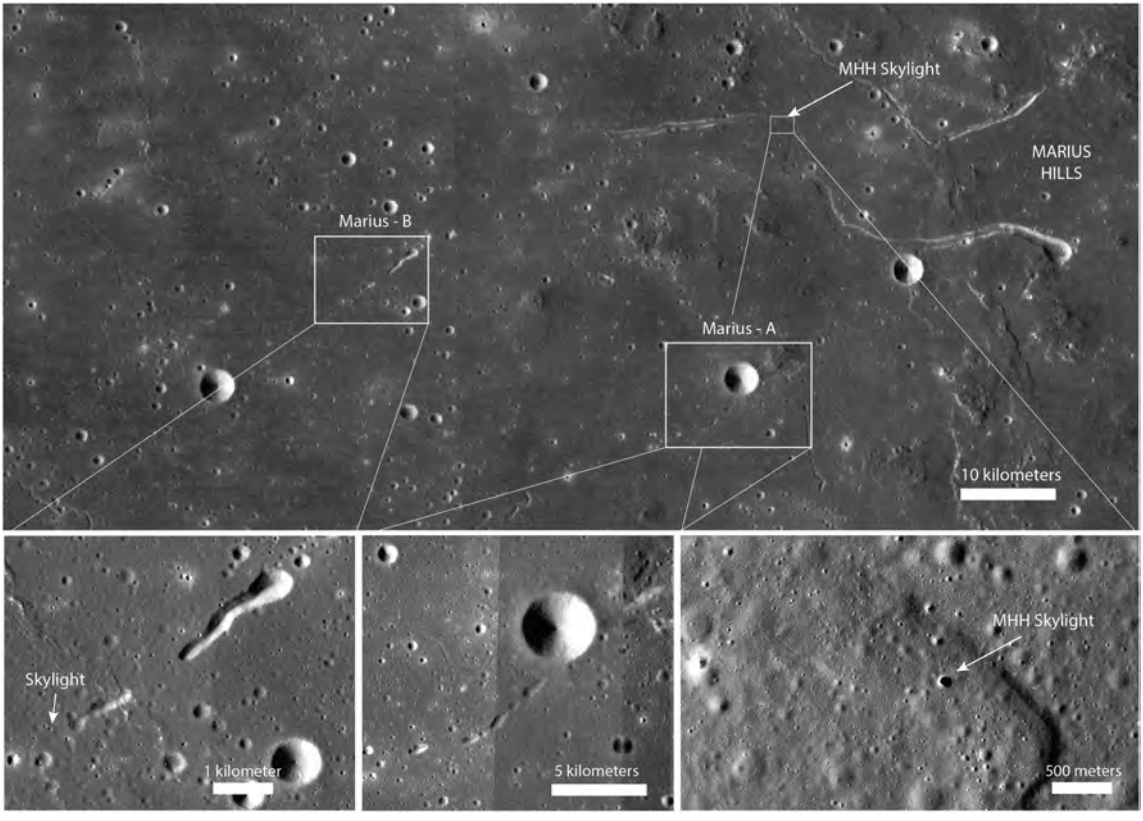
MHH Skylight
MARIUS
HILLS
Marius - B
Marius - A
10 kilometers
Skylight
1 kilometer
5 kilometers
MHH Skylight
500 meters

Figure 10